Chemical Engineering Science 64 (2009) 870 – 882

Contents lists available at ScienceDirect

Chemical Engineering Science

journal homepage: www.elsevier.com/locate/ces

An investigation of the characteristics of Maxwell–Stefan diffusivities of binary mixtures in silica nanopores

R. Krishna*, J.M. van Baten

Van 't Hoff Institute for Molecular Sciences, University of Amsterdam, Nieuwe Achtergracht 166, 1018 WV Amsterdam, The Netherlands

ARTICLE INFO

Article history:
Received 24 August 2008
Received in revised form 24 October 2008
Accepted 25 October 2008
Available online 6 November 2008

Keywords:
Adsorption
Maxwell–Stefan diffusivity
Self-diffusivity
Nanopore
Knudsen diffusivity
Binary mixture
Viscous flow

ABSTRACT

Diffusion of pure components (hydrogen (H_2), argon (Ar), krypton (Kr), methane (C1), ethane (C2), propane (C3), *n*-butane (*n*C4), and *n*-hexane (*n*C6)) in silica nanopores with diameters of 1, 1.5, 2, 3, 4, 5.8, 7.6, and 10 nm were investigated using molecular dynamics (MD). The Maxwell–Stefan (M–S) diffusivity ($Đ_{i,s}$) and self-diffusivities ($D_{i,self,s}$) were determined for pore loadings ranging to 10 molecules nm^{-3}. The MD simulations show that zero-loading diffusivity $Đ_{i,s}(0)$ is consistently lower, by up to a factor of 10, than the values anticipated by the classical Knudsen formula; the differences increase with increasing adsorption strength. Only when the adsorption is negligible does the $Đ_i(0)$ approach the Knudsen diffusivity value.
MD simulations of diffusion in binary mixtures C1–H_2, C1–Ar, C1–C2, C1–C3, C1–*n*C4, C1–*n*C6, C2–*n*C4, C2–*n*C6, and *n*C4–*n*C6 in the different pores were also performed to determine the three parameters $Đ_{1,s}$, $Đ_{2,s}$, and $Đ_{12}$, arising in the M–S formulation for binary mixture diffusion. The $Đ_{i,s}$ in the mixture were found to be practically the same as the values obtained for unary diffusion, when compared at the same total pore loading. Also, the $Đ_{i,s}$ of any component was practically the same, irrespective of the partner molecules in the mixture. Furthermore the intermolecular species interaction parameter $Đ_{12}$, could be identified with the binary M–S diffusivity in a *fluid* mixture at the same concentration as within the silica nanopore. The obtained results underline the overwhelming advantages of the M–S theory for mixture diffusion in nanopores.
Our study underlines the limitations of the commonly used dusty-gas approach to pore diffusion in which Knudsen and surface diffusion mechanisms are considered to be additive.

© 2008 Elsevier Ltd. All rights reserved.

1. Introduction

A wide variety of nanoporous materials such as zeolites, carbon nanotubes, carbon molecular sieves, metal–organic frameworks, titanosilicates, MCM-41, and SBA-16, with pore sizes smaller than about 10 nm, are used in adsorptive and membrane separations and catalysis. In the development of process technologies it is often necessary to have a good description of mixture diffusion within the nanosized pores (Arora and Sandler, 2005; Chen and Sholl, 2004; Chen et al., 1994; Ciesla and Schüth, 2005; Düren and Snurr, 2004; Himeno et al., 2007; Keskin et al., 2008; Krishna and Paschek, 2000; Krishna and van Baten, 2006b, 2007; Kuznicki et al., 2001; Li et al., 2007; Marathe et al., 2004; Schlünder et al., 2006; Snurr et al., 2004; Yoshioka et al., 2001).

If the pore sizes are smaller than about 0.8 nm, as is the case of zeolites, the molecules are always within the influence of the force field exerted with the wall and we have to reckon with the motion of *adsorbed* molecules; there is no "bulk" fluid phase to speak of. This can be illustrated in the case of diffusion of methane inside a zeolite pore. The Lennard–Jones size parameter σ for interaction of methane with the oxygen atoms of the zeolite structure is 0.347 nm (Dubbeldam et al., 2004). The minimum in the potential energy for interaction with the wall surface occurs at a distance $2^{1/6}\sigma = 0.39$ nm from the wall. This implies that the methane molecule at the centre of a pore of radius 0.4 nm will experience significant interactions with the surrounding walls. Diffusion inside pores smaller than 0.8 nm has been examined in detail in several recent publications (Kärger et al., 2003; Krishna and van Baten, 2008a,b) and will not be discussed further in this paper. The main focus of the present communication is on mixture diffusion in materials that have pore sizes ranging from about 1 to 10 nm, such as MCM-41, SBA-16, and Vycor glass. In such cases there is central core region where the influence of interactions with the wall is either small or negligible. Diffusion in this case is governed both by molecule–molecule and molecule–pore wall interactions.

In the Onsager theory, used for example by Bhatia and Nicholson (2008), the molecular fluxes N_i, defined in a reference

* Corresponding author. Tel.: +31 20 257007; fax: +31 20 5255604.
E-mail address: r.krishna@uva.nl (R. Krishna).

0009-2509/$ - see front matter © 2008 Elsevier Ltd. All rights reserved.
doi:10.1016/j.ces.2008.10.045

frame with respect to the pore walls, are related to the chemical potential gradients by

$$N_i = -\frac{1}{k_B T}\sum_{j=1}^{2} L_{ij}\frac{\mathrm{d}\mu_j}{\mathrm{d}x}, \quad i = 1,2 \tag{1}$$

The Onsager reciprocal relations prescribe

$$L_{12} = L_{21} \tag{2}$$

In the alternative Maxwell–Stefan (M–S) formulation (Krishna and Wesselingh, 1997), we write

$$-\frac{c_1}{k_B T}\frac{\mathrm{d}\mu_1}{\mathrm{d}x} = \frac{x_2 N_1 - x_1 N_2}{Đ_{12}} + \frac{N_1}{Đ_{1,s}} \tag{3}$$

$$-\frac{c_2}{k_B T}\frac{\mathrm{d}\mu_2}{\mathrm{d}x} = \frac{x_1 N_2 - x_2 N_1}{Đ_{21}} + \frac{N_2}{Đ_{2,s}} \tag{4}$$

In Eqs. (3) and (4) the $Đ_{i,s}$ are the M–S diffusivities of species 1 and 2, respectively, portraying the interaction between component i in the mixture with the surface (s), or wall, of the pore. The $Đ_{12}$ and $Đ_{21}$ are M–S diffusivities representing interaction between components 1 with component 2. The Onsager reciprocal relations require

$$Đ_{12} = Đ_{21} \tag{5}$$

The c_i are the loadings within the pore and x_i represent the component mole fractions

$$x_i = c_i/(c_1 + c_2) = c_i/c_t; \quad i = 1,2 \tag{6}$$

For unary diffusion, Eqs. (1), (3), and (4) simplify to yield

$$N_i = -\frac{c_i}{k_B T} Đ_{i,s}\frac{\mathrm{d}\mu_i}{\mathrm{d}x} = -\frac{1}{k_B T} L_i \frac{\mathrm{d}\mu_i}{\mathrm{d}x} \tag{7}$$

where $L_i = c_i Đ_{i,s}$ is the Onsager coefficient for pure component i. By introducing the thermodynamic factor Γ_i

$$\frac{c_i}{k_B T}\frac{\mathrm{d}\mu_i}{\mathrm{d}x} = \Gamma_i \frac{\mathrm{d}c_i}{\mathrm{d}x}; \quad \Gamma_i \equiv \frac{c_i}{f_i}\frac{\partial f_i}{\partial c_i}; \quad \text{unary system} \tag{8}$$

we can re-write Eq. (7) as

$$N_i = -Đ_{i,s}\Gamma_i \frac{\mathrm{d}c_i}{\mathrm{d}x} = -D_{Fick,i,s}\frac{\mathrm{d}c_i}{\mathrm{d}x} \tag{9}$$

where the Fick diffusivity $D_{Fick,i,s}$ for unary diffusion inside the pore is defined as

$$D_{Fick,i,s} = Đ_{i,s}\Gamma_i \tag{10}$$

The thermodynamic factor Γ_i can be obtained by differentiating the pure component adsorption isotherm.

The fluxes N_i in the foregoing Eqs. (1), (3), (4), and (7) include the viscous flow contributions. Therefore the phenomenological Onsager coefficients L_{ij} and the M–S diffusivities $Đ_{i,s}$ include the viscous shear contributions to the diffusivity (Bhatia and Nicholson, 2008). In this context it must be noted that our Eqs. (3) and (4) do *not* correspond to those of the dusty-gas model (DGM) (Mason and Malinauskas, 1983) used, for example, to interpret experimental data in porous glass membrane permeation (Yang et al., 2005), and mixture adsorption dynamics (Delgado and Rodrigues, 2001). The DGM been the subject of severe criticisms in recent years because of a number of flaws and inconsistencies highlighted by Kerkhof (1996), Kerkhof and Geboers (2005a,b), and Young and Todd (2005); these authors eloquently point out several flaws in the Mason development of the DGM, especially pertaining to the accounting of the viscous

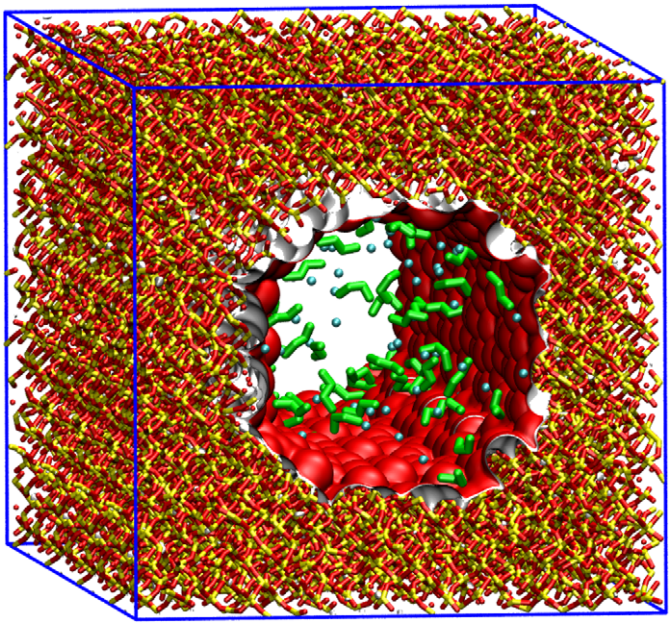

Fig. 1. Structure and wall surface landscape for 3 nm silica nanopore. Also shown is a snapshot of the equilibrium positions of C1 and *n*C4 molecules.

contribution. Formally, Eqs. (3) and (4) correspond with the binary friction model of Kerkhof (1996), Kerkhof and Geboers (2005a,b), derived by combining the mass and momentum balance relations for binary mixtures; our $Đ_{i,s}$ can be viewed as the inverse of Kerkhof's wall-friction coefficients. Following Kerkhof, we get

$$Đ_{i,s} = D_{i,Kn} + \frac{B_0 c_i k_B T}{\eta_i} \tag{11}$$

where $D_{i,Kn}$ is the Knudsen diffusivity, and B_0 representing the permeability of the pore. The second term on the right-hand side of Eq. (11) represents the viscous contribution. An important difference between our approach in the current paper with the work of Kerkhof is that we do not neglect the influence of adsorption at the pore wall, and attendant surface diffusion along the pore surface. Indeed, one of the major objectives is to underline the influence of surface adsorption on the $Đ_{i,s}$. At this stage in the model development, $Đ_{i,s}$ represents a conglomerate of "Knudsen", "surface", and "viscous" effects; in the molecular dynamics (MD) simulations that we shall employ, this lumped parameter is determined, without deconvolution into the individual contributions.

For binary mixtures the relation between the Onsager L_{ij} and the M–S diffusivities $Đ_{i,s}$ and $Đ_{12}$ are (see supplementary material for detailed derivations)

$$L_{11} = \frac{c_1 Đ_{1,s}\left(1 + \dfrac{x_1 Đ_{2,s}}{Đ_{12}}\right)}{1 + \dfrac{x_1 Đ_{2,s} + x_2 Đ_{1,s}}{Đ_{12}}} \tag{12}$$

$$L_{22} = \frac{c_2 Đ_{2,s}\left(1 + \dfrac{x_2 Đ_{1,s}}{Đ_{12}}\right)}{1 + \dfrac{x_2 Đ_{1,s} + x_1 Đ_{2,s}}{Đ_{12}}} \tag{13}$$

$$L_{12} = \frac{c_2 Đ_{1,s}\dfrac{x_1 Đ_{2,s}}{Đ_{12}}}{1 + \dfrac{x_1 Đ_{2,s} + x_2 Đ_{1,s}}{Đ_{12}}} \tag{14}$$

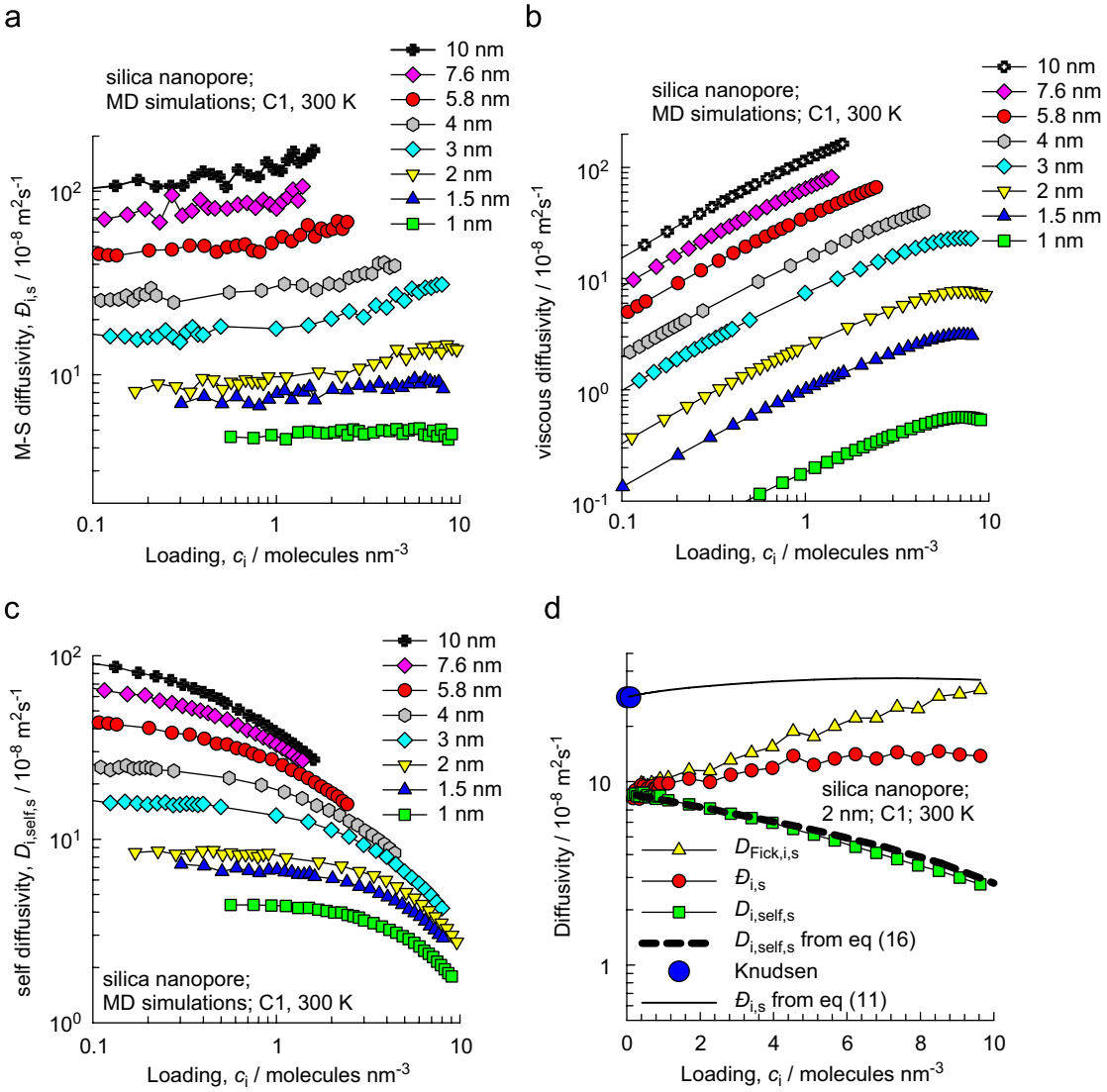

Fig. 2. (a) Maxwell–Stefan, $Đ_{i,s}$, (b) viscous contribution, and (c) self-diffusivities $D_{i,self,s}$ of methane (C1) in silica pores of various diameters at 300 K. (d) Comparison of Fick, Maxwell–Stefan, and self-diffusivities for C1 in 2 nm silica pore at 300 K.

$$L_{21} = \frac{c_1 Đ_{2,s} \dfrac{x_2 Đ_{1,s}}{Đ_{12}}}{1 + \dfrac{x_1 Đ_{2,s} + x_2 Đ_{1,s}}{Đ_{12}}} \tag{15}$$

From a practical viewpoint an important advantage of the M–S equations (3) and (4), over the Onsager formulation (1) is that $Đ_{i,s}$ can be identified with the corresponding *pure* component values. This advantage does not hold for the Onsager formulation, and the diagonal elements L_{ii} cannot be identified with the pure component L_i. Furthermore, the $Đ_{12}$ in the M–S formulation can be identified with the binary M–S diffusivity in the corresponding *fluid* mixture at the same mixture composition and total pore loading. The main objectives of the present communication are to critically examine the general validity of the perceived advantages of the M–S approach. Specifically, we aim to provide answers to the following questions:

(1) Can the $Đ_{i,s}$, defined in Eqs. (3) and (4), be identified with the corresponding values for unary diffusion, defined by Eq. (7)?
(2) How does adsorption at the wall affect $Đ_{i,s}$? Under what conditions can $Đ_{i,s}$ be identified with the Knudsen diffusivity $D_{i,Kn}$?
(3) Can the molecule–molecule interaction parameter, $Đ_{12}$, defined in Eqs. (3) and (4), be identified with the M–S diffusivity in a binary fluid mixture at the same total loading as within the pore?

To obtain answers of reasonably wide applicability we carried out MD simulations of diffusion in a variety of pure components (hydrogen (H_2), argon (Ar), krypton (Kr), methane (C1), ethane (C2), propane (C3), *n*-butane (*n*C4), and *n*-hexane (*n*C6)) and a variety of binary mixtures (C1–H_2, C1–Ar, C1–C2, C1–C3, C1–*n*C4, C1–*n*C6, C2–*n*C4, C2–*n*C6, and *n*C4–*n*C6) in silica pores of diameters 1, 1.5, 2, 3, 4, 5.8, 7.6, and 10 nm. The silica pore structures have been prepared using a method based on Coasne et al. (2008); Fig. 1 shows the landscape for a pore of 3 nm diameter, as an example. In every case the following simulations were conducted: (1) Configurational-bias Monte Carlo (CBMC) simulations in the grand canonical ensemble were performed to determine the pure component adsorption isotherms; these simulations allow calculation of the thermodynamic factors required for the determination of the Fick diffusivities using Eq. (10). (2) MD simulations of the pure component self-diffusivities $D_{i,self,s}$ and M–S diffusivities $Đ_{i,s}$ inside the pores for a range of molecular loadings. (3) MD simulations for diffusion in

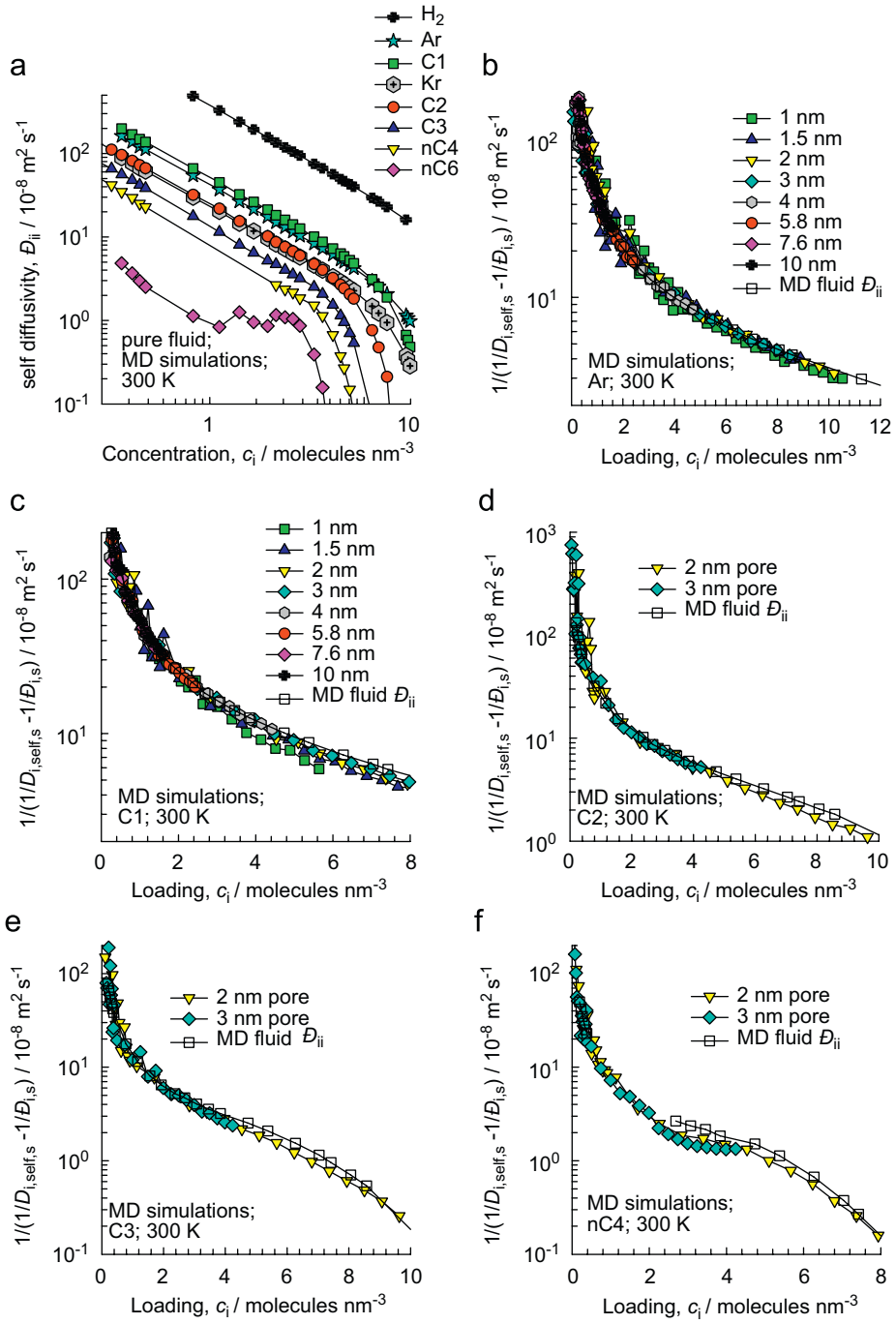

Fig. 3. (a) MD simulations of self-diffusivities $Đ_{ii}$ of H_2, Ar, Kr, C1,C2, C3, *n*C4, and *n*C6 at 300 K as a function of the fluid concentration c_i. Plots of $1/(1/D_{i,self,s} - 1/Đ_{i,s})$ for (b) Ar, (c) C1, (d) C2, (e) C3, and (f) *n*C4, respectively, in the silica pores of different diameters are compared with corresponding data on $Đ_{ii}$.

binary mixtures in the various pores to determine the L_{ij}; with the help of Eqs. (12)–(15) the $Đ_{i,s}$ and $Đ_{12}$ can be backed-out. (4) Determination of pure component self-diffusivities $Đ_{ii}$, along with the M–S diffusivity $Đ_{12}$ and the shear viscosity η_i in *fluids* (i.e. without the constraining influence of the silica pore wall) for varying concentrations. Most of the simulations were performed for $T = 300$ K. Additionally, a few simulations were carried out at 200, 500, 700, and 1200 K to vary the adsorption strength. The entire data base of simulation results is available in the supplementary material accompanying this publication; this material includes details of the MD simulation methodology, description of the force fields used, simulation data (fluid phase $Đ_{ii}$, $Đ_{12}$, and η_i; pure component isotherms; $D_{i,self,s}$; comparison of $Đ_{i,s}$ obtained from both unary and binary systems; comparison of $Đ_{12}$ obtained from diffusion inside pore with that for binary fluid mixtures), snapshots showing the location of molecules inside the pores, detailed derivations of the explicit formulae for backing out the $Đ_{1,s}$, $Đ_{2,s}$, and $Đ_{12}$ from the MD simulations of the L_{ij} for mixture diffusion.

We should emphasize here that though specific silica structures are used in the simulations, along with chosen force fields, the conclusions we draw in relation to the three questions posed above have general validity for diffusion in rough cylindrical pores in the

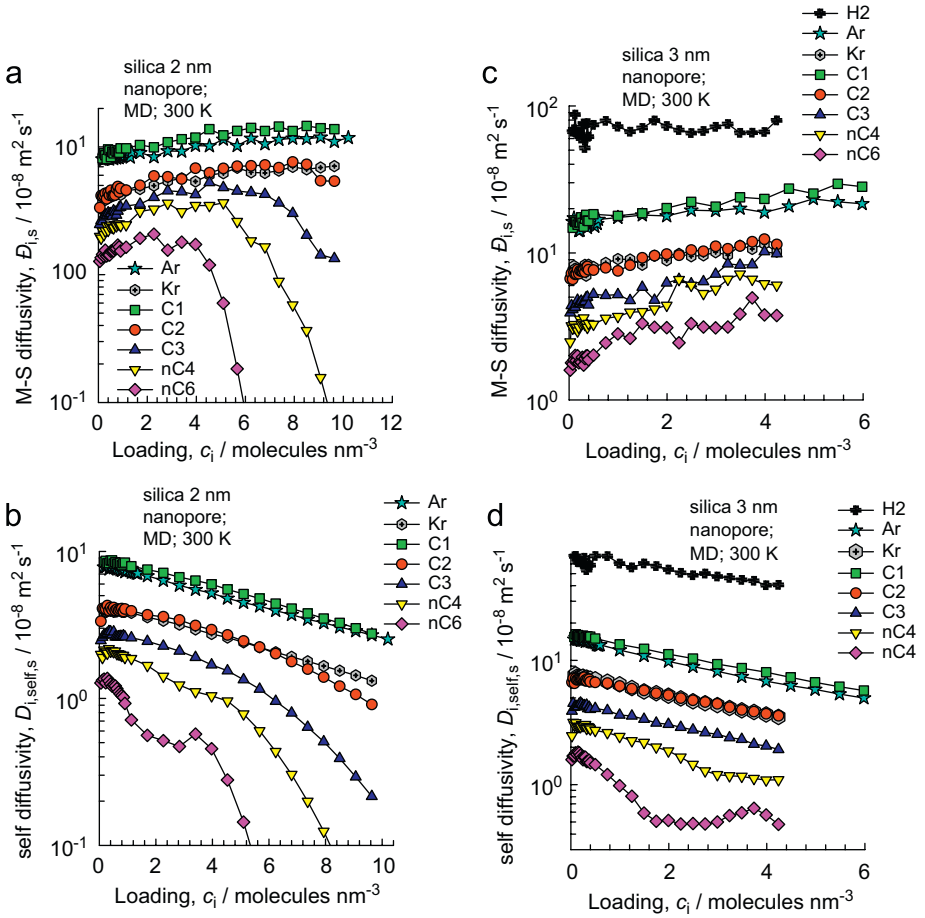

Fig. 4. Maxwell–Stefan diffusivities, $Đ_{i,s}$, and self-diffusivities $D_{i,self,s}$ for H_2, Ar, Kr, C1, C2, C3, *n*C4, and *n*C6 in (a, b) 2 nm and (c, d) 3 nm silica pores at 300 K.

1–10 nm range; this aspect will be further underlined in the ensuing discussions.

2. Pure component diffusion inside pores

Fig. 2a shows the simulation results for $Đ_{i,s}$ of C1 as a function of the loading c_i inside the silica pores of eight different diameters. The c_i is expressed in units of molecules per nm^3 of pore volume; for conversion to engineering units we note that 1 molecule nm^{-3} = 1.66 kmol m^{-3}. The $Đ_{i,s}$ increases with c_i due to the viscous contribution increasing with c_i. Fig. 2b shows the calculations of the viscous contribution for different pore sizes using the second term of the right member of Eq. (11), taking $B_0 = d_{p,eff}^2/32$, along with MD simulated values of the viscosity η_i. These calculations only provide the right *qualitative* trends for the viscous contribution with increasing c_i; for more accurate calculations we need to account for the radial variation of c_i within the pore as in the work of Bhatia et al. (2004) and Bhatia and Nicholson (2006). The self-diffusivity $D_{i,self,s}$ of C1 shows a pronounced decrease with increasing pore loadings c_i; see Fig. 2c. At any finite loading, the self-diffusivity inside the pore is related to the $Đ_{i,s}$ by

$$\frac{1}{D_{i,self,s}} = \frac{1}{Đ_{i,s}} + \frac{1}{Đ_{ii}} \tag{16}$$

where $Đ_{ii}$ is the self-diffusivity in the pure fluid; this diffusivity arises from molecule–molecule interactions. The derivation of Eq. (16) is available in the supplementary material. MD simulations of self-diffusivities in pure fluids, $Đ_{ii}$, of a variety of molecules used in this study are plotted in Fig. 3a as a function of the fluid density c_i. In the low density range, say $c_i < 2$ molecule nm^{-3} the $Đ_{ii}$ decreases *linearly* with increasing c_i; this is the low-density gas limit. For $c_i > 5$ molecule nm^{-3} we have high density fluid characteristics with a much sharper decline in $Đ_{ii}$ with increasing c_i. Eq. (16) implies that the parameter $1/(1/D_{i,self,s} - 1/Đ_{i,s})$ should be (a) independent of the pore diameter, and (b) equal the self-diffusivity of pure component i in the fluid phase at the same loading as within the pore. Figs. 3b–f present the $1/(1/D_{i,self,s} - 1/Đ_{i,s})$ data for Ar, C1, C2, C3, and *n*C4, respectively, in silica pores of different sizes; this data confirms that this parameter is pore size independent for every molecule, and in good agreement with the corresponding value of $Đ_{ii}$ determined from independent fluid self-diffusion simulations. For estimation purposes, the self-diffusivity inside the pore $D_{i,self,s}$ can be *calculated* using $Đ_{i,s}$ and fluid phase $Đ_{ii}$ (from Fig. 3a) as data inputs; these calculations are shown by the dashed line in Fig. 2c for the 2 nm pore.

From the simulated adsorption isotherms the thermodynamic factor Γ_i can be calculated and the Fick diffusivity determined using Eq. (10). The $D_{Fick,i,s}$ data for the 2 nm pore are plotted in Fig. 2c. In the limit of zero loading inside the pores molecule–molecule interactions and viscous contributions are both of negligible importance, and the self, M–S, and Fick diffusivities converge to the same value $Đ_{i,s}(0)$. Results analogous to that in Fig. 2c are obtained for C1 in all other pore diameters and also for other guest–pore combinations investigated; see supplementary material.

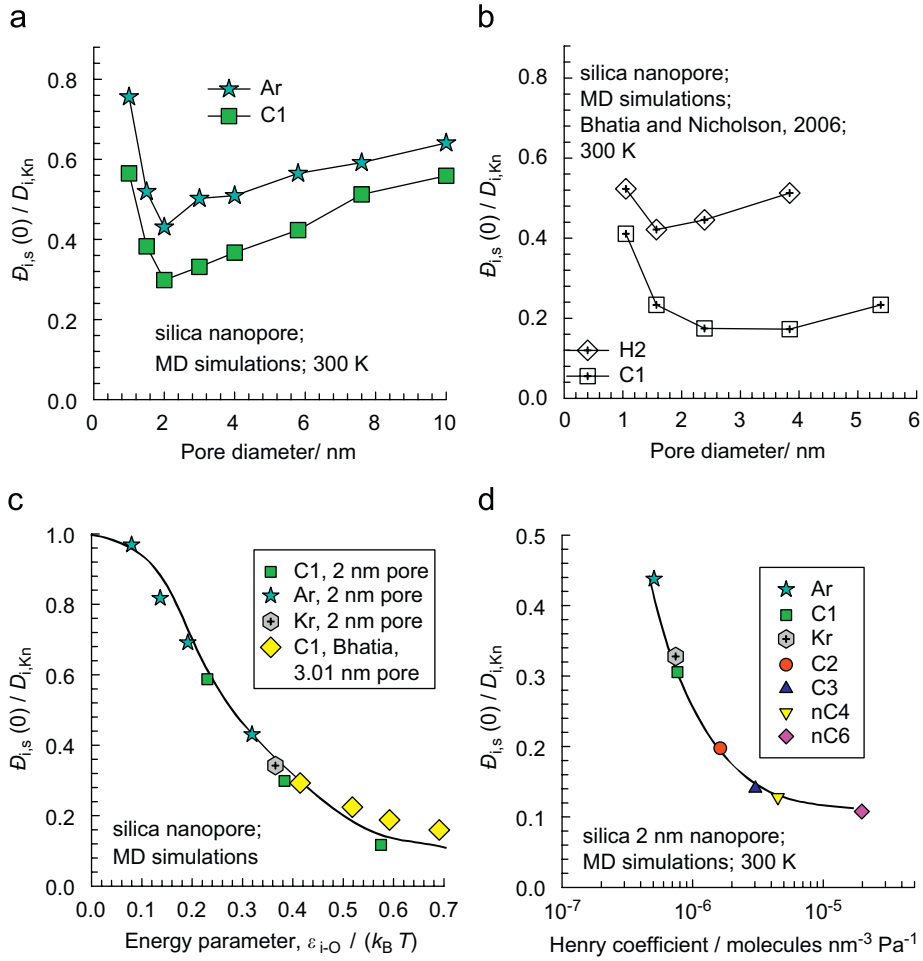

Fig. 5. (a) MD data for the ratio of zero-loading Maxwell–Stefan diffusivity to Knudsen diffusivity, $Đ_{i,s}(0)/D_{i,Kn}$ for diffusion of C1 and Ar as a function of the pore diameter. (b) MD data for $Đ_{i,s}(0)/D_{i,Kn}$ of Bhatia (2006) for diffusion of C1 and H_2 at 300 K as a function of the pore diameter. (c) MD data for $Đ_{i,s}(0)/D_{i,Kn}$ as a function of the energy parameter ε_{i-O}/k_BT for diffusion of C1, Ar and Kr at various temperatures in 2 nm pore. The values of ε_{i-O}/k_B are 115, 95.6, and 109.6 K for C1, Ar, and Kr. Also shown are the data of Bhatia et al. (2004) for C1 at various temperatures in a 3.01 nm pore (the value of ε_{i-O}/k_B is taken to be 207 K, as used in their simulations). (d) MD data for $Đ_{i,s}(0)/D_{i,Kn}$ as a function of the Henry coefficient for diffusion of various molecules in 2 nm pore.

For a pore size of 2 nm, the $Đ_{i,s}$ and $D_{i,self,s}$ data for Ar, Kr, C1, C2, C3, *n*C4, and *n*C6 are shown in Figs. 4a and b. We note that for longer *n*-alkanes *n*C4 and *n*C6 that have significantly higher adsorption strengths, the $Đ_{i,s}$ increases with pore loadings, reaches a maximum and then decreases as pore saturation is approached. The loading dependence of $Đ_{i,s}$ for *n*C4 and *n*C6 are similar to that observed in zeolites and metal–organic frameworks (Chmelik et al., 2009; Krishna and van Baten, 2008a,b), and is characteristic of diffusion of adsorbed molecules, i.e. surface diffusion. Put another way, with increased adsorption strength the contribution of surface diffusion to $Đ_{i,s}$ becomes increasingly important. Figs. 4c, and d present the corresponding $Đ_{i,s}$ and $D_{i,self,s}$ data for H_2, Ar, C1, C2, C3, *n*C4, and *n*C6 in a 3 nm pore.

We now try to obtain an answer to the second question posed in the Introduction. When the mean free path of the molecule is significantly larger than the pore diameter, molecule–wall surface collisions are predominant and Knudsen diffusion is normally assumed to hold, with the diffusivity given by Albo et al. (2006), Arya et al. (2003a,b), Bhatia (2006), Bhatia and Nicholson (2006), and Zschiegner et al. (2007)

$$D_{i,Kn} = \frac{d_{p,eff}}{3}\sqrt{\frac{8RT}{\pi M_i}} \tag{17}$$

Following Bhatia and Nicholson (2006) we define the effective pore diameter, $d_{p,eff}$ by

$$d_{p,eff} = d_p - 0.92(\sigma_i + \sigma_O) \tag{18}$$

where d_p is the centre-to-centre distance between the O atoms on the surface of the pore, σ_i is the Lennard–Jones size parameter for molecule–molecule interaction, and σ_O is the Lennard–Jones size parameter for O atoms in the silica structure (the Lennard–Jones parameters are tabulated in the supplementary material). The correction to the pore diameter is especially relevant for pores smaller than about 3 nm. Eq. (17) holds provided the molecules suffer *diffuse* reflections on collision with the wall surface. Diffuse reflections usually result from rough surfaces (Arya et al., 2003b; Bhatia, 2006; Bhatia et al., 2004; Bhatia and Nicholson, 2006; Zschiegner et al., 2007), as is the case with silica pores. Carbon nanotubes, in contrast, have smooth walls and the reflections are *specular*; this results in diffusivity values about 2–3 orders of magnitude higher than those predicted by Eq. (17) (Bhatia, 2006; Jakobtorweihen et al., 2007). In deriving Eq. (17) it is also assumed that the molecules do not adsorb, or stick, to the walls on collision. Furthermore, the Knudsen formula (17) implies low pore concentrations, $c_i \to 0$, with no molecule–molecule interactions.

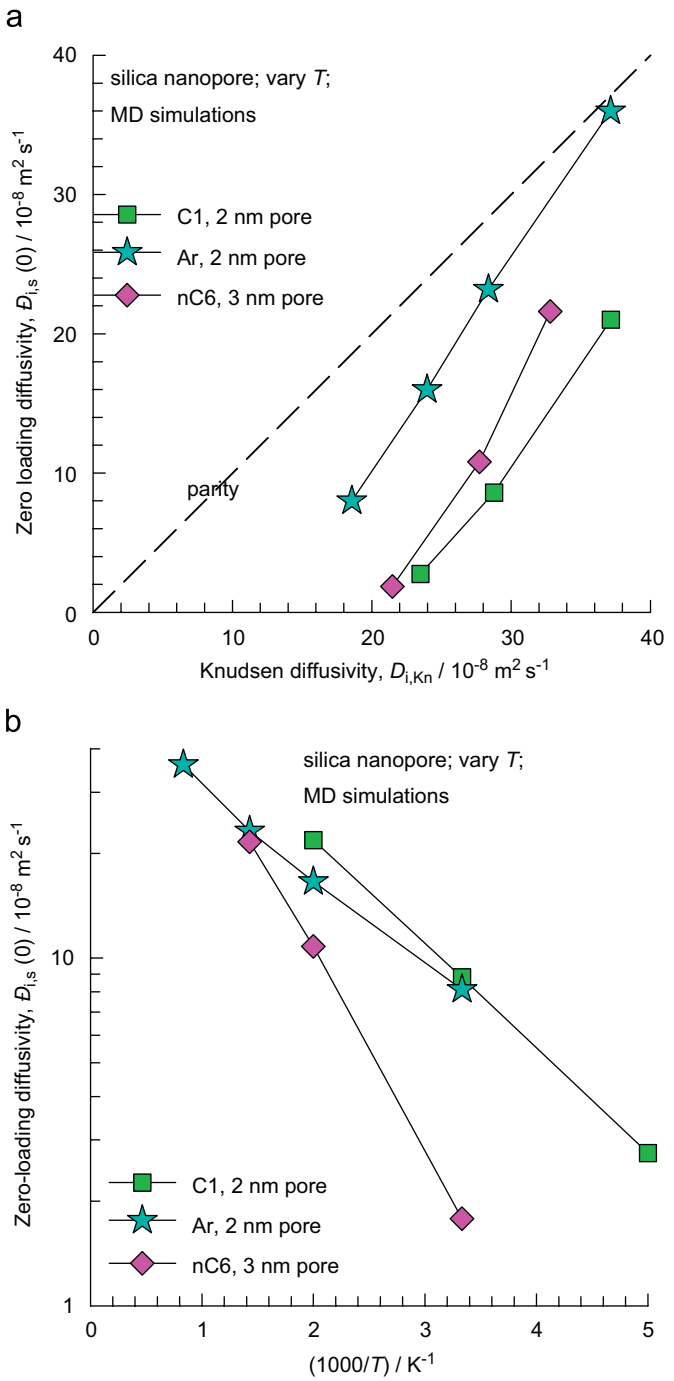

Fig. 6. MD data on $Đ_{i,s}(0)$ for C1 and Ar in a 2 nm pore, and *n*C6 in 3 nm pore at a variety of temperatures plotted against the (a) Knudsen diffusivity $D_{i,Kn}$ and (b) inverse temperature.

From Eq. (11), we note that in the limit of low pore loadings, $c_i \to 0$, molecule–molecule interactions will be negligible, the viscous flow contribution is of negligible importance and the $Đ_{i,s}(0)$ should approach $D_{i,Kn}$; we now address the question of whether $Đ_{i,s}(0)$ can indeed be identified with the classical formula for Knudsen diffusivity.

For diffusion of methane in the 2 nm pore, the $D_{i,Kn}$ is also plotted in Fig. 2c (large blue circle), along with the calculations of $Đ_{i,s}$ using the commonly used formula (11), that includes the viscous contribution. In the calculations for Eq. (11) we use MD simulated values of the viscosity η_i taking $B_0 = d_{p,eff}^2/32$. The Knudsen diffusivity value calculated from Eq. (17) is significantly higher than the $Đ_{i,s}(0)$. Similar results are obtained for other pores; data on $Đ_{i,s}(0)/D_{i,Kn}$ at 300 K for a variety of pore sizes for C1 and for Ar are plotted in Fig. 5a against d_p. Both data sets are consistently below unity. Interestingly, the $Đ_{i,s}(0)$ for C1 deviate to a greater extent from $D_{i,Kn}$ than the Ar data. The $Đ_{i,s}(0)/D_{i,Kn}$ values for C1 are lower than that for Ar because C1 has a higher adsorption strength than Ar; we return to this point in later discussions. For both data sets in Fig. 5a the ratio $Đ_{i,s}(0)/D_{i,Kn}$ appears to approach unity as the pore diameter is increased beyond 10 nm.

From the MD simulation results of Bhatia and Nicholson (2006) for diffusion of C1 and H_2 in a variety of pores at 300 K, we constructed a similar plot; see Fig. 5b. We note that the $Đ_{i,s}(0)/D_{i,Kn}$ values of both C1 and H_2 lie significantly below unity, signifying departures from the Knudsen formula. Again, the data of the more strongly adsorbed C1 deviate to a greater extent than the corresponding results for the weakly adsorbed H_2. Comparison of our results for C1 (Fig. 5a) with those of Bhatia and Nicholson (2006) in Fig. 5b shows that our values of $Đ_{i,s}(0)/D_{i,Kn}$ for a given pore size tend to be higher. The reason is that the Lennard–Jones energy parameter for interaction of C1 with the O atoms, ε_{i-O}/k_B, in our simulations is taken to be 115 K, in line with the force field for zeolites (Dubbeldam et al., 2004); the corresponding value used by Bhatia and Nicholson (2006) is significantly higher, and equals 207 K. The adsorption strength is dictated by ε_{i-O}/k_BT; consequently, the adsorption strength of C1 is much stronger in the Bhatia simulations when compared to ours, resulting in lower $Đ_{i,s}(0)/D_{i,Kn}$. We stress this point in Fig. 5c by plotting our results for $Đ_{i,s}(0)/D_{i,Kn}$ against ε_{i-O}/k_BT for C1, Ar, Kr at a variety of temperatures (200, 300, 500, 700, and 1200 K) in a 2 nm pore. The simulation results of Bhatia et al. (2004) for C1 at a variety of temperatures in a 3.01 nm pore are also plotted in Fig. 5c. The two different sets of results, with two different ε_{i-O}/k_BT parameter values, produce similar results for $Đ_{i,s}(0)/D_{i,Kn}$, suggesting that the plot in Fig. 5c has, perhaps, a generic validity. We note that for Ar at 1200 K in the 2 nm pore, $Đ_{i,s}(0)/D_{i,Kn} \approx 1$. On the basis of this plot we can conclude that only for poorly adsorbing molecules at high T is the approximation $Đ_{i,s}(0) \approx D_{i,Kn}$ of reasonable accuracy. We note that the $Đ_{i,s}(0)/D_{i,Kn}$ tends to approach an asymptotic value of about 0.1 for low values of T. The practical consequence is that the adoption of the Knudsen formula (17) for diffusion of say *n*C6 in silica pores will lead to 10-fold overestimation of the fluxes. The fundamental reasons for the deviation $Đ_{i,s}(0)$ from the Knudsen formula in cases where there is significant Lennard–Jones interaction with wall is to be found in the model of Bhatia and Nicholson (2006) who assume oscillatory motion of molecules within pores in the 1–10 nm range after suffering diffuse reflections from the pore walls; this aspect needs further detailed investigation. Such oscillatory motion can also been discerned on viewing animations of MD simulations, that is available on our web-site (van Baten and Krishna, 2008).

For molecules with more than one pseudo-atom, such as *n*-alkanes, it is difficult to plot the results in the same manner as in Fig. 5c because ε/k_B for the terminal CH_3 groups are not the same as for intermediate CH_2 groups (Dubbeldam et al., 2004). For this reason, for *n*-alkanes, we chose to plot the $Đ_{i,s}(0)/D_{i,Kn}$ for various molecules against the Henry coefficient for adsorption; see Fig. 5d. The Henry coefficients were determined from CBMC simulations of the adsorption isotherms. It is interesting to note that $Đ_{i,s}(0)/D_{i,Kn}$ approaches an asymptotic value of about 0.1 for high values of the Henry coefficient, consonant with the results in Fig. 5c.

With increased adsorption at the pore walls, the importance of surface diffusion increases. Surface diffusion is an activated process (Krishna, 1990) and the temperature dependence on the surface diffusivity can be expected to follow an Arrhenius behaviour rather than the $\sqrt{T}$ characteristic of Knudsen diffusion. Data on $Đ_{i,s}(0)$ for

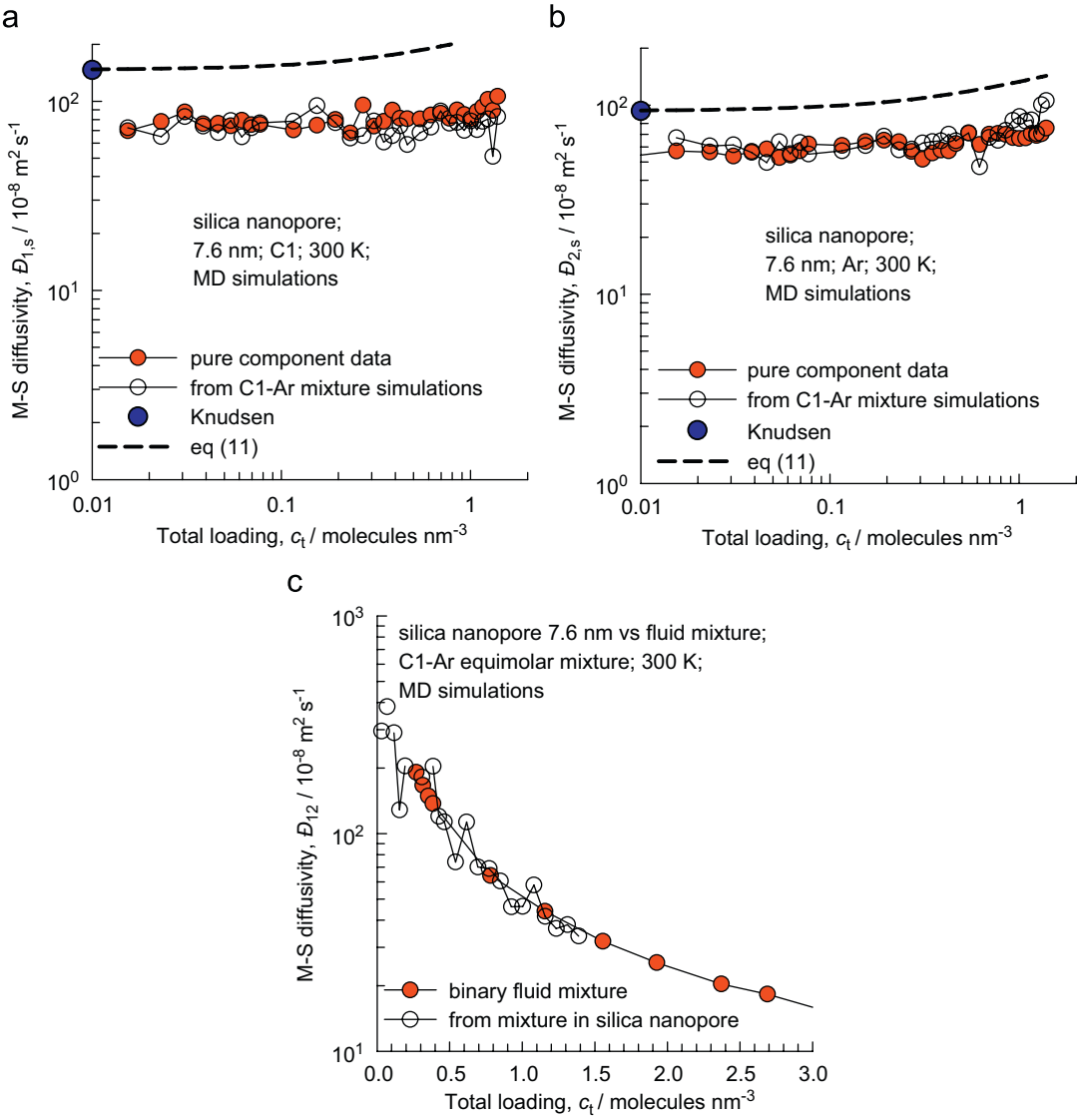

Fig. 7. The Maxwell–Stefan diffusivities (a) $Đ_{1,s}$, (b) $Đ_{2,s}$, and (c) $Đ_{12}$ for diffusion of equimolar ($c_1 = c_2$) binary mixture (open symbols) of C1 (1) and Ar (2) in 7.6 nm pore at 300 K as a function of the total fluid concentration, c_t. The procedure for backing out these parameters from binary mixture simulations are discussed in detail in the supplementary material. Also shown in (a) and (b) are the corresponding pure component $Đ_{i,s}$ (filled symbols), along with the calculations using Eq. (11). The $Đ_{12}$ for binary fluid C1–Ar mixture diffusion, obtained from independent MD simulations, is also presented in (c).

C1, Ar, and *n*C6 obtained at different temperatures in 2 and 3 nm pores are plotted against the calculated values of $D_{i,Kn}$ in Fig. 6a; we note that the $Đ_{i,s}(0)$ data sets are not parallel to the parity line for all three molecules; this signifies that the $Đ_{i,s}(0)$ does not follow a $\sqrt{T}$ dependence; the T-dependence of $Đ_{i,s}(0)$ is closer to Arrhenius behaviour, as is evidenced by the Arrhenius plots in Fig. 6b. The results in Fig. 6b are in agreement with earlier work of Bhatia and Nicholson (2003). A further point to note is that for Ar at 1200 K in the 2 nm pore, $Đ_{i,s}(0) \approx D_{i,Kn}$.

From Figs. 5 and 6 we can broadly conclude for any molecule that $Đ_{i,s}(0)$ tends to approach the classical Knudsen value $D_{i,Kn}$ with increasing pore diameter and/or increasing temperature. Our conclusions are in line with the work of Albo et al. (2006) who report MD simulation results of pores in the 10–150 nm range. Even though Figs. 5 and 6 provide a good indication of the degree of departure of the $Đ_{i,s}(0)$ from $D_{i,Kn}$, *a priori* estimation procedure for $Đ_{i,s}$ of general validity for all types of molecules have yet to be developed. In this connection the theory of Bhatia et al. (2004) and Bhatia and Nicholson (2006, 2008) provides a good starting point, but needs to be tested for molecules other than the simple molecules such as C1 and H_2 used in their studies.

In the commonly used DGM, Knudsen and surface diffusion are treated as combinatorial phenomena (Mason and Malinauskas, 1983). We believe this approach to be fundamentally flawed because dynamic adsorption–desorption processes at the wall have a significant influence on the "Knudsen" contribution to the fluxes. For molecules with strong adsorption strength the actual "Knudsen" contribution could be a factor 10 lower than that anticipated by the classical Knudsen formula (17) as is implied in the results presented in Fig. 5. Adding a surface diffusion contribution on the right-hand side of Eq. (17) exacerbates this problem. Kerkhof and Geboers (2005a,b) and Young and Todd (2005) underline other flaws in the DGM formulation but ignore adsorption–desorption at the pore walls in their suggested alternative models.

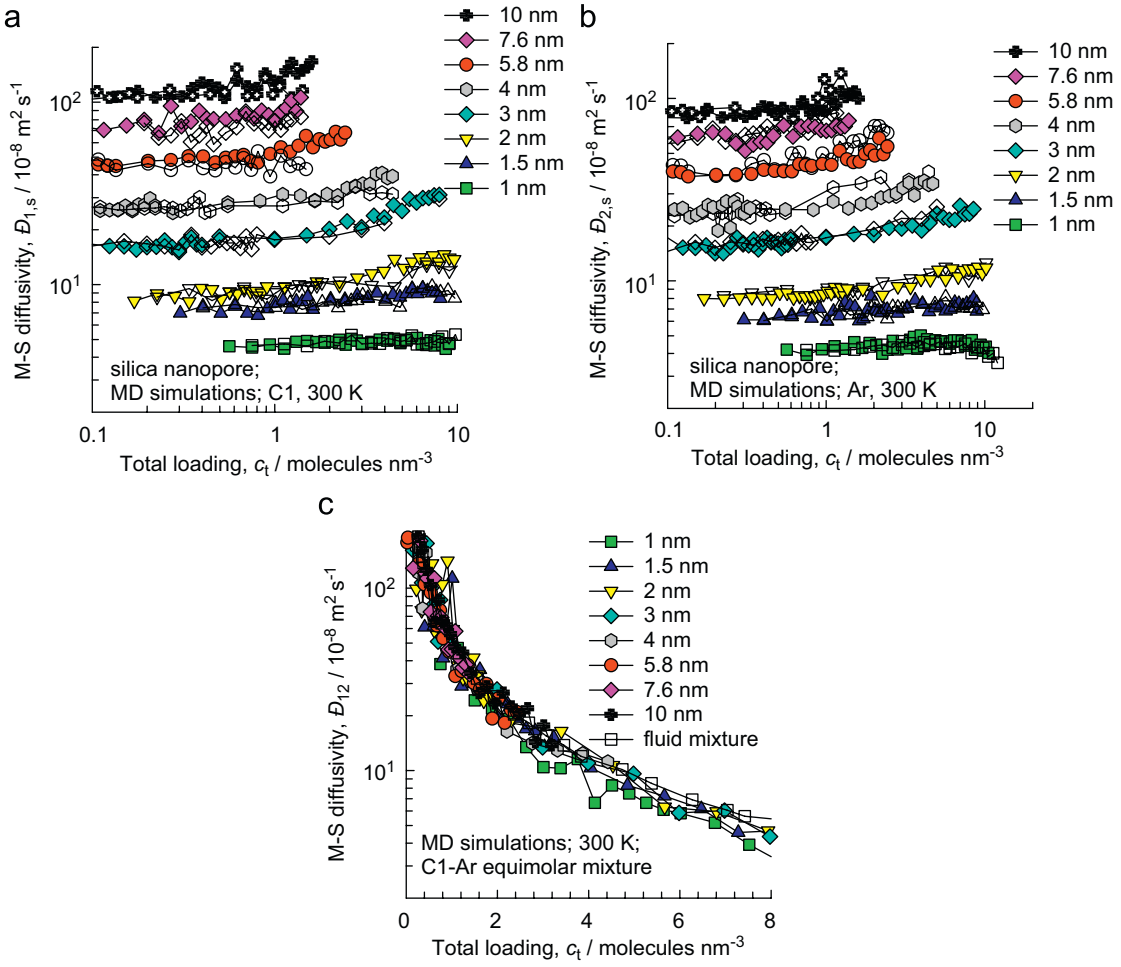

Fig. 8. The Maxwell–Stefan parameters (a) $Đ_{1,s}$, (b) $Đ_{2,s}$, and (c) $Đ_{12}$ for diffusion of equimolar ($c_1 = c_2$) binary mixture (open symbols) of C1 (1) and Ar (2) in eight different pores at 300 K. Also shown in (a) and (b) are the corresponding pure component $Đ_{i,s}$ (filled symbols). The $Đ_{12}$ data for binary fluid C1–Ar mixture diffusion, obtained from independent MD simulations, is also presented in (c).

3. Binary mixture diffusion inside silica pores

Consider diffusion of an equimolar ($c_1 = c_2$) binary mixture of C1 (1) and Ar (2) in the 7.6 nm pore at a temperature of 300 K. The values of $Đ_{1,s}$, $Đ_{2,s}$, and $Đ_{12}$ determined from MD mixture simulations are presented in Figs. 7a–c, respectively, as a function of the total mixture loading $c_t = c_1 + c_2$. Also shown in (a) and (b) are the $Đ_{i,s}$ for diffusion of pure component C1 and Ar, as function of the corresponding c_i. We note a good agreement between the $Đ_{i,s}$ obtained from mixture simulations with the corresponding pure component values. Eq. (11) is seen to significantly over-predict the $Đ_{i,s}$ values for both components, but the c_i dependence is qualitatively correct. The $Đ_{12}$ for mixture diffusion inside the 2 nm pore is also in excellent agreement with the M–S diffusivity for the equimolar binary fluid mixture, determined by *independent* simulations using the method described in earlier publications (Krishna and van Baten, 2005, 2006a,b).

The results presented in Fig. 7 are typical of C1–Ar mixtures in all other pore diameters investigated in this study (see supplementary material for plots analogous to Fig. 7). A summary of the C1–Ar mixture diffusion simulation results in eight different pore diameters is given in Fig. 8. In Fig. 8a the $Đ_{1,s}$ of C1 (component 1) in C1–Ar mixtures (denoted by open symbols) are compared with the corresponding pure component value (shown by the filled symbols) in pores of various diameters. There is good agreement between the two sets of results, when compared at the same total loading within the pore. Fig. 8b shows the analogous set of results for the $Đ_{1,s}$ of Ar (component 2) in C1–Ar mixtures (open symbols) with pure component values (filled symbols) in various pores; again good agreement between the two sets is obtained. Furthermore, the M–S formulation implies that the parameter $Đ_{12}$, quantifying molecule–molecule interactions should not depend on the pore size; this is confirmed by the simulation results for $Đ_{12}$ in C1–Ar mixture in eight different pores (filled symbols); see Fig. 8c. Also, shown in Fig. 8c is the $Đ_{12}$ obtained from MD simulations in an equimolar *fluid* mixture (open symbols); there is good agreement between the different sets of results.

A further implication of the M–S equations is that the $Đ_{i,s}$ of any species i in a binary mixture should be independent of the partner molecule in that mixture. As a test of this premise, Fig. 9a compares the M–S diffusivity of pure component C1 in a 3 nm pore with that in equimolar binary C1–H_2, C1–Ar, C1–C2, C1–C3, C1–*n*C4, and C1–*n*C6 mixtures in the same pore at the same temperature. The good agreement between the different sets of simulation results underlines the efficacy of the M–S formulation in predicting mixture diffusion on the basis of pure component diffusivity data. The remarkable thing to note about the results in Fig. 9a is that the extremely wide variation in the molar masses of the partner molecules, ranging from 0.002 mol kg^{-1} for H_2 to 0.086 mol kg^{-1} for *n*C6, the M–S diffusivity of pure component C1 is practically unaffected for the range of

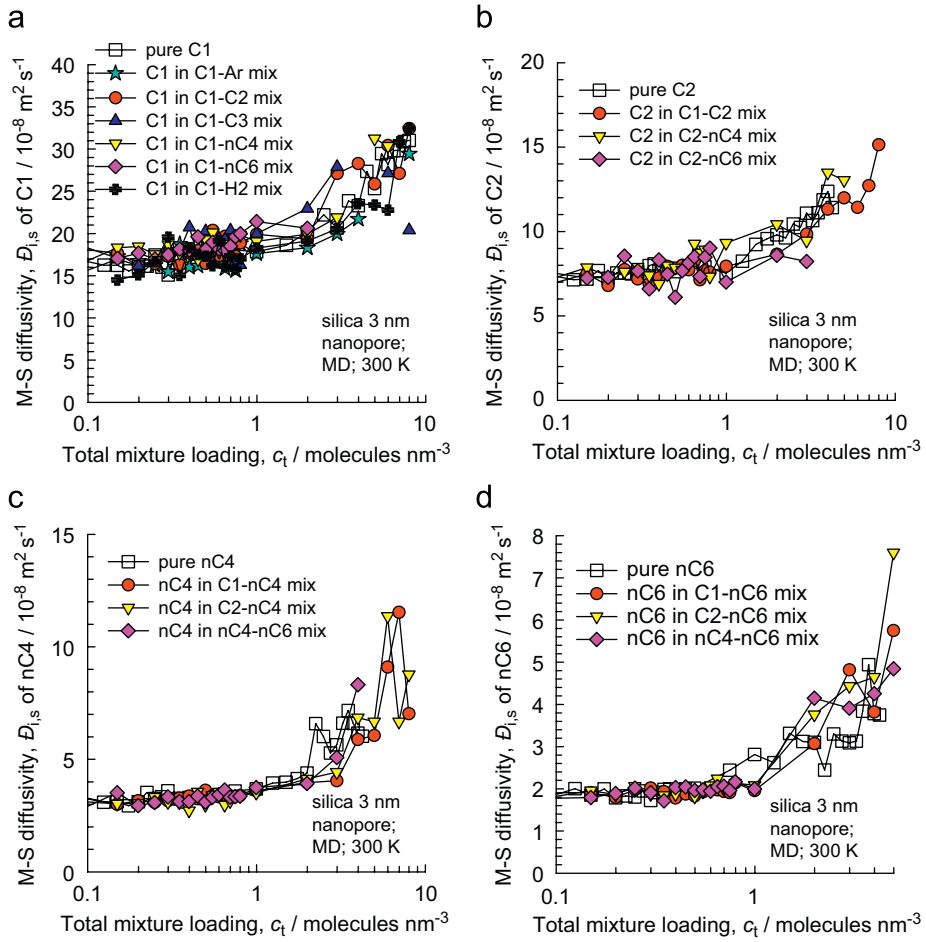

Fig. 9. The Maxwell–Stefan diffusivity $Đ_{i,s}$ of pure component (a) C1, (b) C2, (c) *n*C4, and (d) *n*C6 in 3 nm pore at 300 K compared with the corresponding values in equimolar binary C1–H_2, C1–Ar, C1–C2, C1–C3, C1–*n*C4, C1–*n*C6, C2–*n*C4, C2–*n*C6, and *n*C4–*n*C6 mixtures in 3 nm pore.

loadings considered here. Analogous results for C2, *n*C4, and *n*C6 are obtained in for the 3 nm pore; see Figs. 9b–d.

The precise estimation of $Đ_{i,s}$ for pure component diffusion is, however, the key to good estimation of mixture diffusion characteristics. In practical applications, such as membrane permeation, unary permeation experiments are performed to determine the permeances (Higgins et al., 2008). From the data on the permeances as a function of the upstream pressures, the $Đ_{i,s}$ can be determined using information on the adsorption isotherm. There is no need to determine the viscous permeability B_0 as the viscous contributions are subsumed into the $Đ_{i,s}$. These $Đ_{i,s}$ are then to be used to calculate the fluxes in binary mixtures by solving Eqs. (3) and (4). For applications in practice, Eqs. (12)–(15) can be used to estimate the L_{ij} from information on the pure component $Đ_{i,s}$, along with the binary $Đ_{12}$ in the *fluid* mixture. We illustrate the application by considering equimolar C1–H_2 and C1–*n*C4 mixtures in a 3 nm pore. These two mixtures are specifically chosen to represent extremes in the mixture diffusion characteristics. In the C1–H_2 mixture, C1 is more strongly adsorbed but is tardier, and H_2 is poorly adsorbed but is more mobile. In the C1–*n*C4 mixture, C1 is the component that is relatively less strongly adsorbed but is more mobile, and *n*C4 is much more strongly adsorbed but is much tardier. The pure component $Đ_{i,s}$, along with "empirical" fits of this data, is shown in Fig. 10a. The data on $Đ_{12}$ for equimolar C1–H_2 and C1–*n*C4 *fluid* mixtures are obtained from the MD simulation results; see Fig. 10b. The calculations of L_{ij} using Eqs. (12)–(14), using the fitted $Đ_{i,s}$, estimated at the total mixture loading, c_t, are in good agreement with the MD simulated values; see Figs. 10c and d.

The expressions for the self-diffusivities in a binary mixture inside a pore can be derived (see supplementary material) as follows:

$$\frac{1}{D_{1,self,s}} = \frac{1}{Đ_{1,s}} + \frac{x_1}{Đ_{11}} + \frac{x_2}{Đ_{12}} \tag{19}$$

$$\frac{1}{D_{2,self,s}} = \frac{1}{Đ_{2,s}} + \frac{x_2}{Đ_{22}} + \frac{x_1}{Đ_{12}} \tag{20}$$

The predictions of $D_{i,self}$ for both components using the fitted values of $Đ_{i,s}$ along with the $Đ_{ii}$ and $Đ_{12}$ from *binary fluid mixture* MD simulations are shown in Figs. 10e and f. The predictions are in good agreement with the M–S model equations.

The $Đ_{12}$ for fluid mixtures can be estimated from component self-diffusivities $Đ_{ii}$ using the Darken relations (Krishna and van Baten, 2005).

$$Đ_{12} = x_2 Đ_{11} + x_1 Đ_{22} \tag{21}$$

Procedures for estimation of the pure component self-diffusivities, $Đ_{ii}$, for Lennard–Jones fluids are discussed by Yu and Gao (2000). To illustrate the accuracy of Eq. (21), Fig. 11 shows MD simulations of self-diffusivities, $Đ_{ii}$, of C1 and C3, along with the $Đ_{12}$ for equimolar binary C1–C3 fluid mixture as a function of the

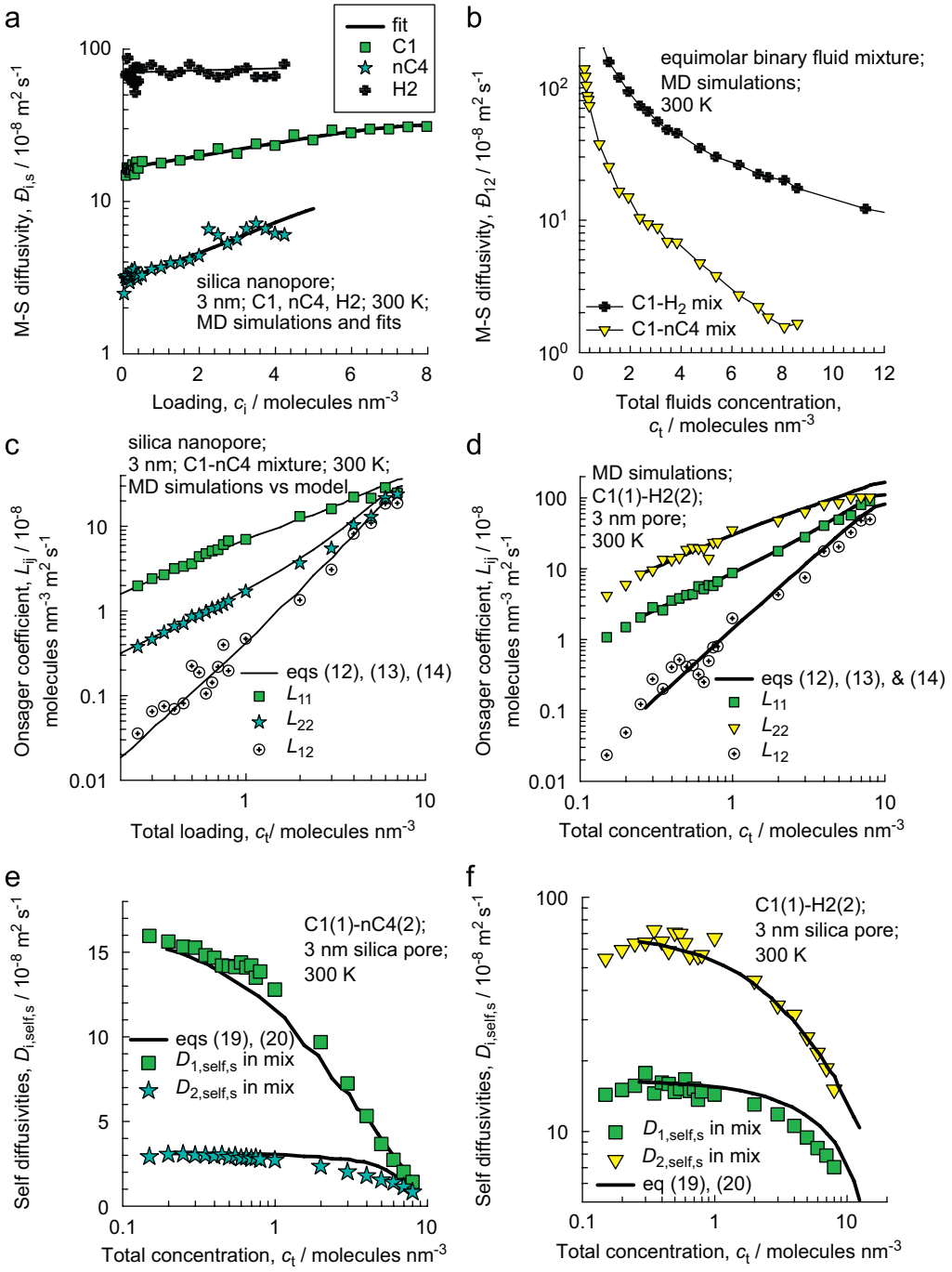

Fig. 10. (a) The MD simulated Maxwell–Stefan diffusivity $Đ_{i,s}$ of pure component C1, *n*C4, and H_2 (symbols) in 3 nm pore at 300 K, along with fits (continuous solid lines). (b) MD simulated Maxwell–Stefan diffusivity $Đ_{12}$ of binary *fluid* mixtures C1–H_2, and C1–*n*C4 at 300 K. MD simulated values of the Onsager coefficients L_{ij} (symbols), for (c) C1–*n*C4 and (d) C1–H_2 equimolar mixtures in 3 nm pore, are compared with calculations (continuous solid lines) following Eqs. (12)–(14). MD simulated values of the self-diffusivities $Đ_{i,self,s}$ (symbols), for (e) C1–*n*C4 and (f) C1–H_2 equimolar mixtures in 3 nm pore, are compared with calculations (continuous solid lines) following Eqs. (19), and (20).

total fluid concentration, c_t. The calculations of $Đ_{12}$ according to Eq. (21), shown by the continuous solid line, are in excellent agreement with the MD simulated values of $Đ_{12}$ for an equimolar fluid mixture over the entire range of concentrations. Furthermore, Eq. (21) is also in good agreement with the data for $Đ_{12}$ backed out from mixture diffusion inside a 3 nm pore.

The identification of the $Đ_{12}$ parameter in the M–S equations with molecule–molecule interactions in the fluid phase is an important advantage of the M–S formulation. In sharp contrast the cross-coefficient L_{12} in the Onsager formulation cannot be identified solely with molecule–molecule interactions as is evident by close examination of Eq. (14). The L_{12} is also influenced by molecule–wall interactions.

4. Conclusions

On the basis of a large data set of MD simulations of unary and binary diffusion of a variety guest species in silica nanopores of eight

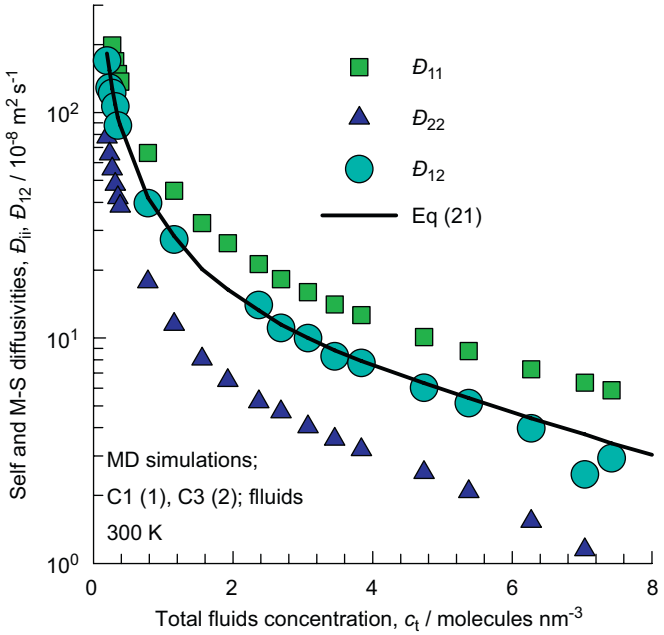

Fig. 11. MD simulations of self-diffusivities, $Đ_{i,i}$, of C1 and C3, along with the $Đ_{12}$ for equimolar binary C1–C3 fluid mixture as a function of the total fluid concentration, c_t. The calculations of $Đ_{12}$ according to Eq. (21) are shown by the continuous solid line.

different diameters, answers to the three questions posed in the Introduction can be obtained.

(1) For all systems investigated the $Đ_{i,s}$ describing binary mixture diffusion, defined in Eqs. (3) and (4), can be identified with the corresponding values for unary diffusion, defined by Eq. (7). The equality holds provided the pure component values are determined at the total mixture loading, c_t. For molecules that adsorb strongly at the pore walls, the $Đ_{i,s}$ tends to increase with c_i, reach a maximum and then decrease to near-zero values as pore saturation is attained. The assumption of loading-independent $Đ_{i,s}$ is not a good one for such molecules, except perhaps for low loadings. Further work is required to provide *a priori* estimations of $Đ_{i,s}$ as a function of the pore loadings. For this purpose, it will be necessary to quantify the viscous flow and surface diffusion contributions in more detail.

(2) For rough surface walls, as is typical of silica nanopores, the $Đ_{i,s}(0)$ is lower than the Knudsen diffusivity value $D_{i,Kn}$ calculated using Eq. (17). The stronger the adsorption characteristics, the lower is the value of $Đ_{i,s}(0)/D_{i,Kn}$. For any given molecule, our MD simulation results show that $Đ_{i,s}(0)$ tends to approach the classical Knudsen value $D_{i,Kn}$ with increasing pore diameter and/or increasing temperature; these results complement the work of Albo et al. (2006) who investigated pore sizes in the 10–150 nm range. For engineering purposes the ratio $Đ_{i,s}(0)/D_{i,Kn}$ can be estimated using the trends in Figs. 5 and 6. At any given pore loading, c_i, the $Đ_{i,s}$ can be estimated from $Đ_{i,s} = Đ_{i,s}(0) + B_0 c_i k_B T/\eta_i$, with the added cautionary note that for more reliable estimation of the viscous contribution we need to account for radial distribution of c_i within the pore following the work of Bhatia and Nicholson (2006).

(3) The molecule–molecule interaction parameter, $Đ_{12}$, defined in Eqs. (3) and (4), can be identified with the M–S diffusivity in the binary fluid mixture at the same loading as within the pore. For practical purposes $Đ_{12}$ can be estimated from pure component transport properties (Krishna and van Baten, 2005).

Notation

B_0	permeability of pore, m^2
c_i	concentration of species i, molecule m^{-3}
c_t	total concentration in mixture, molecule m^{-3}
d_p	pore diameter, m
$d_{p,eff}$	effective pore diameter defined by Eq. (18), m
$Đ_{Fick,i,s}$	Fick diffusivity for unary diffusion inside pore, $m^2\ s^{-1}$
$D_{i,Kn}$	Knudsen diffusivity of species i, $m^2\ s^{-1}$
$Đ_{i,s}$	Maxwell–Stefan diffusivity for species–pore wall interaction, $m^2\ s^{-1}$
$Đ_{i,s}(0)$	zero-loading M–S diffusivity for species–pore wall interaction, $m^2\ s^{-1}$
$D_{i,self,s}$	self-diffusivity of species i within pore, $m^2\ s^{-1}$
$Đ_{ii}$	self-diffusivity of species i in fluid phase, $m^2\ s^{-1}$
$Đ_{12}$	Maxwell–Stefan diffusivity for species–species interaction, $m^2\ s^{-1}$
f_i	fugacity of species i, Pa
k_B	Boltzmann constant, 1.38×10^{-23} J molecule^{-1} K^{-1}
L_i	Onsager coefficients for pure component i, molecule $nm^{-3}\ m^2\ s^{-1}$
L_{ij}	Onsager coefficients for mixture diffusion, molecule $nm^{-3}\ m^2\ s^{-1}$
M_i	molar mass of species i, kg mol^{-1}
N_i	molecular flux of species i, molecule $m^{-2}\ s^{-1}$
R	gas constant, 8.314 J mol^{-1} K^{-1}
T	absolute temperature, K
x_i	mole fraction of species i based on loading within pore, dimensionless
x	spatial distance, m

Greek letters

Γ_i	thermodynamic factor for unary diffusion, dimensionless
ε/k_B	Lennard–Jones energy parameter, K
η_i	viscosity of species i, Pa s
μ_i	molar chemical potential, J mol^{-1}
σ	Lennard–Jones size parameter, m

Subscripts

eff	effective pore diameter
i	referring to component i
Kn	referring to Knudsen
O	referring to O atoms in silica
p	referring to pore
s	referring to surface, or wall of pore
t	referring to total mixture

Acknowledgements

R.K. acknowledges the grant of a TOP subsidy from the Netherlands Foundation for Fundamental Research (NWO-CW) for intensification of reactors.

Appendix A. Supplementary data

Supplementary data associated with this article can be found in the online version at doi:10.1016/j.ces.2008.10.045.

References

Albo, S.E., Broadbelt, L.J., Snurr, R.Q., 2006. Multiscale modeling of transport and residence times in nanostructured membranes. American Institute of Chemical Engineers Journal 52, 3679–3687.

Arora, G., Sandler, S.I., 2005. Air separation by single wall carbon nanotubes: thermodynamics and adsorptive selectivity. Journal of Chemical Physics 123, 044705.

Arya, G., Chang, H.C., Maginn, E.J., 2003a. Molecular simulations of Knudsen wall-slip: effect of wall morphology. Molecular Simulation 29, 697–709.

Arya, G., Chang, H.C., Maginn, E.J., 2003b. Knudsen diffusivity of a hard sphere in a rough slit pore. Physical Review Letters 91, 026102.

Bhatia, S.K., 2006. Influence of adsorbate interaction on transport in confined spaces. Adsorption Science & Technology 24, 101–116.

Bhatia, S.K., Nicholson, D., 2003. Molecular transport in nanopores. Journal of Chemical Physics 119, 1719–1730.

Bhatia, S.K., Nicholson, D., 2006. Transport of simple fluids in nanopores: theory and simulation. American Institute of Chemical Engineers Journal 52, 29–38.

Bhatia, S.K., Nicholson, D., 2008. Modeling mixture transport at the nanoscale: departure from existing paradigms. Physical Review Letters 100, 236103.

Bhatia, S.K., Jepps, O., Nicholson, D., 2004. Tractable molecular theory of transport of Lennard–Jones fluids in nanopores. Journal of Chemical Physics 120, 4472–4485.

Chen, H.B., Sholl, D.S., 2004. Rapid diffusion of CH_4/H_2 mixtures in single-wall carbon nanotubes. Journal of the American Chemical Society 126, 7778–7779.

Chen, Y.D., Yang, R.T., Uawithya, P., 1994. Diffusion of oxygen, nitrogen and their mixtures in carbon molecular-sieve. American Institute of Chemical Engineers Journal 40, 577–585.

Chmelik, C., Kärger, J., Wiebcke, M., Caro, J., van Baten, J.M., Krishna, R., 2009. Adsorption and diffusion of alkanes in CuBTC crystals investigated using infrared microscopy and molecular simulations. Microporous and Mesoporous Materials 117, 22–32.

Ciesla, U., Schüth, F., 2005. Ordered mesoporous materials. Microporous and Mesoporous Materials 27, 131–149.

Coasne, B., Di Renzo, F., Galarneau, A., Pellenq, R.J.M., 2008. Adsorption of simple fluid on silica surface and nanopore: effect of surface chemistry and pore shape. Langmuir 24, 7285–7293.

Delgado, J.A., Rodrigues, A.E., 2001. A Maxwell–Stefan model of bidisperse pore pressurization for Langmuir adsorption of gas mixtures. Industrial & Engineering Chemistry Research 40, 2289–2301.

Dubbeldam, D., Calero, S., Vlugt, T.J.H., Krishna, R., Maesen, T.L.M., Smit, B., 2004. United atom forcefield for alkanes in nanoporous materials. Journal of Physical Chemistry B 108, 12301–12313.

Düren, T., Snurr, R.Q., 2004. Assessment of isoreticular metal–organic frameworks for adsorption separations: a molecular simulation study of methane/*n*-butane mixtures. Journal of Physical Chemistry B 108, 15703–15708.

Higgins, S., DeSisto, W., Ruthven, D.M., 2008. Diffusive transport through mesoporous silica membranes. Microporous and Mesoporous Materials ⟨http://dx.doi.org/10.1016/j.micromeso.2008.06.030⟩.

Himeno, S., Tomita, T., Suzuki, K., Nakayama, K., Yoshida, S., 2007. Synthesis and permeation properties of a DDR-type zeolite membrane for separation of CO_2/CH_4 gaseous mixtures. Industrial & Engineering Chemistry Research 46, 6989–6997.

Jakobtorweihen, S., Lowe, C.P., Keil, F.J., Smit, B., 2007. Diffusion of chain molecules and mixtures in carbon nanotubes: the effect of host lattice flexibility and theory of diffusion in the Knudsen regime. Journal of Chemical Physics 127, 024904.

Kärger, J., Vasenkov, S., Auerbach, S.M., 2003. Diffusion in zeolites. In: Auerbach, S.M., Carrado, K.A., Dutta, P.K. (Eds.), Handbook of Zeolite Science and Technology. Marcel Dekker, New York, pp. 341–422 (Chapter 10).

Kerkhof, P.J.A.M., 1996. A modified Maxwell–Stefan model for transport through inert membranes: the binary friction model. Chemical Engineering Journal 64, 319–343.

Kerkhof, P.J.A.M., Geboers, M.A.M., 2005a. Toward a unified theory of isotropic molecular transport phenomena. American Institute of Chemical Engineers Journal 51, 79–121.

Kerkhof, P.J.A.M., Geboers, M.A.M., 2005b. Analysis and extension of the theory of multicomponent fluid diffusion. Chemical Engineering Science 60, 3129–3167.

Keskin, S., Liu, J., Rankin, R.B., Johnson, J.K., Sholl, D.S., 2008. Progress, opportunities, and challenges for applying atomically detailed modeling to molecular adsorption and transport in metal–organic framework materials. Industrial & Engineering Chemistry Research ⟨http://dx.doi.org/10.1021/ie800666s⟩.

Krishna, R., 1990. Multicomponent surface diffusion of adsorbed species—a description based on the generalized Maxwell–Stefan equations. Chemical Engineering Science 45, 1779–1791.

Krishna, R., Paschek, D., 2000. Separation of hydrocarbon mixtures using zeolite membranes: a modelling approach combining molecular simulations with the Maxwell–Stefan theory. Separation and Purification Technology 21, 111–136.

Krishna, R., van Baten, J.M., 2005. The Darken relation for multicomponent diffusion in liquid mixtures of linear alkanes. An investigation using molecular dynamics (MD) simulations. Industrial & Engineering Chemistry Research 44, 6939–6947.

Krishna, R., van Baten, J.M., 2006a. Validating the Darken relation for diffusivities in fluid mixtures of varying densities by use of MD simulations. Chemical Engineering & Technology 29, 761–765.

Krishna, R., van Baten, J.M., 2006b. Describing binary mixture diffusion in carbon nanotubes with the Maxwell–Stefan equations. An investigation using molecular dynamics simulations. Industrial & Engineering Chemistry Research 45, 2084–2093.

Krishna, R., van Baten, J.M., 2007. Using molecular simulations for screening of zeolites for separation of CO_2/CH_4 mixtures. Chemical Engineering Journal 133, 121–131.

Krishna, R., van Baten, J.M., 2008a. Onsager coefficients for binary mixture diffusion in nanopores. Chemical Engineering Science 63, 3120–3140.

Krishna, R., van Baten, J.M., 2008b. Insights into diffusion of gases in zeolites gained from molecular dynamics simulations. Microporous and Mesoporous Materials 109, 91–108.

Krishna, R., Wesselingh, J.A., 1997. The Maxwell–Stefan approach to mass transfer. Chemical Engineering Science 52, 861–911.

Kuznicki, S.M., Bell, V.A., Nair, S., Hillhouse, H.W., Jacubinas, R.M., Braunbarth, C.M., Toby, B.H., Tsapatsis, M., 2001. A titanosilicate molecular sieve with adjustable pores for size-selective adsorption of molecules. Nature 412, 720–724.

Li, S., Falconer, J.L., Noble, R.D., Krishna, R., 2007. Interpreting unary, binary and ternary mixture permeation across a SAPO-34 membrane with loading-dependent Maxwell–Stefan diffusivities. Journal of Physical Chemistry C 111, 5075–5082.

Marathe, R.P., Mantri, K., Srinivasan, M.P., Farooq, S., 2004. Effect of ion exchange and dehydration temperature on the adsorption and diffusion of gases in ETS-4. Industrial & Engineering Chemistry Research 43, 5281–5290.

Mason, E.A., Malinauskas, A.P., 1983. Gas Transport in Porous Media: The Dusty-Gas Model. Elsevier, Amsterdam.

Schlünder, E.U., Yang, J., Seidel-Morgenstern, A., 2006. Competitive diffusion and adsorption in Vycor glass membranes—a lumped parameter approach. Catalysis Today 118, 113–120.

Snurr, R.Q., Hupp, J.T., Nguyen, S.T., 2004. Prospects for nanoporous metal–organic materials in advanced separations processes. American Institute of Chemical Engineers Journal 50, 1090–1095.

van Baten, J.M., Krishna, R., 2008. MD Animations of Diffusion in Nanoporous Materials. University of Amsterdam, Amsterdam. ⟨http://www.science.uva.nl/research/cr/animateMD/, 20 October 2008⟩.

Yang, J., Čermáková, J., Uchytil, P., Hamel, C., Seidel-Morgenstern, A., 2005. Gas phase transport, adsorption and surface diffusion in a porous glass membrane. Catalysis Today 104, 344–351.

Yoshioka, T., Tsuru, T., Asaeda, M., 2001. Molecular dynamics studies on gas permeation properties through microporous silica membranes. Separation and Purification Technology 25, 441–449.

Young, J.B., Todd, B., 2005. Modelling of multi-component gas flows in capillaries and porous solids. International Journal of Heat and Mass Transfer 48, 5338–5353.

Yu, Y.X., Gao, G.H., 2000. Lennard–Jones chain model for self-diffusion of *n*-alkanes. International Journal of Thermophysics 21, 57–70.

Zschiegner, S., Russ, S., Bunde, A., Kärger, J., 2007. Pore opening effects and transport diffusion in the Knudsen regime in comparison to self- (or tracer-) diffusion. Europhysics Letters 78, 20001.

Supplementary Material to accompany:

An investigation of the characteristics of Maxwell-Stefan diffusivities of binary mixtures in silica nanopores

R. Krishna*, J.M. van Baten

Van 't Hoff Institute for Molecular Sciences, University of Amsterdam, Nieuwe Achtergracht 166,

1018 WV Amsterdam, The Netherlands

CORRESPONDING AUTHOR *Tel +31 20 257007 ; Fax: + 31 20 5255604;

email: r.krishna@uva.nl

1. Construction of the structure of silica nanopores

The silica structures have been prepared using a method based on Coasne et al.[1]. An initial β-cristobalite (unit cell of 8 Si and 16 O atoms, at glass density of 2200 kg/m3, with a box size of 7.132 Å) structure was considered. The total number of β-cristobalite unit cells in the complete box was determined by a minimum of 24 Å in the z-direction, and a minimum of 24 Å plus target pore diameter in the remaining two directions. A cylindrical cavity was cut out of the initial geometry. Subsequently, all Si atoms that was not bound to 4 O atoms were removed. Any non-bound O atoms were removed after that. This causes singly bound O atoms to remain in the structure. Half of these need to be removed to ensure electro-neutrality of the system. Pairs of singly-bound O-atoms were detected for which the O-O distance is less than 2.7 Å. These combinations where replaced by a single O atom to form a Siloxane bridge. The single O atom was placed at the geometric mean location of the two removed O atoms. Half of the remaining singly bound O atoms were removed at random, introducing one bond defect per O atom. Of the remaining structure, all atoms were displaced on a random sphere with 0.7 Å radius to form the amorphous structure. The structure data files we used in our simulations are available on our website [2]. The framework structure, and the landscapes for eight different pore diameters 1, 1.5, 2, 3, 4, 5.8, 7.6 and 10 nm are presented in Figures 1, 2, 3, 4, 5, 6, 7, and 8

.

2. Monte Carlo simulation methodology

The adsorption isotherms were computed using Monte Carlo (MC) simulations in the grand canonical (GC) ensemble. The interaction between the guest molecules and the silica surface is assumed to be dominated by interactions between guest molecules and the O atoms in the silica. The united atom force field for alkanes, developed by Dubbeldam et al. [3] for zeolites, is used to describe Lennard-Jones interactions, both alkane-alkane, and alkane – O atom in the silica pore. For Lennard-Jones parameters are tabulated in Dubbeldam et al. [3]; the potential for the n-alkanes includes bond stretching, bending, and torsion. Simulations were also carried out for Ar, Kr, and H_2. The

intermolecular Lennard-Jones parameters for Ar are those listed in Skoulidas and Sholl[4]. For Kr the parameters are from Talu and Myers [5]. The force field for H_2 corresponds to that given by Kumar et al.[6] In implementing this force field, quantum effects for H_2 have been ignored because the work of Kumar et al.[6] has shown that quantum effects are of negligible importance for temperatures above 200 K; all our simulations were performed at 300 K. The force field of Kumar et al.[6] is quite similar to that used by Gallo et al. [7]. The Lennard-Jones parameters for molecule-molecule interactions of Ar, Kr, Ne, and H_2 are summarized in Tables 1.

For simulations with linear and branched alkanes with two or more C atoms, the Configurational-Bias Monte Carlo (CBMC) simulation technique [8, 9] was employed. The beads in the chain are connected by harmonic bonding potentials. A harmonic cosine bending potential models the bond bending between three neighboring beads, a Ryckaert-Bellemans potential controls the torsion angle. The beads in a chain separated by more than three bonds interact with each other through a Lennard-Jones potential. The Lennard-Jones potentials are shifted and cut at 12 Å. The CBMC simulation details have been given in detail elsewhere [3, 8-10].

All simulations were performed with 1×1×2 unit cells.

The CBMC isotherm simulations were performed using the BIGMAC code developed by T.J.H. Vlugt[11] as basis. From the adsorption isotherms we can calculate the thermodynamic factors, necessary for determination of the Fick diffusivities; this aspect is discussed below.

3. MD simulation methodology

Diffusion is simulated using Newton's equations of motion until the system properties, on average, no longer change in time. The Verlet algorithm is used for time integration. A time step of 1 fs was used in all simulations. For each simulation, *initializing* CBMC moves are used to place the molecules in the domain, minimizing the energy. Next, follows an *equilibration* stage. These are essentially the same as the production cycles, only the statistics are not yet taken into account. This removes any initial large disturbances in the system that do not affect statistics on molecular displacements. After a fixed number of initialization and equilibrium steps, the MD simulation *production* cycles start. For every cycle, the

statistics for determining the mean square displacements (MSDs) are updated. The MSDs are determined for time intervals ranging from 2 fs to 1 ns. In order to do this, an order-*N* algorithm, as detailed in Chapter 4 of Frenkel and Smit[8] is implemented. The Nosé-Hoover thermostat is applied to all the diffusing particles.

The DLPOLY code[12] was used along with the force field implementation as described in the previous section. DL_POLY is a molecular dynamics simulation package written by W. Smith, T.R. Forester and I.T. Todorov and has been obtained from CCLRCs Daresbury Laboratory via the website.[12]

The MD simulations were carried out for a variety of molecular loadings within the pores. All simulations were carried out on the LISA clusters of PCs equipped with Intel Xeon processors running at 3.4 GHz on the Linux operating system[13]. Each MD simulation, for a specified loading, was run for 120 h, determined to be long enough to obtain reliable statistics for determination of the diffusivities.

4. MD simulations for binary mixtures inside cylindrical silica pores

The Maxwell-Stefan (M-S) equations for binary mixture diffusion inside a cylindrical silica pore can be written as

$$-\frac{c_i}{k_B T}\frac{d\mu_i}{dx} = \sum_{\substack{j=1 \\ j\neq i}}^{n} \frac{x_j N_i - x_i N_j}{Đ_{ij}} + \frac{N_i}{Đ_{i,s}}; \quad i = 1,2 \tag{1}$$

In equation (1) the $Đ_{i,s}$ are the M-S diffusivities of species 1 and 2, respectively, portraying the interaction between component *i* in the mixture with the surface (s), or wall, of the silica pore. The $Đ_{12}$ and $Đ_{21}$ are M-S diffusivities representing interaction between component 1 with component 2. The c_i are the loadings within the pore and x_i represent the component mole fractions

$$x_i = c_i / (c_1 + c_2 + ...c_n); \quad i = 1, n \tag{2}$$

The Onsager reciprocal relations require

$$Đ_{ij} = Đ_{ji} \tag{3}$$

For binary mixtures we can define a square 2×2 matrix [B]

$$-\frac{c_i}{k_B T}\frac{d\mu_i}{dx} = \sum_{j=1}^{2} B_{ij} N_j ; \quad i = 1,2 \tag{4}$$

The four elements of the matrix [B] are given explicitly by

$$B_{11} = \frac{1}{Đ_{1,s}} + \frac{x_2}{Đ_{12}} \tag{5}$$

$$B_{22} = \frac{1}{Đ_{2,s}} + \frac{x_1}{Đ_{12}} \tag{6}$$

$$B_{12} = -\frac{x_1}{Đ_{12}} \tag{7}$$

$$B_{21} = -\frac{x_2}{Đ_{12}} \tag{8}$$

Furthermore, we define a matrix [Δ] as the inverse of [B]

$$[\Delta] \equiv [B]^{-1} \tag{9}$$

The inversion can be carried out explicitly to give the following expressions

$$\Delta_{11} = \frac{Đ_{1,s}\left(1 + \dfrac{x_1 Đ_{2,s}}{Đ_{12}}\right)}{1 + \dfrac{x_1 Đ_{2,s} + x_2 Đ_{1,s}}{Đ_{12}}} \tag{10}$$

$$\Delta_{22} = \frac{Đ_{2,s}\left(1 + \dfrac{x_2 Đ_{1,s}}{Đ_{12}}\right)}{1 + \dfrac{x_2 Đ_{1,s} + x_1 Đ_{2,s}}{Đ_{12}}} \tag{11}$$

$$\Delta_{12} = \frac{Đ_{1,s}\dfrac{x_1 Đ_{2,s}}{Đ_{12}}}{1+\dfrac{x_1 Đ_{2,s} + x_2 Đ_{1,s}}{Đ_{12}}} \tag{12}$$

$$\Delta_{21} = \frac{x_2}{x_1}\Delta_{12} = \frac{Đ_{2,s}\dfrac{x_2 Đ_{1,s}}{Đ_{12}}}{1+\dfrac{x_1 Đ_{2,s} + x_2 Đ_{1,s}}{Đ_{12}}} \tag{13}$$

The elements Δ_{ij} can be obtained from MD simulations of molecular displacements using the formula in the direction along the axis of the cylindrical pore

$$\Delta_{ij} = \frac{1}{2}\lim_{\Delta t\to\infty}\frac{1}{n_j}\frac{1}{\Delta t}\left\langle\left(\sum_{l=1}^{n_i}\left(\mathbf{r}_{l,i}(t+\Delta t)-\mathbf{r}_{l,i}(t)\right)\right)\bullet\left(\sum_{k=1}^{n_j}\left(\mathbf{r}_{k,j}(t+\Delta t)-\mathbf{r}_{k,j}(t)\right)\right)\right\rangle \tag{14}$$

In this expression n_i and n_j represent the number of molecules of species i and j respectively, and $\mathbf{r}_{l,i}(t)$ is the position of molecule l of species i at any time t. In this context we note a typographical error in eq (14) as printed in earlier publications [14-16] wherein the denominator in the right member had n_i instead of n_j. The simulation results presented in these publications are, however, correct as the proper formula given in eq (14) was used. Compliance with the Onsager Reciprocal Relations demands that

$$n_j\Delta_{ij} = n_i\Delta_{ji};\quad i,j = 1,2,....n \tag{15}$$

We define a matrix of thermodynamic correction factors $[\Gamma]$

$$\frac{c_i}{k_B T}\frac{d\mu_i}{dx} = \sum_{j=1}^{n}\Gamma_{ij}\nabla c_j;\quad \Gamma_{ij} \equiv \frac{c_i}{c_j}\frac{\partial \ln f_i}{\partial \ln c_j} = \frac{c_i}{f_i}\frac{\partial f_i}{\partial c_j};\quad i,j = 1,..n \tag{16}$$

where f_i represents the fugacity of component i in the bulk fluid phase outside the pore . With this definition equation (4) can be recast in the form

$$-[\Gamma]\frac{d(c)}{dx} = [B](N);\quad (N) = -[B]^{-1}[\Gamma]\frac{d(c)}{dx} = -[\Delta][\Gamma]\frac{d(c)}{dx} \tag{17}$$

The matrix of Fick diffusivities for binary mixture diffusion is defined as

$$\left[D_{Fick,s}\right] = [B]^{-1}[\Gamma] = [\Delta][\Gamma] \tag{18}$$

An alternative to the M-S formulation is the Onsager formulation, in which the flux equations are expressed as

$$N_i = -\frac{1}{k_B T}\sum_{j=1}^{2} L_{ij}\,\frac{d\mu_j}{dx}; \quad i = 1,2 \tag{19}$$

with

$$L_{12} = L_{21} \tag{20}$$

Equation (19) is used, for example, by Bhatia and Nicholson [17].

For binary mixtures the relation between the Onsager matrix [L] and the M-S matrix [Δ] is

$$\begin{bmatrix} L_{11} & L_{12} \\ L_{21} & L_{22} \end{bmatrix} = \begin{bmatrix} \Delta_{11}c_1 & \Delta_{12}c_2 \\ \Delta_{21}c_1 & \Delta_{22}c_2 \end{bmatrix} \tag{21}$$

Equation (21), in combination with eq (Ð14), allows the elements L_{ij} to be obtained from MD simulations. Furthermore, equation (21), used in combination with equations (10), (11), (12), and (13) allows the calculation of the elements L_{ij} from information on c_i, $Ð_{i,s}$ and $Ð_{12}$.

5. Unary diffusion inside cylindrical silica pore

For unary diffusion, equation (1) simplifies to yield

$$-\frac{c_i}{k_B T}\frac{d\mu_i}{dx} = \frac{N_i}{Ð_{i,s}} \tag{22}$$

The corresponding Onsager relation for unary diffusion is

$$-\frac{1}{k_B T}\frac{d\mu_i}{dx} = \frac{N_i}{L_i} \tag{23}$$

with the inter-relationship

$$L_i = c_i Đ_{i,s} \tag{24}$$

The pure component $Đ_{i,s}$ can be obtained from MD simulations of molecular displacements using the formula in the coordinate direction along the axis of the cylindrical pore

$$Đ_{i,s} = \frac{1}{2}\lim_{\Delta t\to\infty}\frac{1}{n_i}\frac{1}{\Delta t}\left\langle\left(\sum_{l=1}^{n_i}\left(\mathbf{r}_{l,i}(t+\Delta t)-\mathbf{r}_{l,i}(t)\right)\right)^2\right\rangle \tag{25}$$

Let us apply equation (1) to a system consisting of two species that are identical with respect to diffusional properties and, furthermore, that we have equimolar diffusion $N_1 + N_2 = 0$

$$-\frac{c_1}{k_B T}\frac{d\mu_1}{dx} = \frac{(x_1+x_2)N_1}{Đ_{11}} + \frac{N_1}{Đ_{1,s}} = \left(\frac{1}{Đ_{11}} + \frac{1}{Đ_{1s}}\right)N_1 \tag{26}$$

The M-S diffusivity $Đ_{11}$ is the self-diffusivity in the fluid mixture. Equation (26) defines the self-diffusivity within a pore

$$-\frac{c_1}{k_B T}\frac{d\mu_1}{dx} = \frac{N_1}{D_{1.se;f.s}} \tag{27}$$

and so we derive the expression

$$\frac{1}{D_{i,self,s}} = \frac{1}{Đ_{i,s}} + \frac{1}{Đ_{ii}} \tag{28}$$

Following Krishna and Paschek [18] the expressions for the self-diffusivities in a binary mixture inside a pore can be derived as follows

$$\frac{1}{D_{1,self,s}} = \frac{1}{Đ_{,s1}} + \frac{x_1}{Đ_{11}} + \frac{x_2}{Đ_{12}} \tag{29}$$

$$\frac{1}{D_{2,self,s}} = \frac{1}{Đ_{2,s}} + \frac{x_2}{Đ_{22}} + \frac{x_1}{Đ_{12}} \tag{30}$$

In equations (29) and (30), the $Đ_{11}$ and $Đ_{22}$ are the self-diffusivities of species 1 and 2 in the binary fluid mixture, and these are not necessarily the same as the corresponding self-diffusivities in pure fluids, encountered in equation (28).

The self-diffusivities $D_{\mathrm{i,self,s}}$ can be computed from MD simulations by analyzing the mean square displacement of each species *i* for the coordinate direction along the pore axis using

$$D_{i,self,s} = \frac{1}{2n_i} \lim_{\Delta t \to \infty} \frac{1}{\Delta t} \left\langle \left(\sum_{l=1}^{n_i} \left(\mathbf{r}_{l,i}(t+\Delta t) - \mathbf{r}_{l,i}(t) \right)^2 \right) \right\rangle \tag{31}$$

By introducing the thermodynamic factor Γ_i

$$\frac{c_i}{k_B T} \frac{d\mu_i}{dx} = \Gamma_i \frac{dq_i}{dx}; \quad \Gamma_i \equiv \frac{\partial \ln f_i}{\partial \ln c_j} = \frac{c_i}{f_i} \frac{\partial f_i}{\partial c_i}; \quad \text{unary system} \tag{32}$$

we can re-write equation (22) as

$$N_i = -D_{Fick,i,s} \frac{dc_i}{dx} = -Đ_{i,s} \Gamma_i \frac{dc_i}{dx} \tag{33}$$

The thermodynamic factor can be obtained by differentiating the pure component adsorption isotherm. The Fick diffusivity for unary diffusion inside the pore is

$$D_{Fick,i,s} = Đ_{i,s} \Gamma_i \tag{34}$$

6. MD simulations of diffusivity and viscosity in pure fluids

The validity of equation (28) was also tested by performing independent simulations to determine the self-diffusivities $Đ_{\mathrm{ii}}$ in the pure fluids at various loadings c_{i}. The MD simulation methodology for self-diffusivities in pure fluids is the same as used in our earlier publications [16, 19, 20].

Figure 9 summarizes the pure component self-diffusivity data for pure fluids $Đ_{\mathrm{ii}}$ of various molecules considered in this publication.

Figures 10 and 11 compare the pure fluid $Đ_{\mathrm{ii}}$ with the data for self-diffusivities in binary fluid mixtures C1-Ar, C1-C2, C1-C3, C1-nC4, C1-nC6, and C1-H_2, C2-nC4, C2-nC6, and nC4-nC6.

Furthermore, the M-S diffusivities $Đ_{12}$ in binary fluid mixtures were determined using the methodology used in our earlier publications [16, 19, 20]. Figure 12 summarizes the data on the M-S diffusivities $Đ_{12}$ in binary fluid mixtures.

In order to determine the viscous contribution to the diffusivity, the shear viscosity η_i was determined for pure fluids using the procedure in the published literature [21, 22]. Figure 13 presents MD simulated data on the shear viscosity of pure fluids, η_i. The η_i data are used to estimate the viscous contribution to the $Đ_{is}$ in different pore structures.

7. Backing out $Đ_{i,s}$ and $Đ_{12}$ from mixture simulations

The MD simulations for binary mixtures yields the 2×2 matrix [Δ] using the formula (14). The first step is to determine the determinant

$$|\Delta| = \Delta_{11}\Delta_{22} - \Delta_{12}\Delta_{21} \tag{35}$$

The elements of [B] are then obtained explicitly using

$$B_{11} = \frac{\Delta_{22}}{|\Delta|} \tag{36}$$

$$B_{22} = \frac{\Delta_{11}}{|\Delta|} \tag{37}$$

$$B_{12} = -\frac{\Delta_{12}}{|\Delta|} \tag{38}$$

$$B_{21} = -\frac{\Delta_{21}}{|\Delta|} \tag{39}$$

Combining equation (7) with (38) we can obtain $Đ_{12}$ explicitly

$$Đ_{12} = -\frac{x_1}{B_{12}} \tag{40}$$

Combining equation (8) with (39) we can obtain $Đ_{12}$ from the equivalent relationship

$$Đ_{12} = -\frac{x_2}{B_{21}} \tag{41}$$

From equations (5), (36), and (40) we get

$$Đ_{1,s} = 1\Big/\left(B_{11} - \frac{x_2}{Đ_{12}}\right) \tag{42}$$

From equations (6), (37), and (40) we get

$$Đ_{2,s} = 1\Big/\left(B_{22} - \frac{x_1}{Đ_{12}}\right) \tag{43}$$

The $Đ_{i,s}$ backed out using equations (42) and (43) can be compared with the MD simulated pure component values using equation (25). These two sets of results are compared at the same total loading inside the pore.

The $Đ_{12}$ backed out using equation (41) are also compared with values for binary mixture diffusion in fluid mixtures of the same composition and total loading; the latter were determined using the methodology described in earlier publications [16, 19, 20].

Bhatia and Nicholson [17] present MD simulation results for the Onsager matrix [L]. From their data the elements of [Δ] can first be calculated using

$$\Delta_{ij} = \frac{L_{ij}}{c_j} \tag{44}$$

and the foregoing explicit relations used for backing out $Đ_{i,s}$ and $Đ_{12}$.

8. Simulation results

The CBMC, and MD simulation results for adsorption and diffusion in the eight different pores are presented graphically in Figures 14 – 59. The comparison of MD simulated $Đ_{i,self,s}$ with those calculated

from equation (28) are presented in the simulation results in the Figures 14 – 59; there is only a brief discussion on this in the main text of the paper.

Also presented graphically are the comparisons of the MD simulated $Đ_{i,s}$ values for pure components with the calculations using the formula of Kerkhof [23-25];

$$Đ_{i,s} = D_{i,Kn} + \frac{B_O c_i k_B T}{\eta_i} \tag{45}$$

wherein we estimate the first term on the right hand side of equation (45) using the classical Knudsen formula

$$D_{i,Kn} = \frac{d_{p,eff}}{3}\sqrt{\frac{8RT}{\pi M_i}} \tag{46}$$

In all the Figures in the Supplementary material, the Knudsen calculations using equation (46) are indicated by a large blue filled circle.

The viscous term (second member on the right hand side of equation (45)) is estimated taking

$$B_0 = \frac{d_{p,eff}^2}{32} \tag{47}$$

and, furthermore, using the MD simulated values of η_i in Figure 13, after empirical fitting.

The effective pore diameter in equations (46), and (47) are calculated from

$$d_{p,eff} = d_p - 0.92(\sigma_i + \sigma_O) \tag{48}$$

where d_p is the centre-to-centre distance between the O atoms on the surface of the pore, σ_i is the Lennard-Jones size parameter for molecule-molecule interaction, and σ_O is the Lennard-Jones size parameter for O atoms in the silica structure (see Table 1).

9. Animations

For visual appreciation of the diffusion phenomena in cylindrical silica pores, animations were created on the basis of the MD simulations; these can be viewed by downloading the movies from our website[2].

10. Acknowledgements

We are grateful to T.J.H. Vlugt, Delft, for providing the BIGMAC code. This code was modified to handle rigid molecular structures and charges, with generous assistance and technical inputs from S. Calero, Seville.

11. Notation

B_O	permeability of pore, m^2
$[B]$	matrix of inverse Maxwell-Stefan coefficients, m^{-2} s
c_i	concentration of species i, molecule m^{-3}
c_t	total concentration in mixture, molecule m^{-3}
d_p	pore diameter, m
$d_{p,eff}$	effective pore diameter defined by equation (48), m
$D_{i,self,s}$	self-diffusivity of species i within pore, m^2 s^{-1}
$Đ_{ii}$	self-diffusivity of species i in fluid phase, m^2 s^{-1}
$Đ_{Fick,i,s}$	Fick diffusivity for unary diffusion inside pore, m^2 s^{-1}
$Đ_{i,s}$	Maxwell-Stefan diffusivity for species-pore wall interaction, m^2 s^{-1}
$Đ_{i,s}(0)$	zero-loading M-S diffusivity for species-pore wall interaction, m^2 s^{-1}
$Đ_{12}$	Maxwell-Stefan diffusivity for species-species interaction, m^2 s^{-1}
$D_{i,Kn}$	Knudsen diffusivity of species i, m^2 s^{-1}
f_i	fugacity of species i, Pa
k_B	Boltzmann constant, 1.38×10^{-23} J $molecule^{-1}$ K^{-1}
L_i	Onsager coefficients for pure component i, molecule nm^{-3} m^2 s^{-1}
L_{ij}	Onsager coefficients for mixture diffusion, molecule nm^{-3} m^2 s^{-1}
M_i	molar mass of species i, kg mol^{-1}
N_i	molecular flux of species i, molecules m^{-2} s^{-1}
n_i	number of molecules of species i in simulation box, dimensionless
n	number of species in mixture, dimensionless
$\mathbf{r}_{l,i}(t)$	position vector for molecule l of species i at any time t, m
R	gas constant, 8.314 J mol^{-1} K^{-1}
x_i	mole fraction of species i based on loading within pore, dimensionless
t	time, s
T	absolute temperature, K

x	spatial distance, m

Greek letters

$[\Delta]$	matrix of Maxwell-Stefan diffusivities, $m^2\ s^{-1}$
ε/k_B	Lennard-Jones interaction energy parameter, K
$[\Gamma]$	matrix of thermodynamic factors, dimensionless
Γ_i	thermodynamic factor for unary diffusion, dimensionless
Γ_{ij}	thermodynamic factors for mixtures, dimensionless
η_i	viscosity of species *i*, Pa s
μ_i	molar chemical potential, J $molecule^{-1}$
σ	Lennard-Jones size parameter, m

Subscripts

i	referring to component *i*
t	referring to total mixture
Kn	referring to Knudsen
O	referring to O atoms in silica

Vector and Matrix Notation

( )	vector
[ ]	square matrix

Table 1. Lennard-Jones parameters for guest molecules CH_4, Ar, and Kr. The interaction between adsorbates was calculated using Lennard-Jones potentials. For adsorbate-adsorbate interactions, Lorentz-Berthelot mixing rules were applied for σ and ε/k_B. Leonard-Jones interaction with the silica was considered to be dominated by interactions with the O atoms. For longer n-alkanes the parameters are as listed by Dubbeldam et al.[3]

(pseudo-) atom	Atom-atom σ / Å	Atom-atom ε/k_B / K	Atom - O in silica σ / Å	Atom - O in silica ε/k_B / K
CH_4	3.72	158.5	3.47	115
Ar	3.42	124.07	3.17	95.61
Kr	3.636	166.4	3.45	109.6
H_2	2.782	38.7	2.713	79.914

12. References

[1] B. Coasne, F. Di Renzo, A. Galarneau, R.J.M. Pellenq, Adsorption of Simple Fluid on Silica Surface and Nanopore: Effect of Surface Chemistry and Pore Shape, Langmuir 24 (2008) 7285-7293.

[2] J.M. van Baten, R. Krishna, MD animations of diffusion in nanoporous materials, University of Amsterdam, Amsterdam, http://www.science.uva.nl/research/cr/animateMD/, 20 October 2008.

[3] D. Dubbeldam, S. Calero, T.J.H. Vlugt, R. Krishna, T.L.M. Maesen, B. Smit, United Atom Forcefield for Alkanes in Nanoporous Materials, J. Phys. Chem. B 108 (2004) 12301-12313.

[4] A.I. Skoulidas, D.S. Sholl, Transport diffusivities of CH_4, CF_4, He, Ne, Ar, Xe, and SF_6 in silicalite from atomistic simulations, J. Phys. Chem. B 106 (2002) 5058-5067.

[5] O. Talu, A.L. Myers, Reference potentials for adsorption of helium, argon, methane and krypton in high-silica zeolites, Colloids Surf., A 187-188 (2001) 83-93.

[6] A.V.A. Kumar, H. Jobic, S.K. Bhatia, Quantum effects on adsorption and diffusion of hydrogen and deuterium in microporous materials, J. Phys. Chem. B 110 (2006) 16666-16671.

[7] M. Gallo, T.M. Nenoff, M.C. Mitchell, Selectivities for binary mixtures of hydrogen/methane and hydrogen/carbon dioxide in silicalite and ETS-10 by Grand Canonical Monte Carlo techniques, Fluid Phase Equilib. 247 (2006) 135-142.

[8] D. Frenkel, B. Smit, Understanding molecular simulations: from algorithms to applications, Academic Press, 2nd Edition, San Diego, 2002.

[9] T.J.H. Vlugt, R. Krishna, B. Smit, Molecular simulations of adsorption isotherms for linear and branched alkanes and their mixtures in silicalite, J. Phys. Chem. B 103 (1999) 1102-1118.

[10] D. Dubbeldam, S. Calero, T.J.H. Vlugt, R. Krishna, T.L.M. Maesen, E. Beerdsen, B. Smit, Force Field Parametrization through Fitting on Inflection Points in Isotherms, Phys. Rev. Lett. 93 (2004) 088302.

[11] T.J.H. Vlugt, BIGMAC, University of Amsterdam, http://molsim.chem.uva.nl/bigmac/, 1 November 2000.

[12] W. Smith, T.R. Forester, I.T. Todorov, The DL_POLY Molecular Simulation Package, Warrington, England, http://www.cse.clrc.ac.uk/msi/software/DL_POLY/index.shtml, March 2006.

[13] SARA, Computing & Networking Services, Amsterdam, https://subtrac.sara.nl/userdoc/wiki/lisa/description, 16 January 2008.

[14] R. Krishna, J.M. van Baten, Diffusion of alkane mixtures in zeolites. Validating the Maxwell-Stefan formulation using MD simulations, J. Phys. Chem. B 109 (2005) 6386-6396.

[15] J.M. van Baten, R. Krishna, Entropy effects in adsorption and diffusion of alkane isomers in mordenite: An investigation using CBMC and MD simulations, Microporous Mesoporous Mater. 84 (2005) 179-191.

[16] R. Krishna, J.M. van Baten, Describing binary mixture diffusion in carbon nanotubes with the Maxwell-Stefan equations. An investigation using molecular dynamics simulations, Ind. Eng. Chem. Res. 45 (2006) 2084-2093.

[17] S.K. Bhatia, D. Nicholson, Modeling Mixture Transport at the Nanoscale: Departure from Existing Paradigms, Phys. Rev. Lett. 100 (2008) 236103.

[18] R. Krishna, D. Paschek, Self-diffusivities in multicomponent mixtures in zeolites, Phys. Chem. Chem. Phys. 4 (2002) 1891-1898.

[19] R. Krishna, J.M. van Baten, The Darken relation for multicomponent diffusion in liquid mixtures of linear alkanes. An investigation using Molecular Dynamics (MD) simulations, Ind. Eng. Chem. Res. 44 (2005) 6939-6947.

[20] R. Krishna, J.M. van Baten, Validating the Darken relation for diffusivities in fluid mixtures of varying densities by use of MD simulations, Chem Eng Technol 29 (2006) 761-765.

[21] G.A. Fernández, J. Vrabec, H. Hasse, A molecular simulation study of shear and bulk viscosity and thermal conductivity of simple real fluids, Fluid Phase Equilibr 221 (2004) 157-163.
[22] H. Zhang, B.J. Zhang, J.J. Zhang, Shear viscosity of simple fluids in porous media: molecular dynamics simulations and correlation models (II) – methane in silicate pores, Chem. Phys. Lett. 397 (2004) 233-236.
[23] P.J.A.M. Kerkhof, A modified Maxwell-Stefan model for transport through inert membranes: the binary friction model, Chem. Eng. J. 64 (1996) 319-343.
[24] P.J.A.M. Kerkhof, M.A.M. Geboers, Analysis and extension of the theory of multicomponent fluid diffusion, Chem. Eng. Sci. 60 (2005) 3129-3167.
[25] P.J.A.M. Kerkhof, M.A.M. Geboers, Toward a Unified Theory of Isotropic Molecular Transport Phenomena, A.I.Ch.E.J. 51 (2005) 79-121.

13. Captions for Figures

Figure 1. 1 nm pore structure and landscape.

Figure 2. 1.5 nm pore structure and landscape.

Figure 3. 2 nm pore structure and landscape.

Figure 4. 3 nm pore structure and landscape.

Figure 5. 4 nm pore structure and landscape.

Figure 6. 5.8 nm pore structure and landscape.

Figure 7. 7.6 nm pore structure and landscape.

Figure 8. 10 nm pore structure and landscape.

Figure 9. MD simulation results for self-diffusivities $Đ_{ii}$ in pure fluids.

Figure 10. MD simulation results for self-diffusivities $Đ_{ii}$ in pure fluids compared with those in equimolar binary C1-Ar, C1-C2, C1-C3, C1-nC4, C1-nC6, and C1-H_2 fluid mixtures.

Figure 11. MD simulation results for self-diffusivities $Đ_{ii}$ in pure fluids compared with those in equimolar binary C2-nC4, C2-nC6, and nC4-nC6 mixtures.

Figure 12. MD simulation results for Maxwell-Stefan diffusivities $Đ_{12}$ in equimolar binary fluid mixtures C1-Ar, C1-C2, C1-C3, C1-nC4, C1-nC6, and C1-H_2.

Figure 13. MD simulation results for shear viscosity η_i of pure fluids.

Figure 14 - 59. Simulation results for unary and binary diffusion in the variety of silica pores.

Figure 1

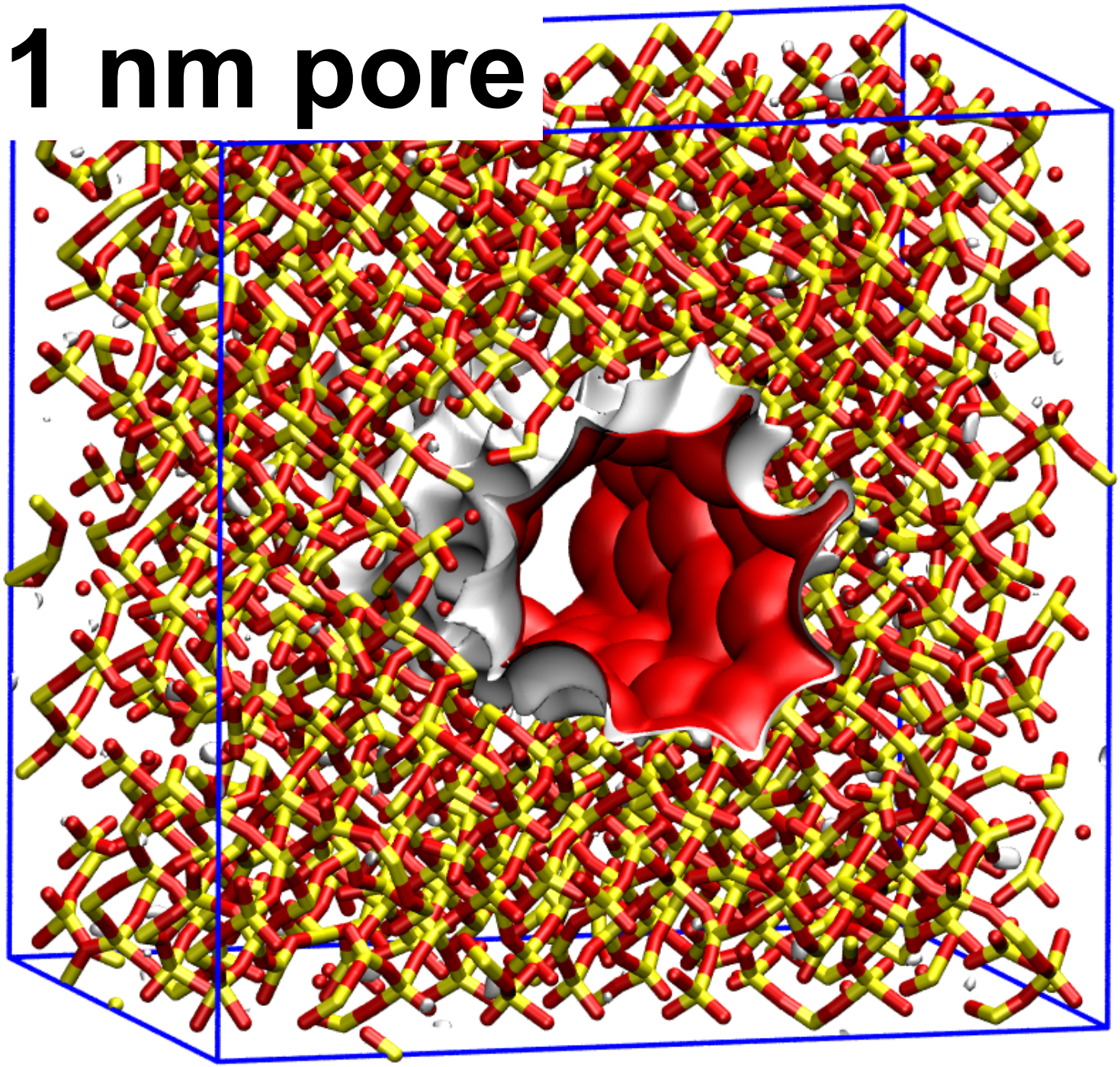

Figure 2

1.5 nm pore

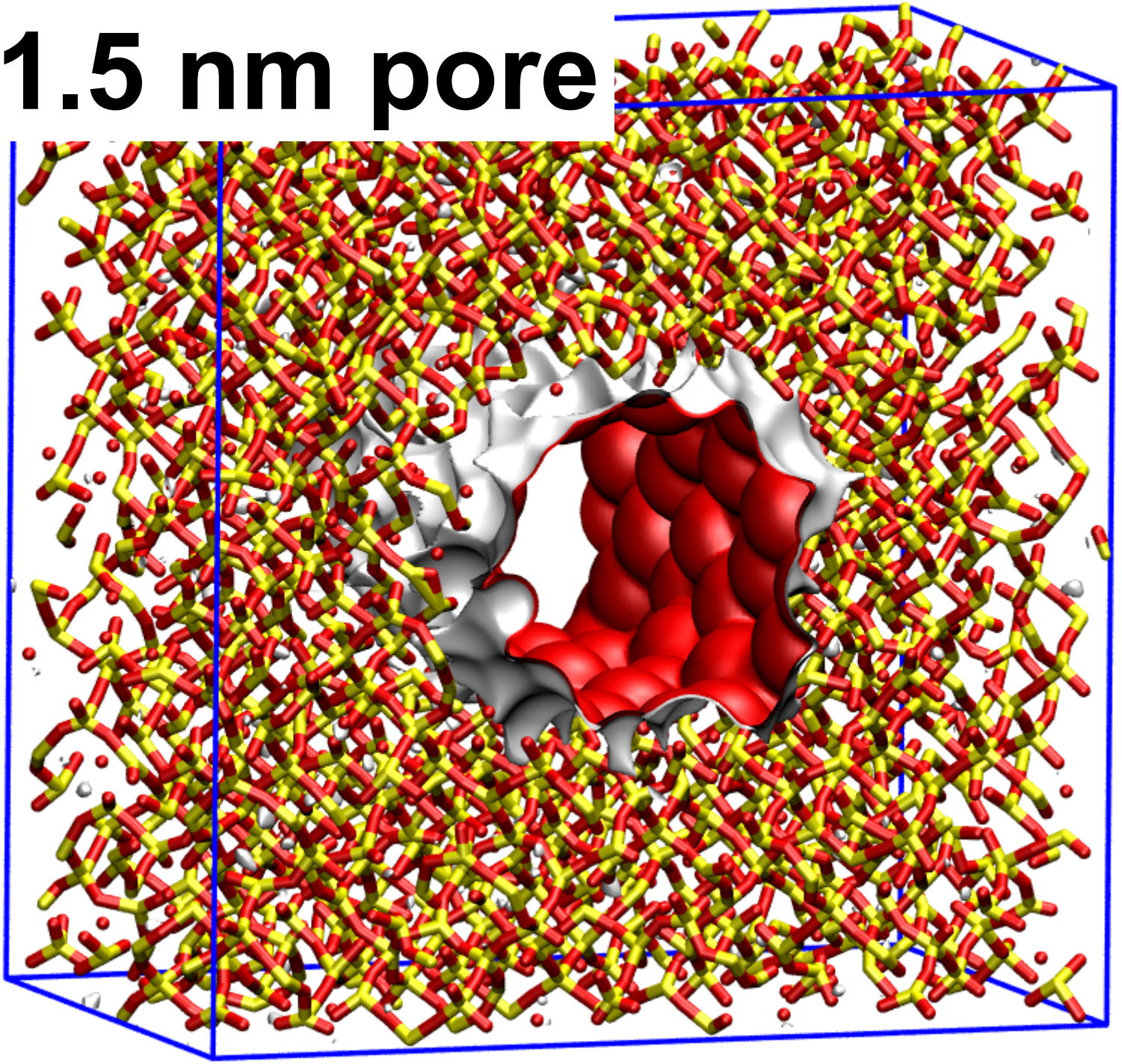

2 nm pore

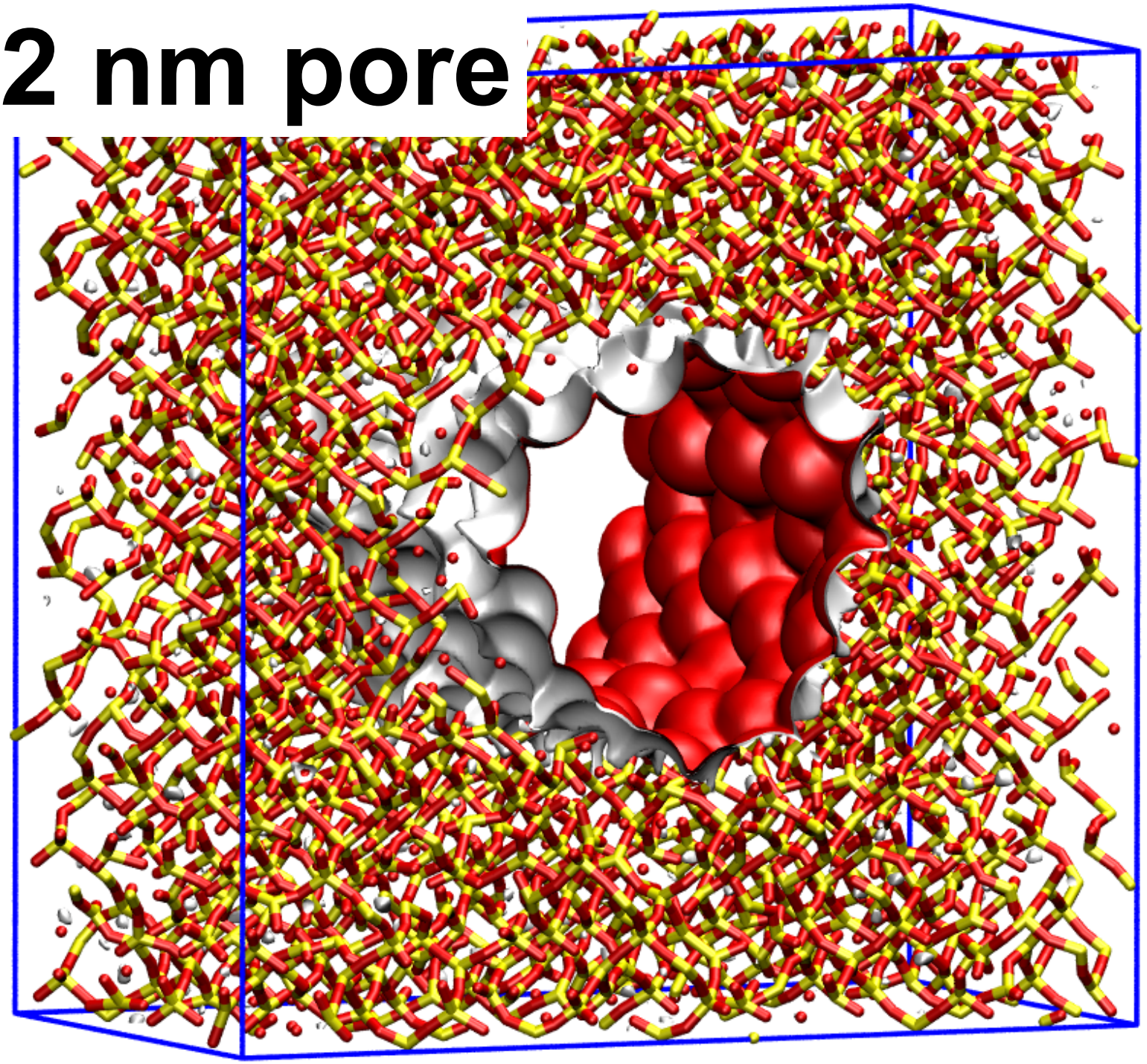

Figure 3

Figure 4

3 nm pore

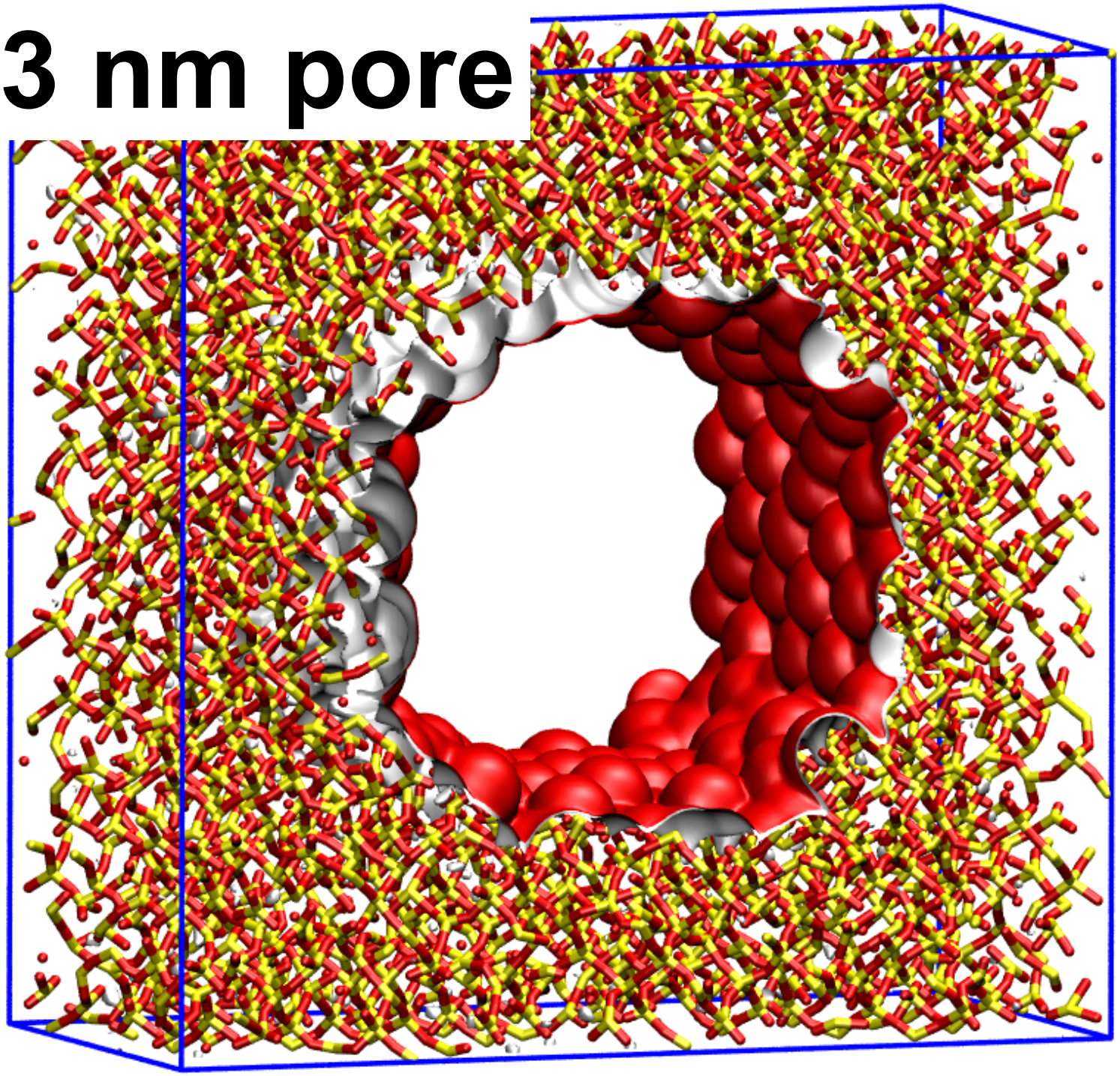

Figure 5

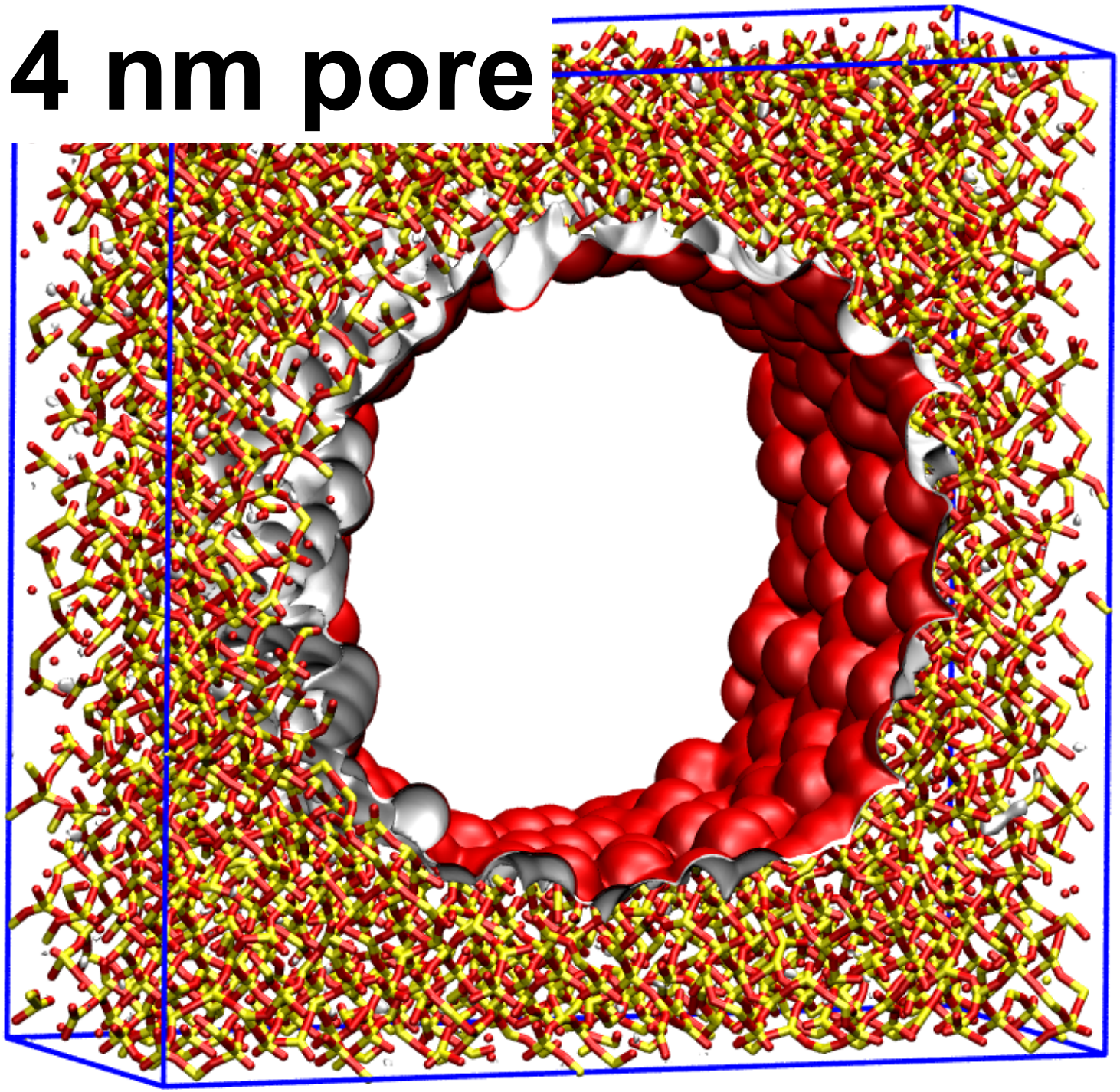

Figure 6

5.8 nm pore

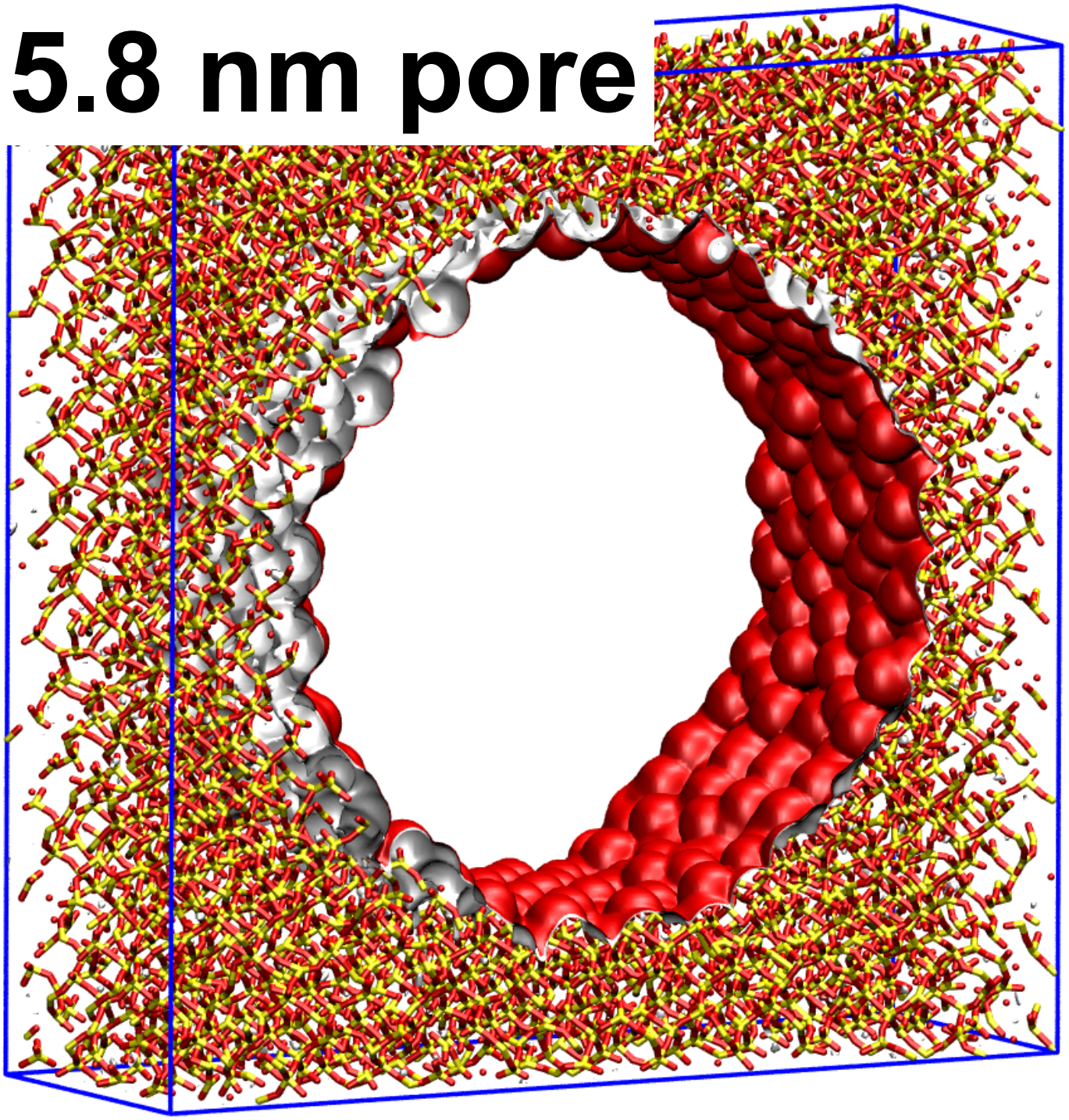

Figure 7

7.6 nm pore

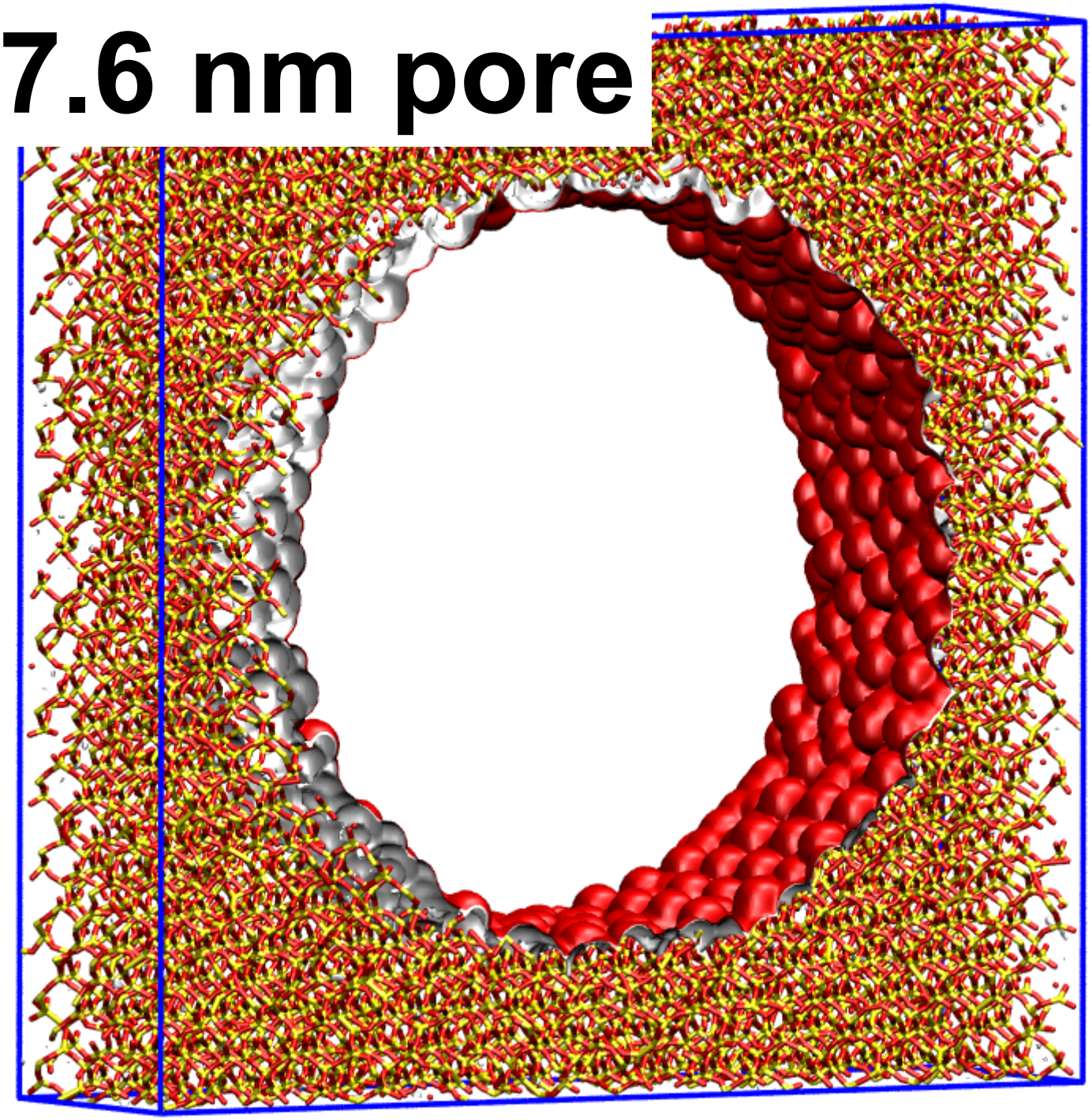

Figure 8

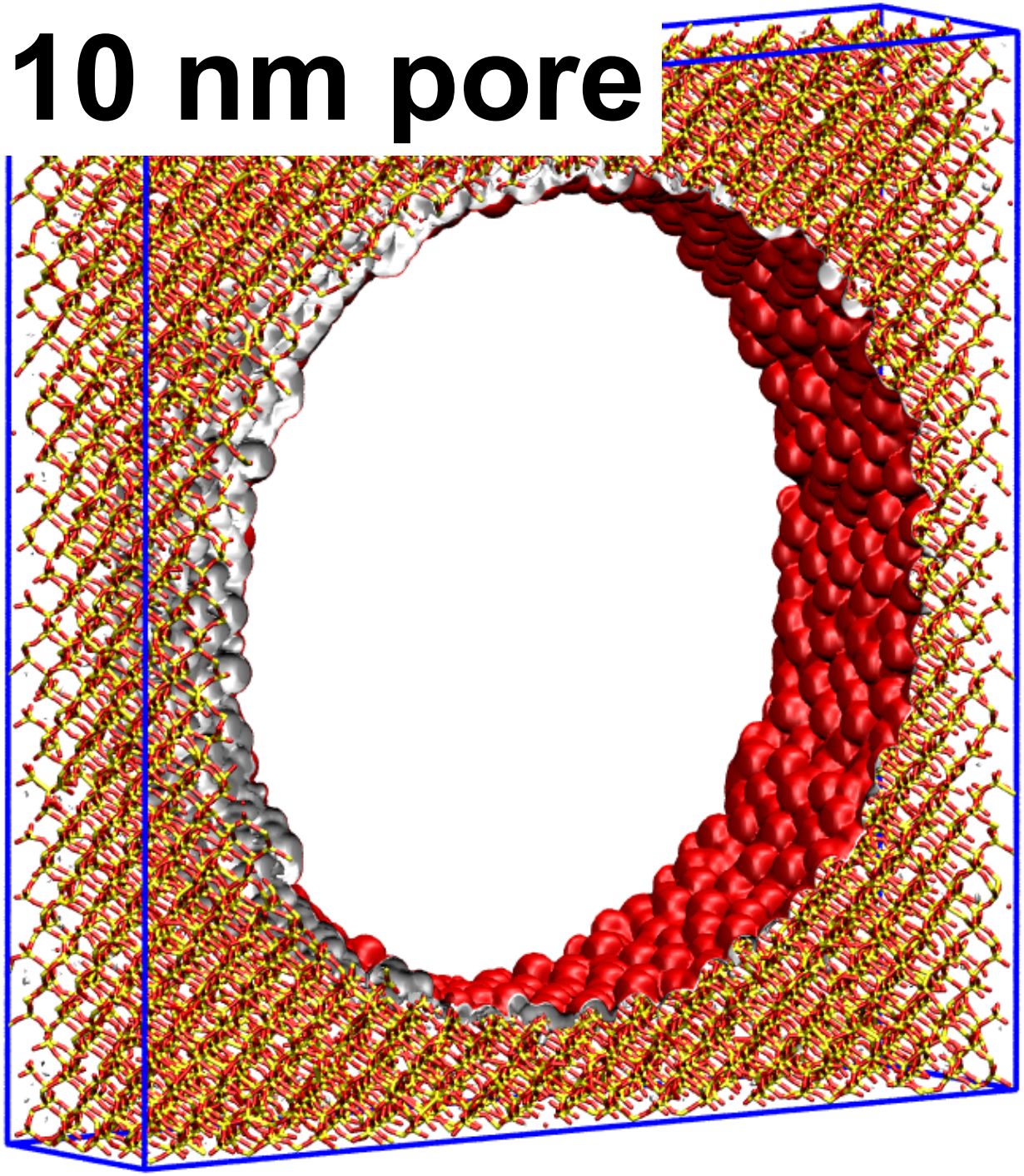

Pure fluids, 300 K

Figure 9

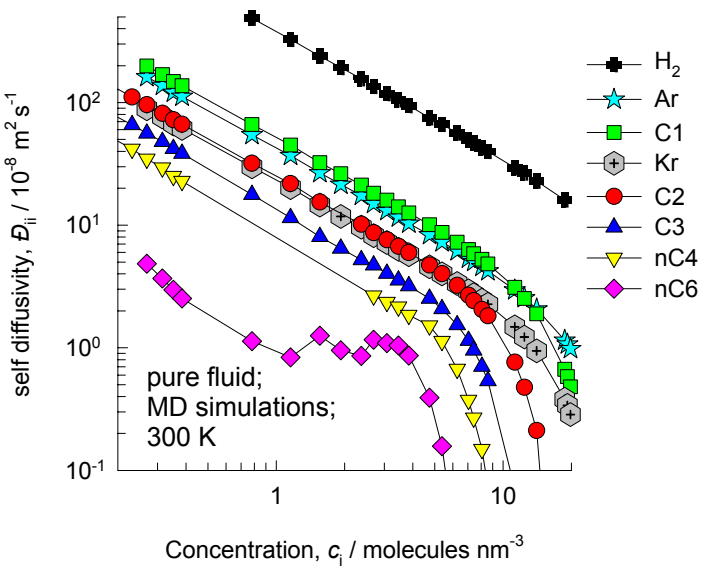

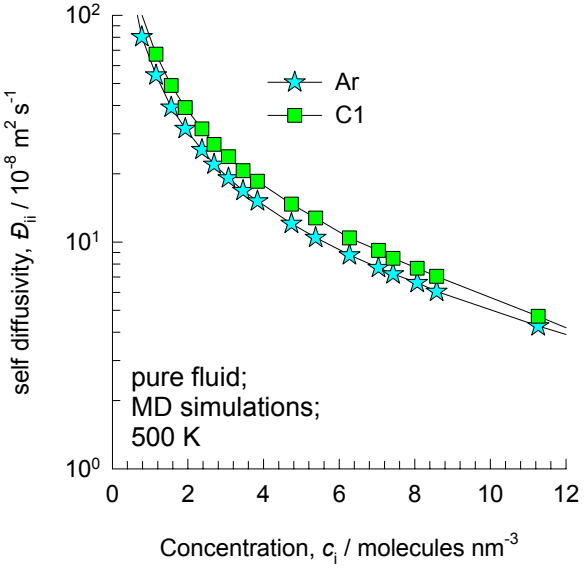

Pure & binary fluid mixtures, self diffusivities, 300 K

Figure 10

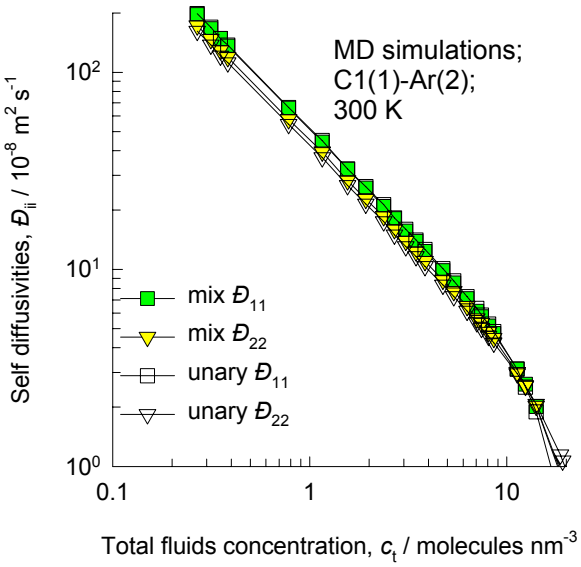

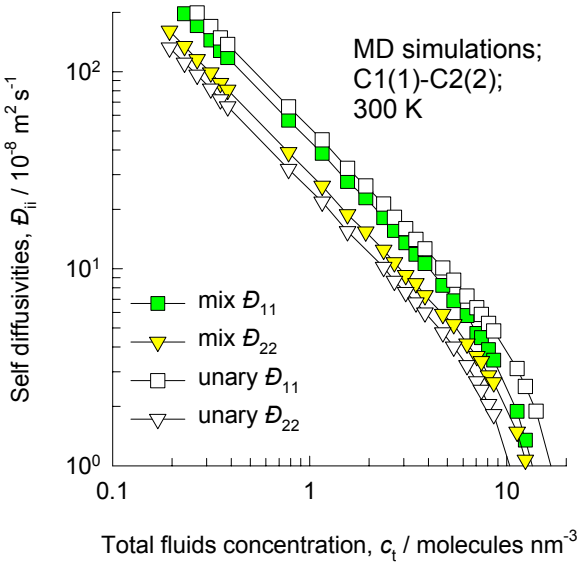

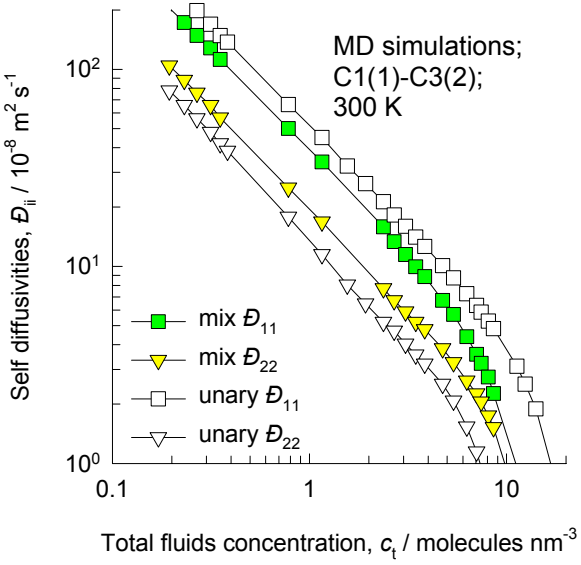

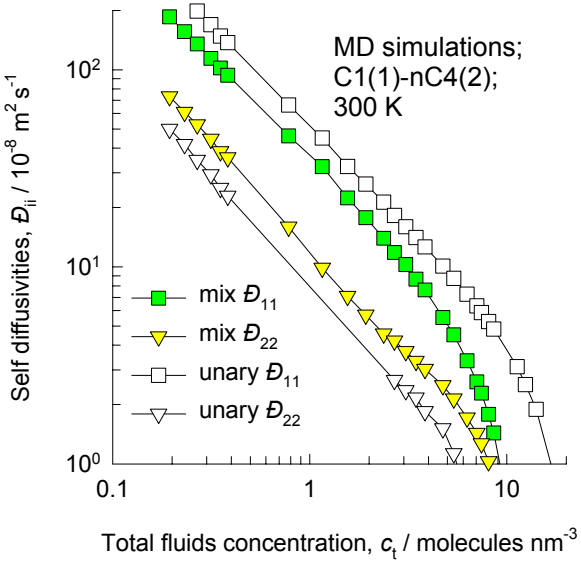

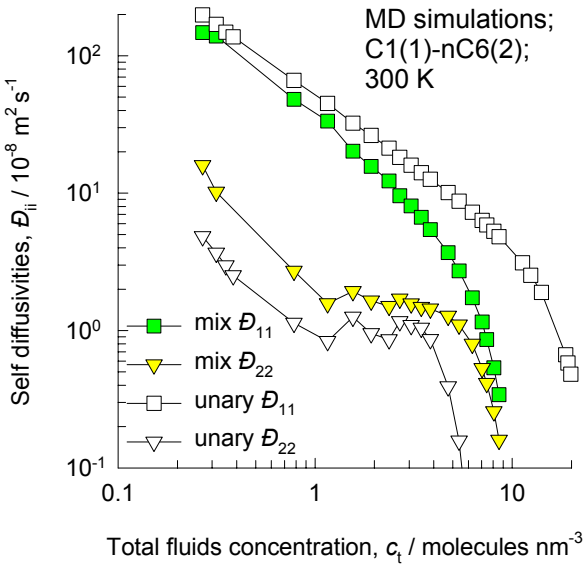

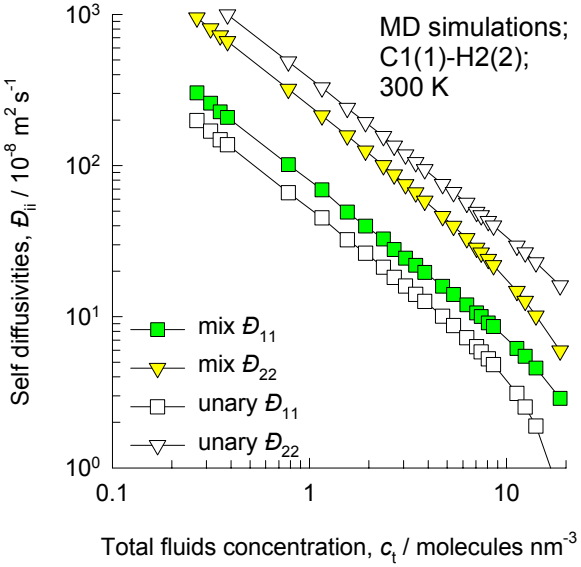

Pure & binary fluid mixtures, self-diffusivities, 300 K

Figure 11

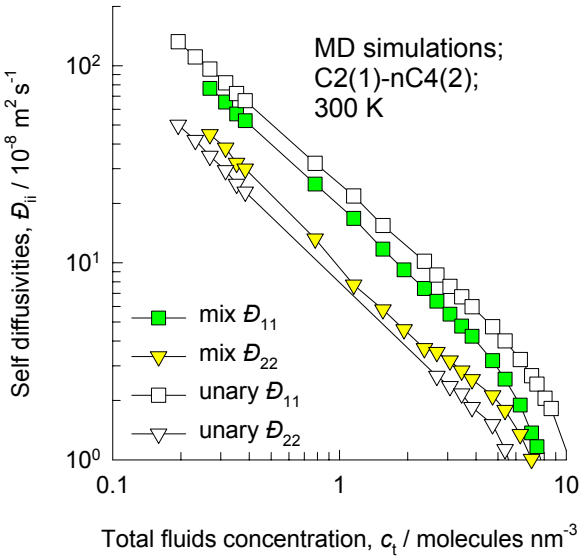

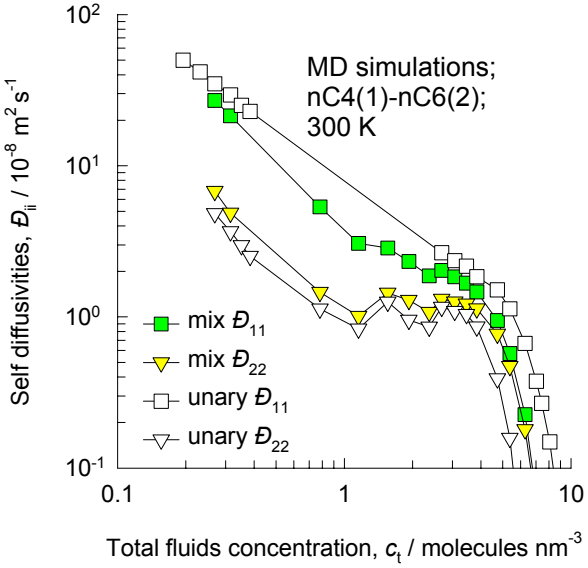

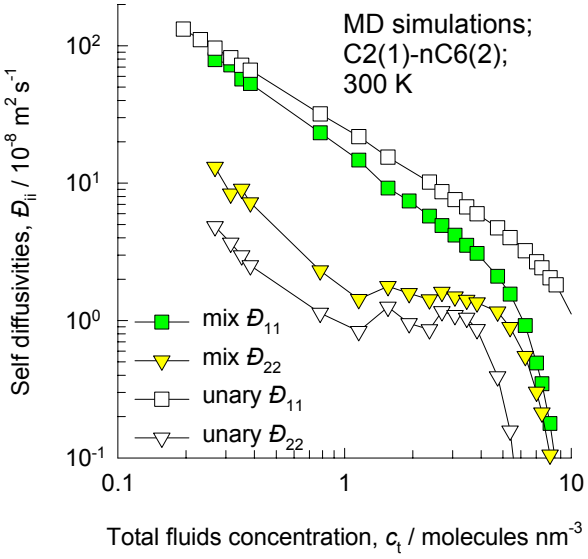

Binary fluid mixtures, M-S diffusivity, 300 K

Figure 12

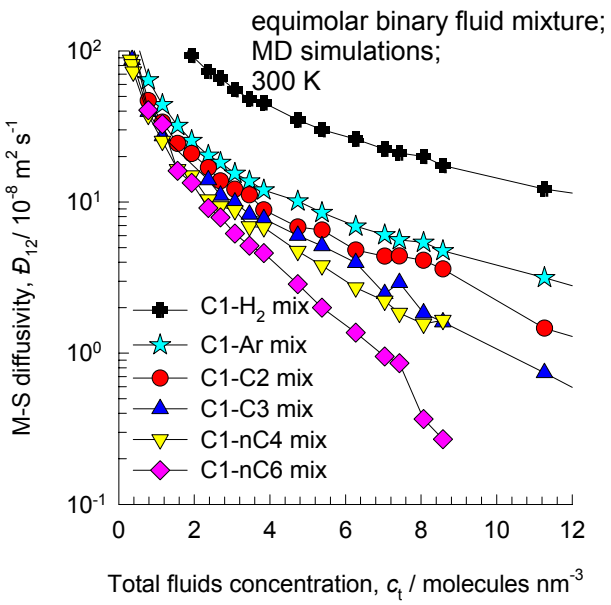

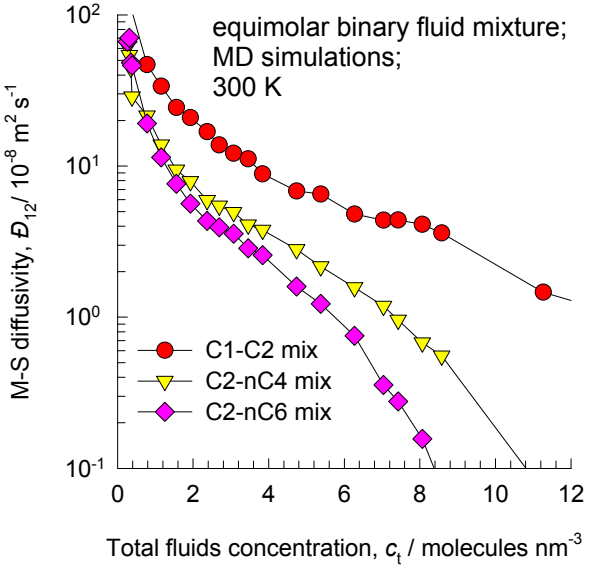

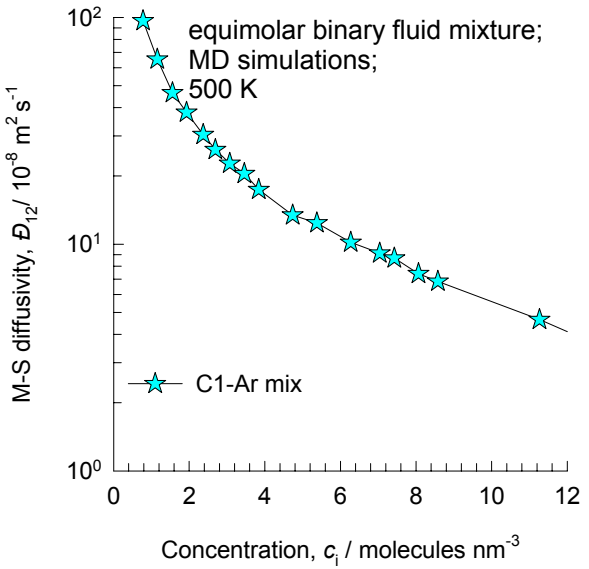

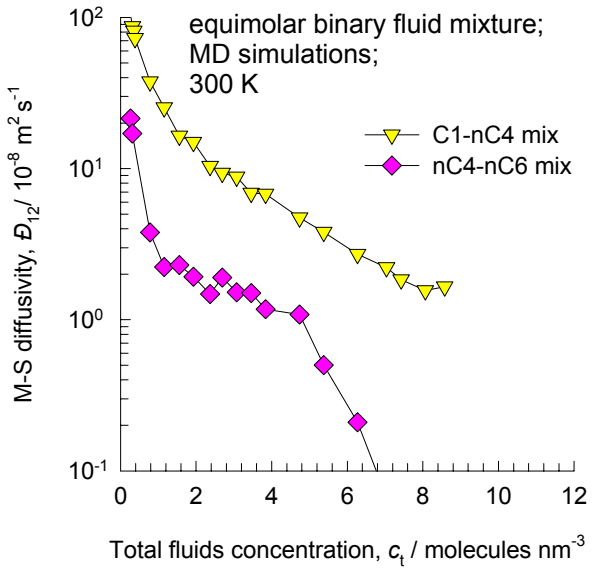

Shear viscosity of pure fluids, 300 K

Figure 13

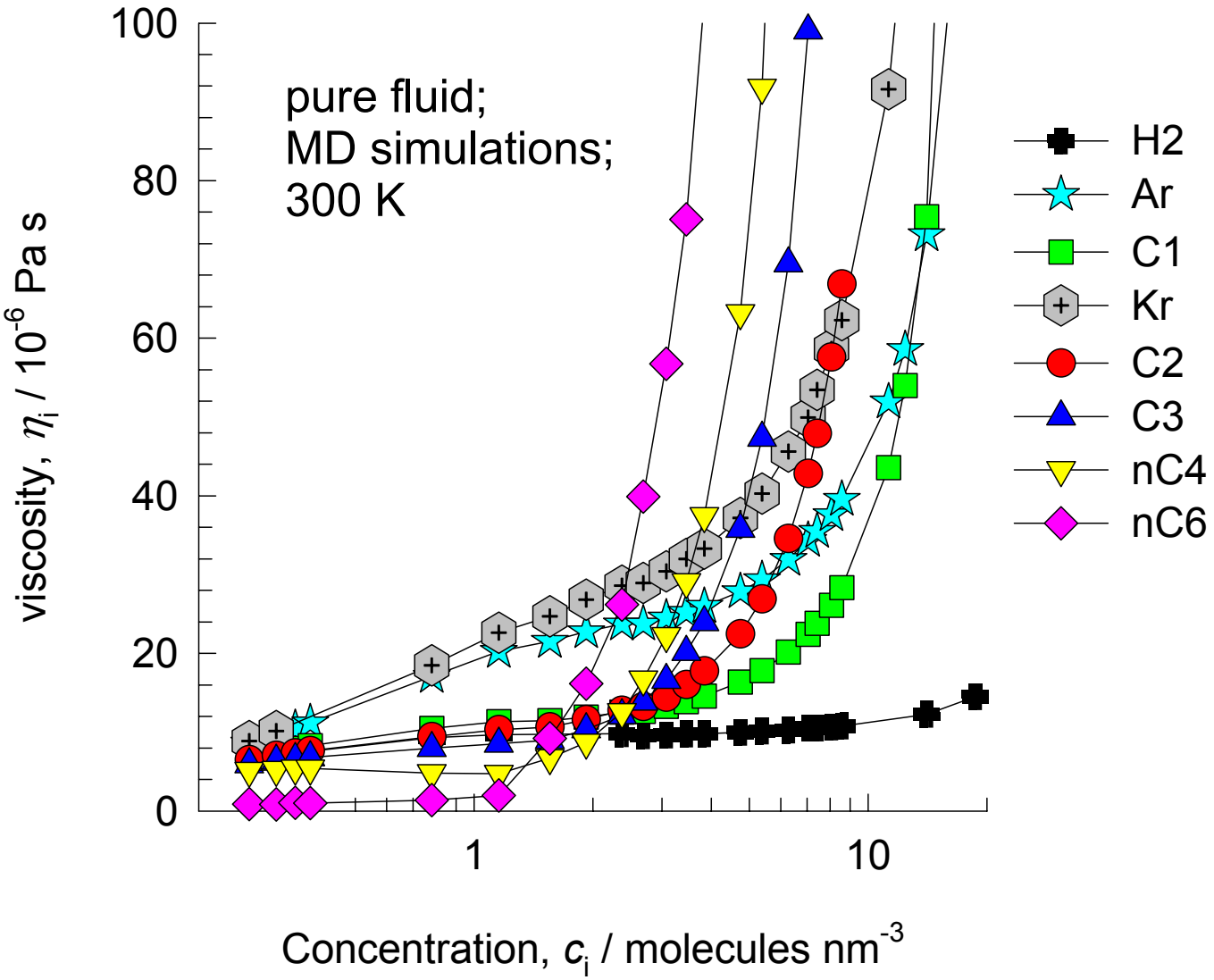

Figure 14

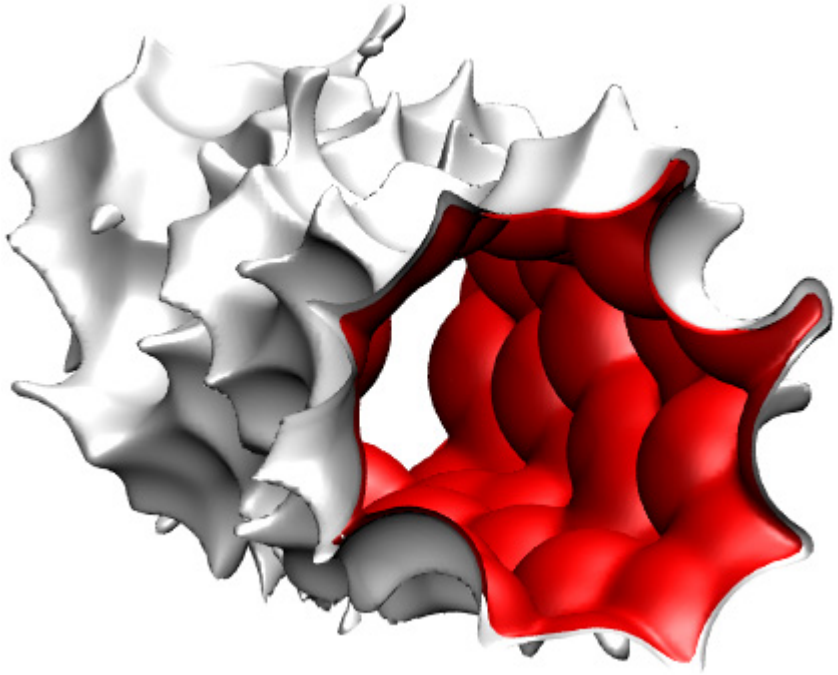

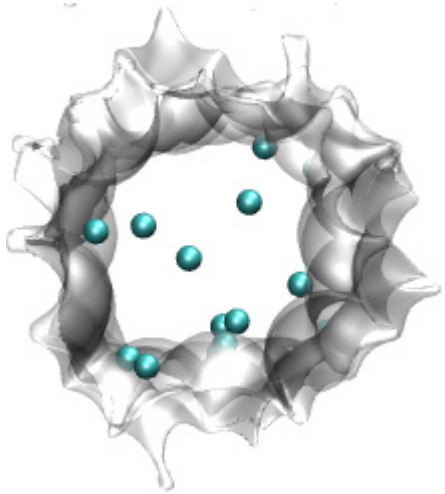

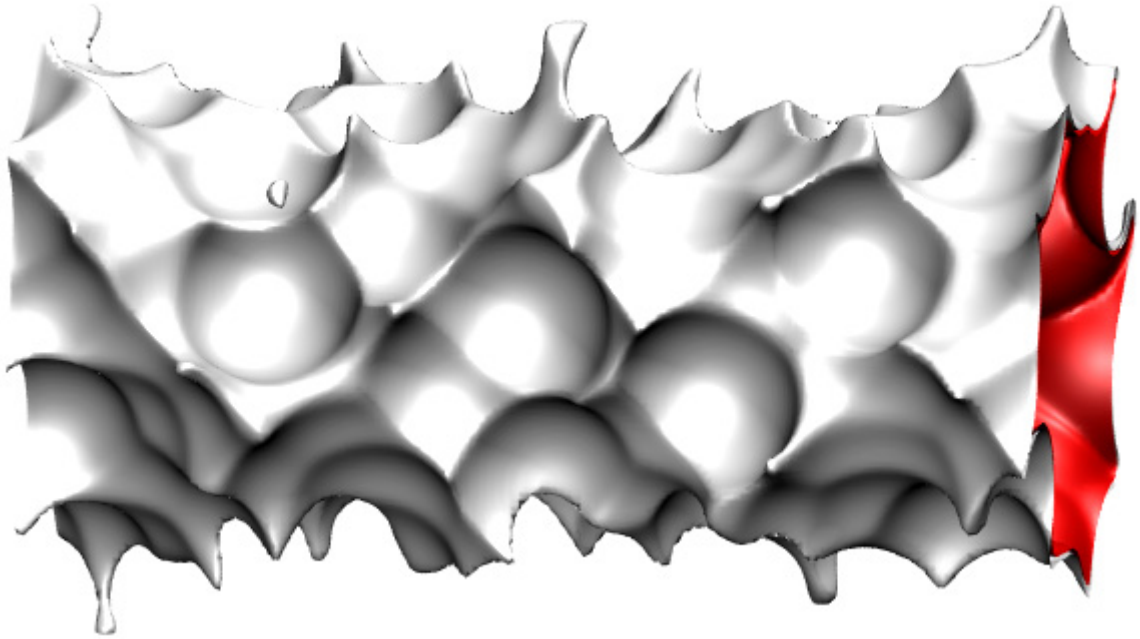

1 nm pore simulation results follow

Pure C1 and pure Ar, 1 nm pore, 300 K

Figure 15

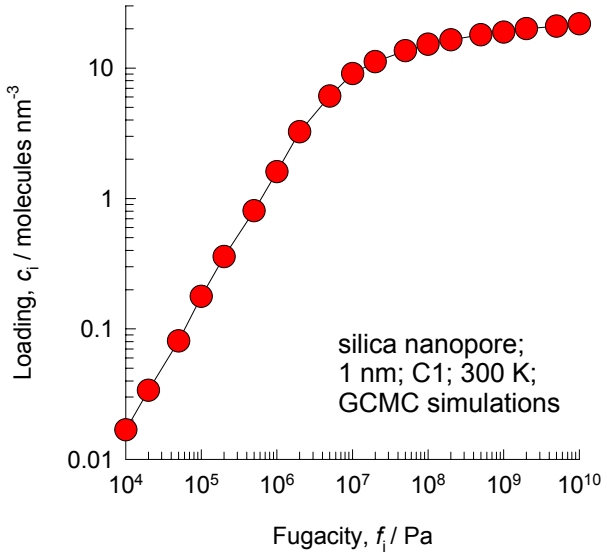

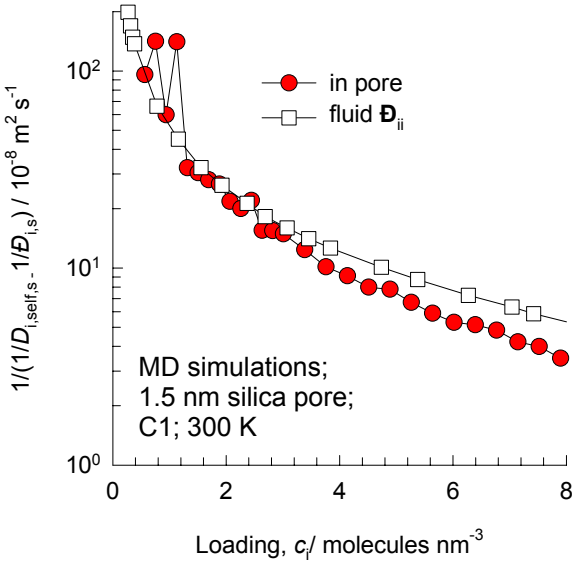

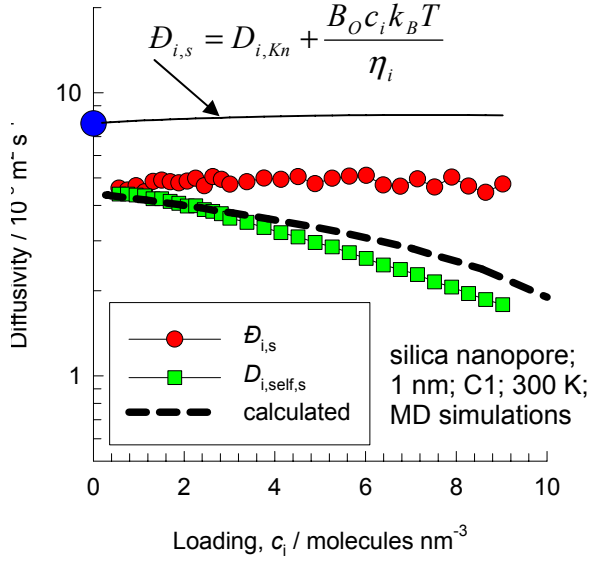

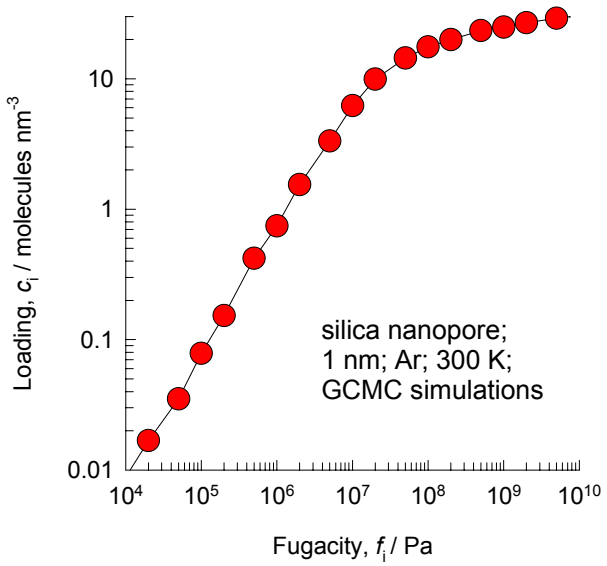

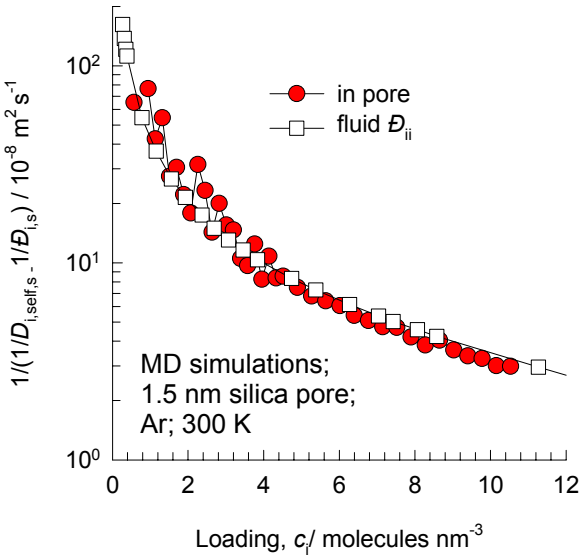

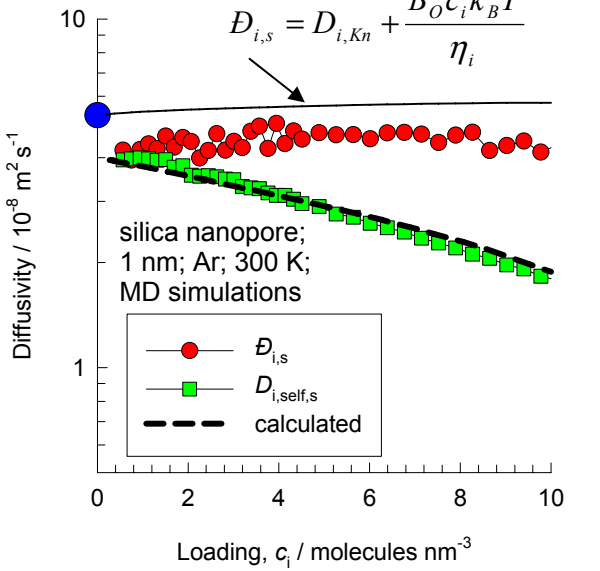

C1 –Ar mixture, 1 nm pore, 300 K

Figure 16

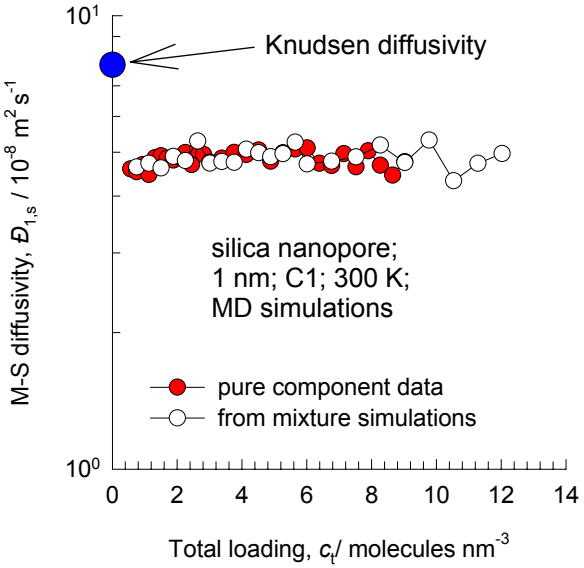

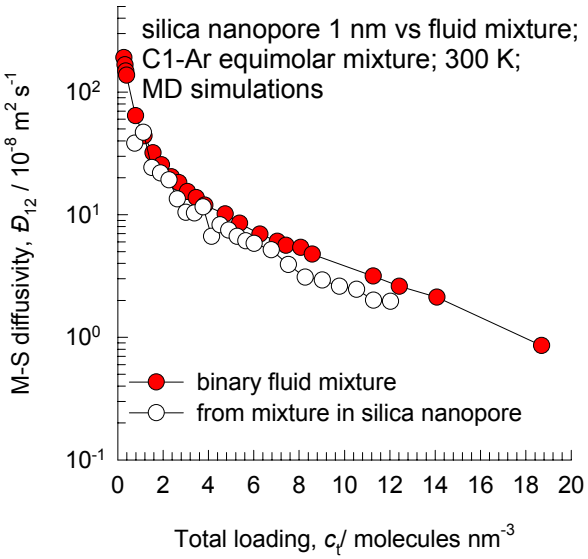

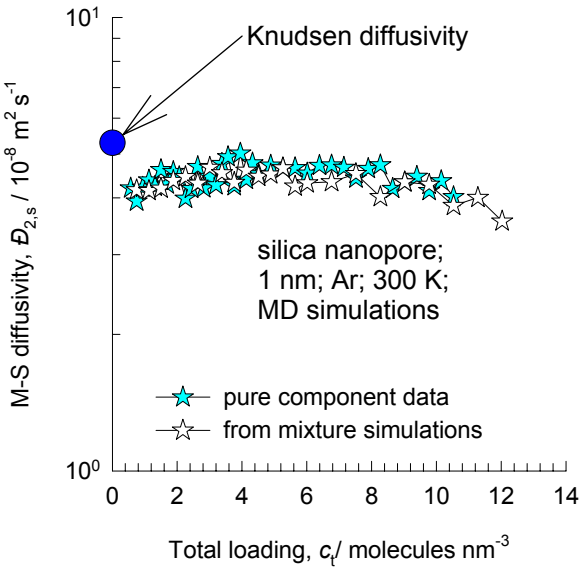

Figure 17

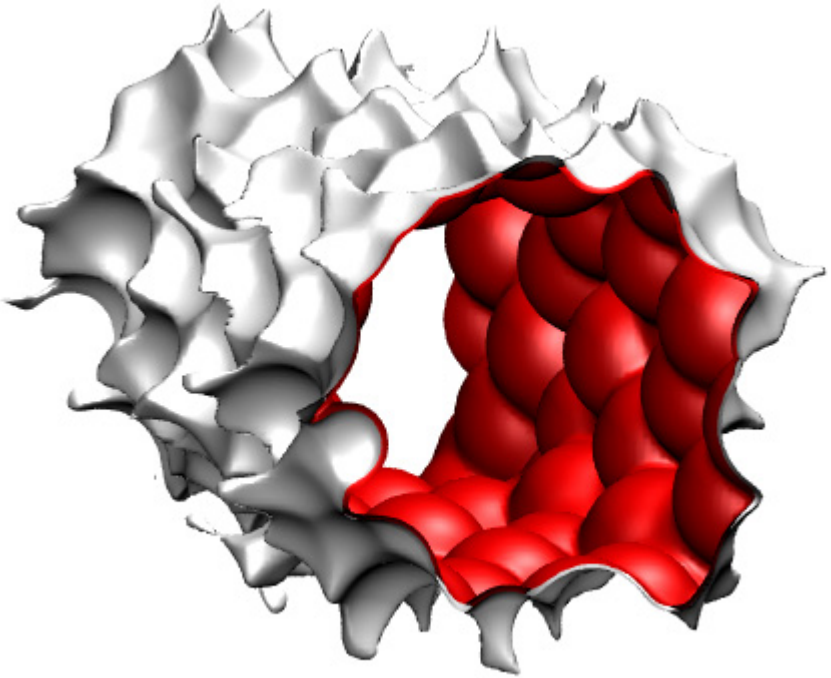

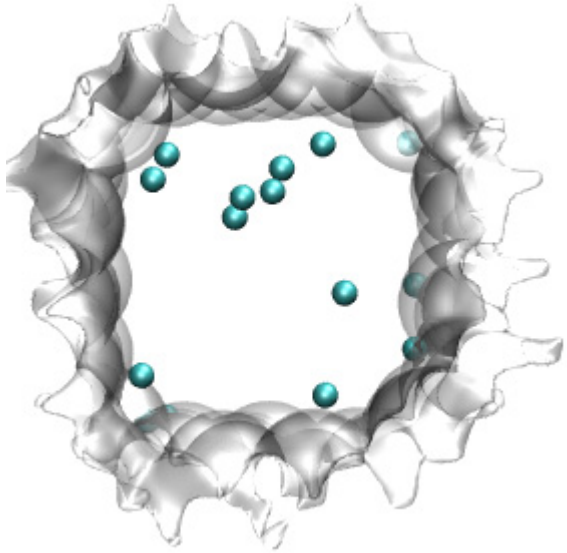

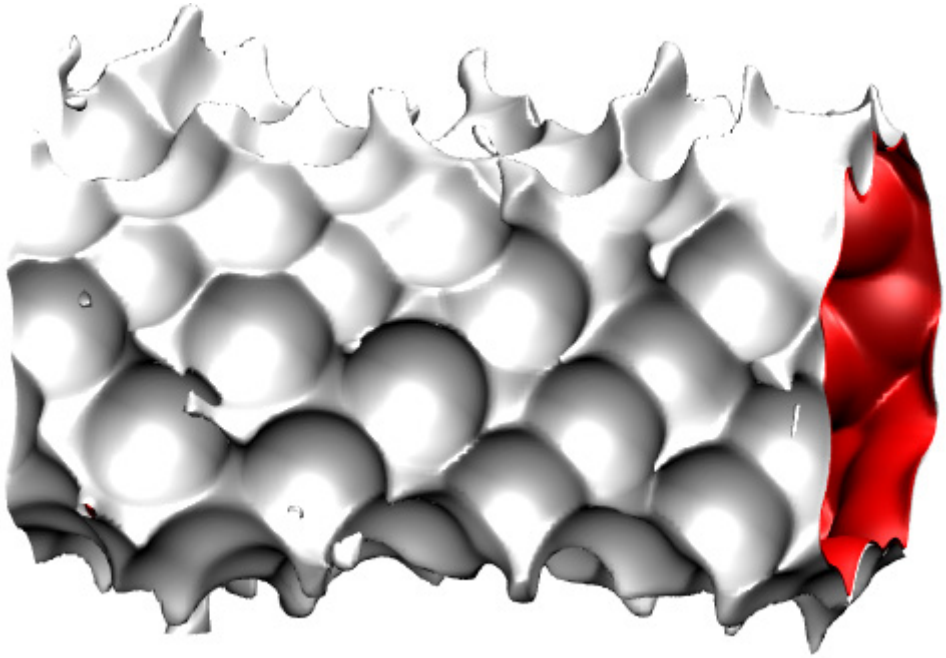

1.5 nm pore simulation results follow

Pure C1 and pure Ar, 1.5 nm pore, 300 K

Figure 18

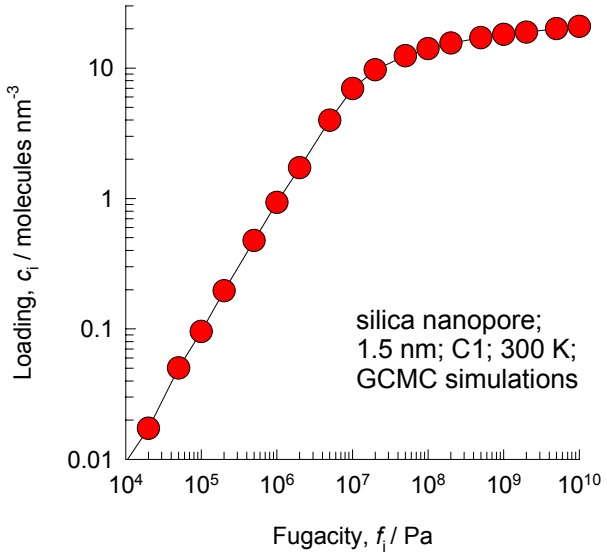

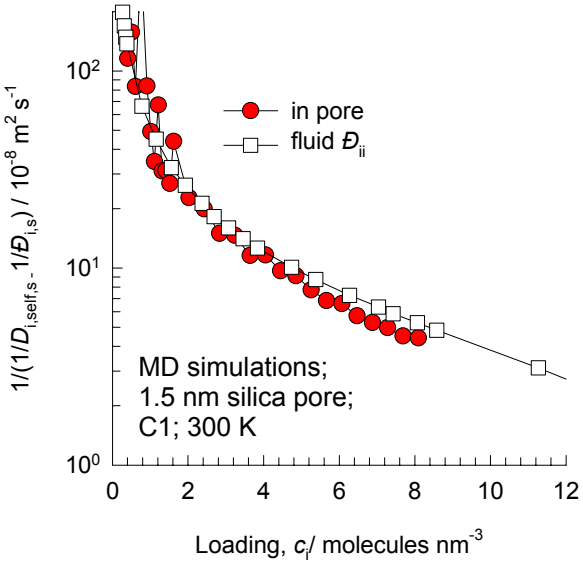

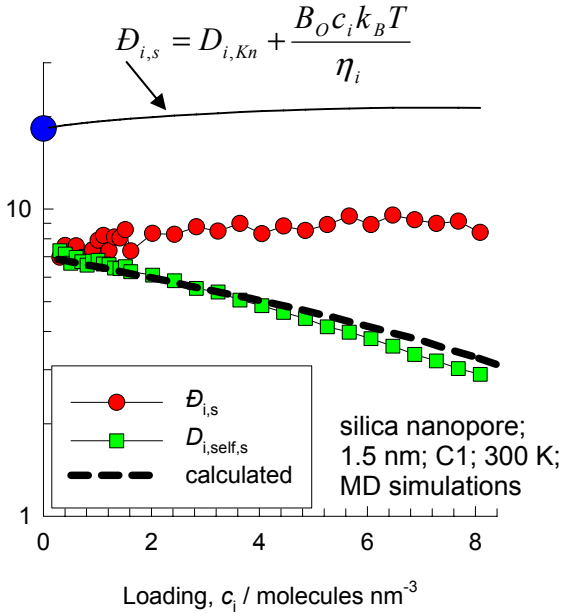

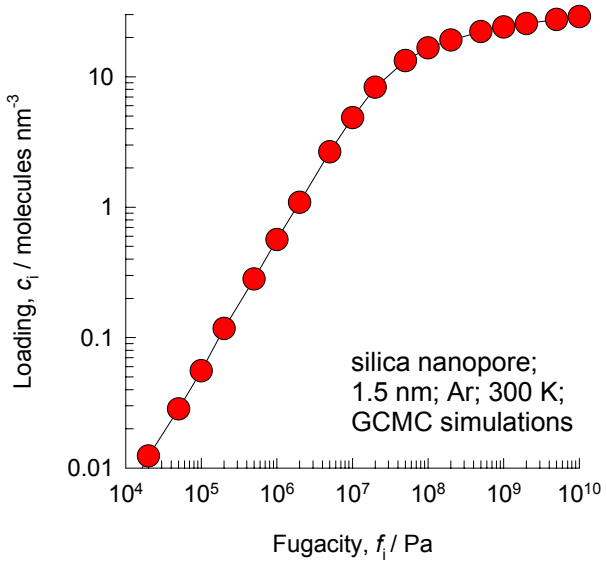

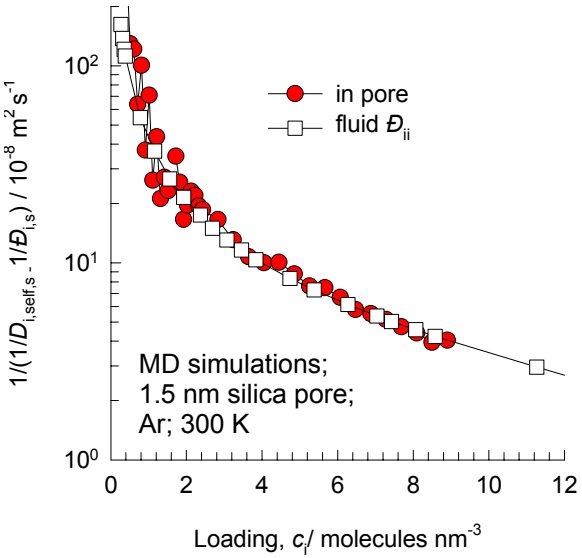

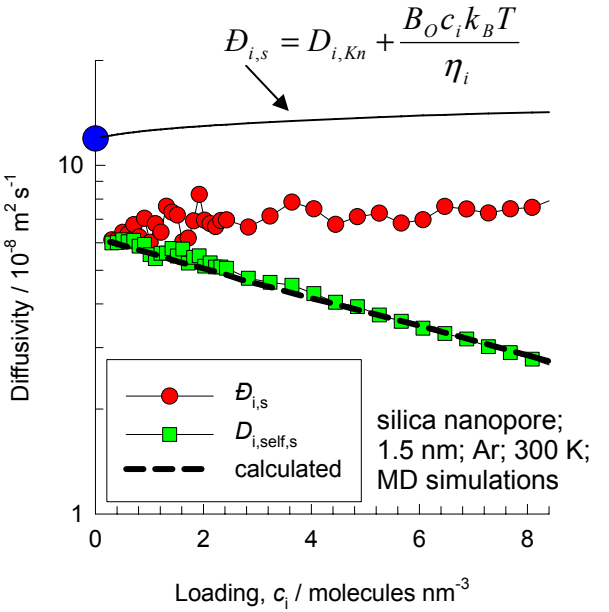

C1 –Ar mixture, 1.5 nm pore, 300 K

Figure 19

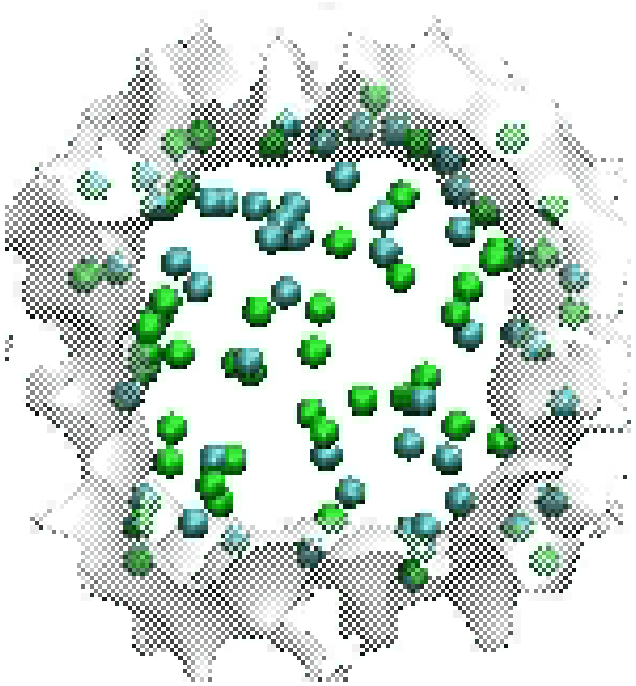

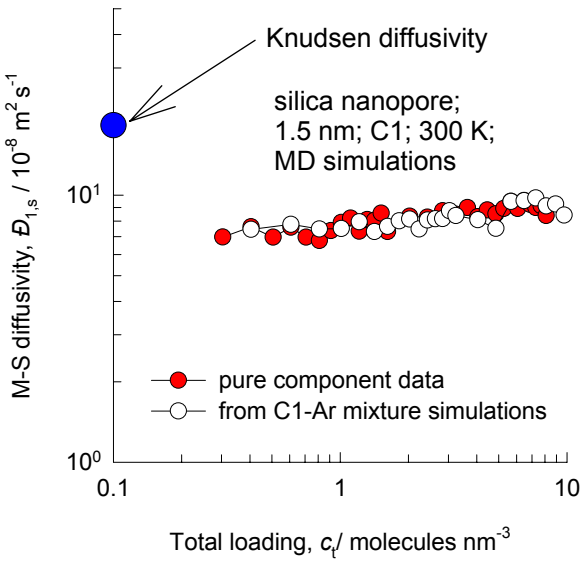

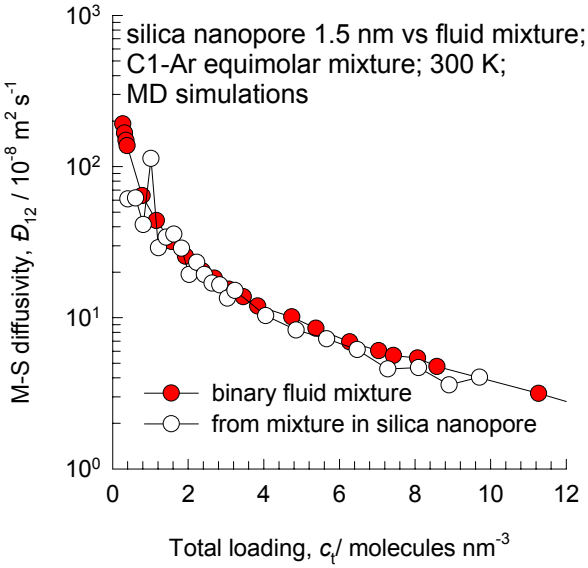

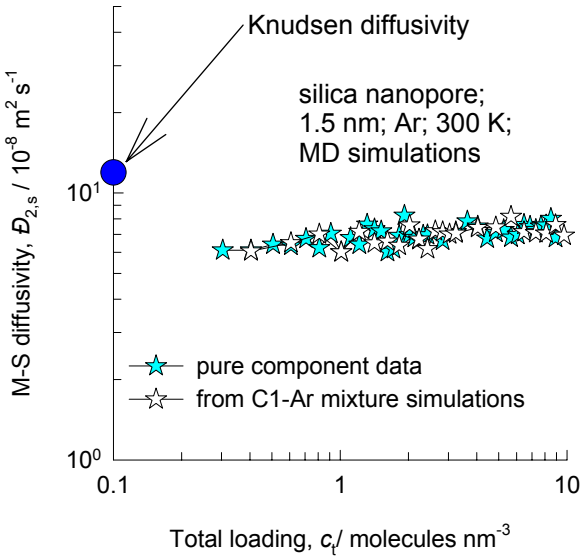

Figure 20

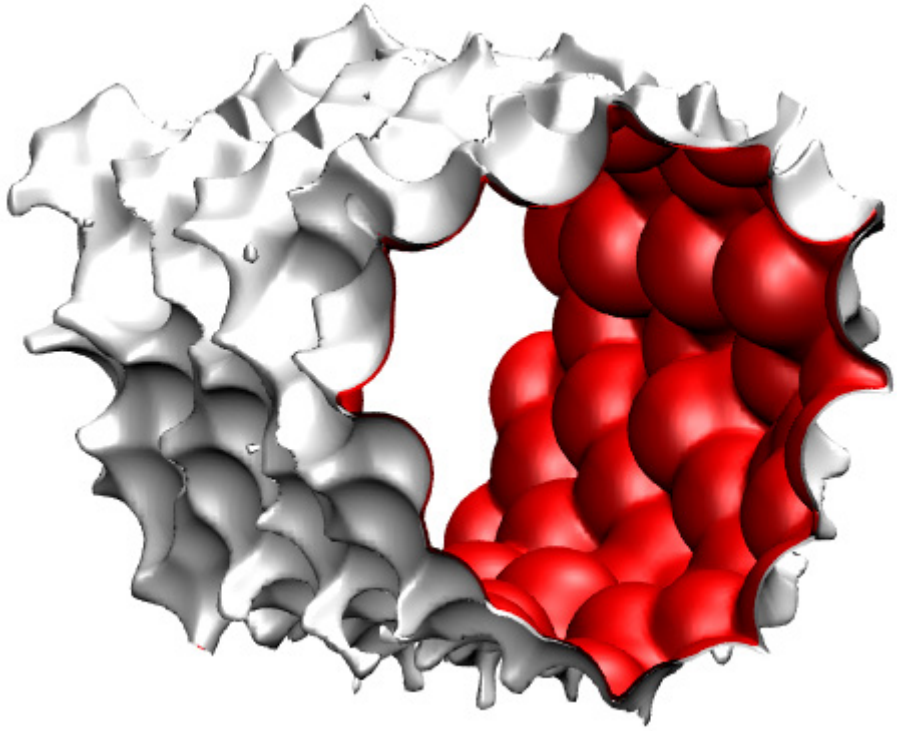

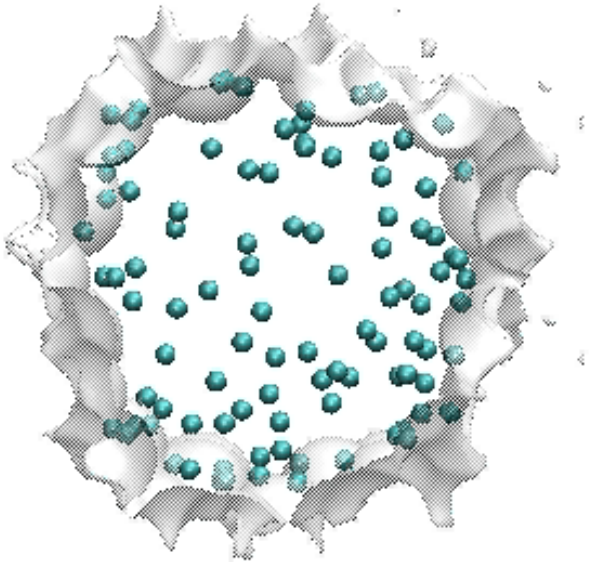

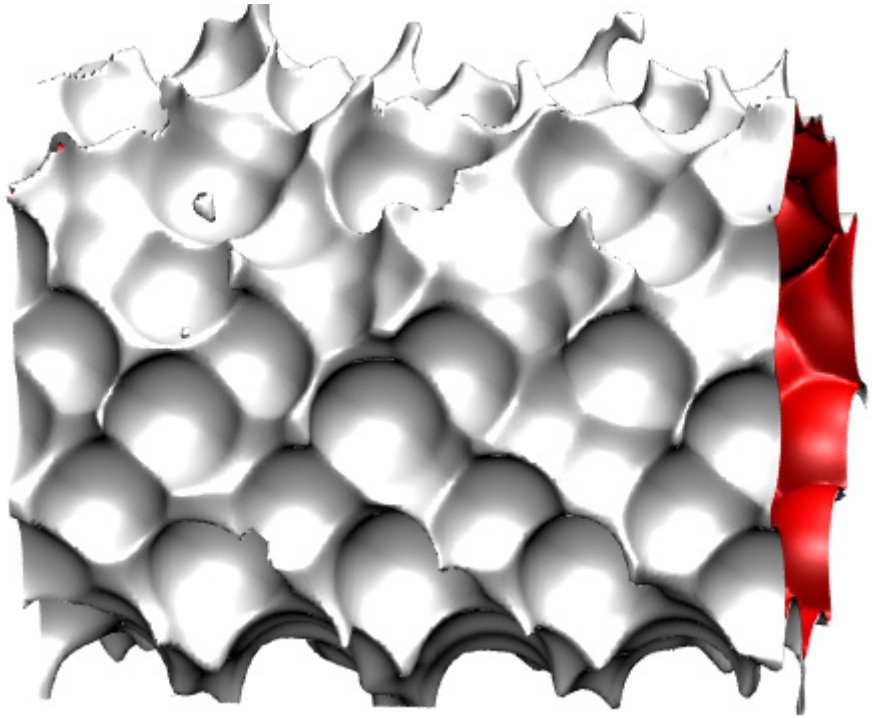

2 nm pore simulation results follow

Pure C1 and pure Ar, 2 nm pore, 300 K

Figure 21

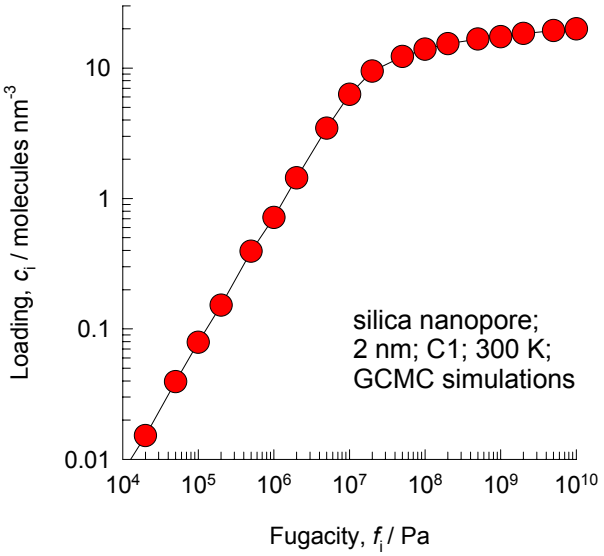

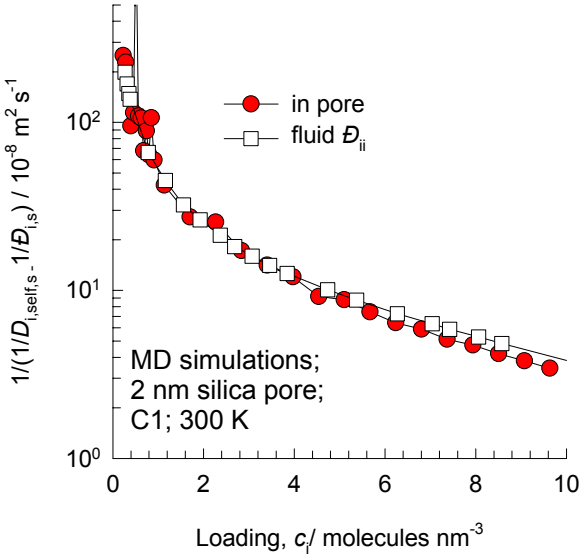

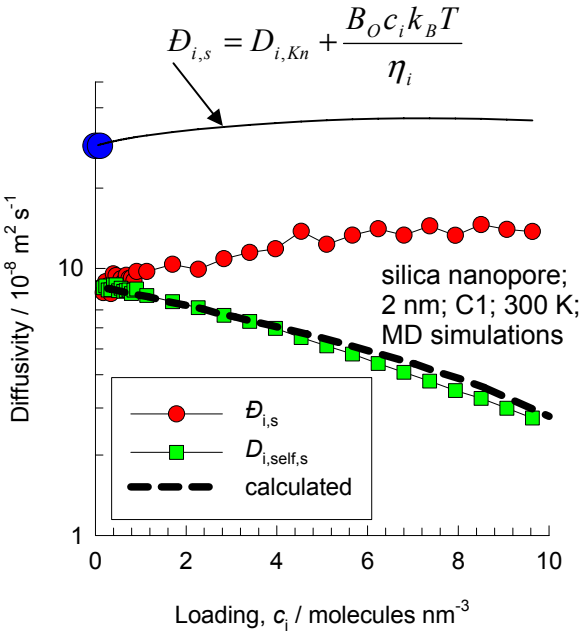

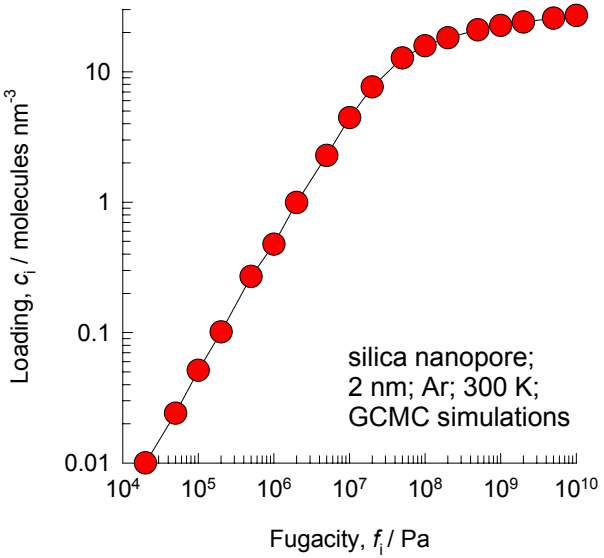

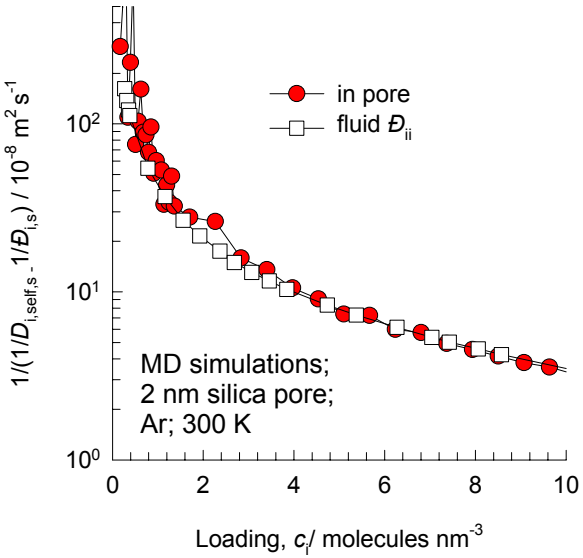

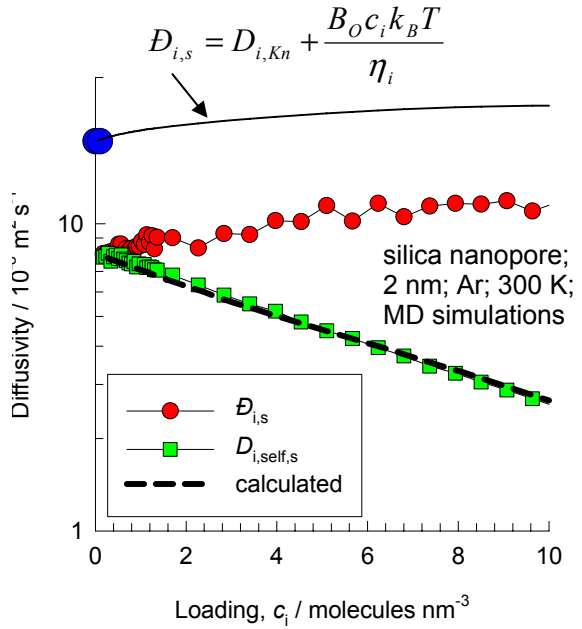

C1 –Ar mixture, 2 nm pore, 300 K

Figure 22

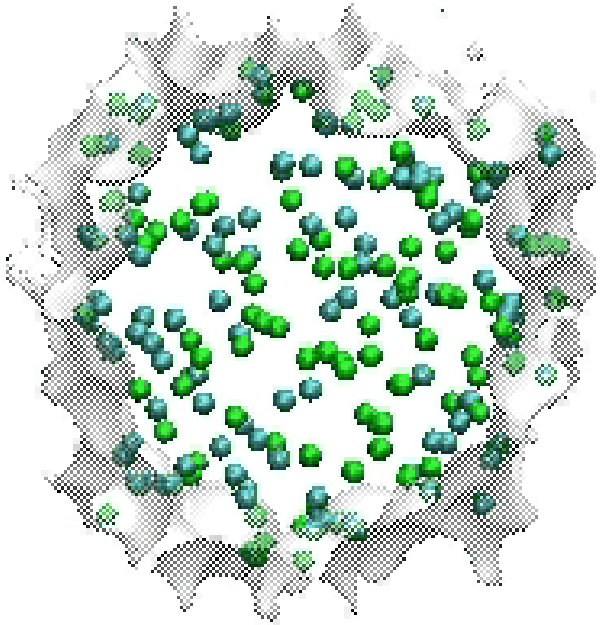

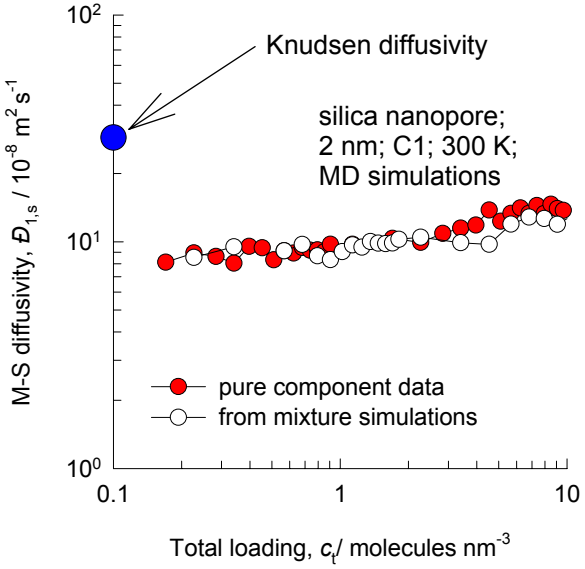

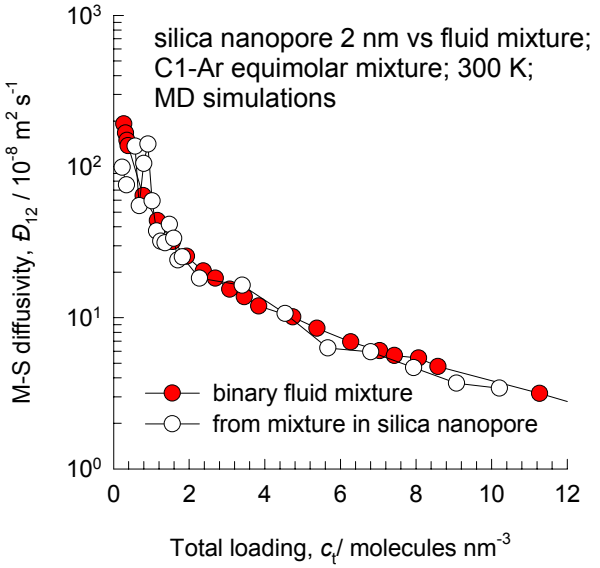

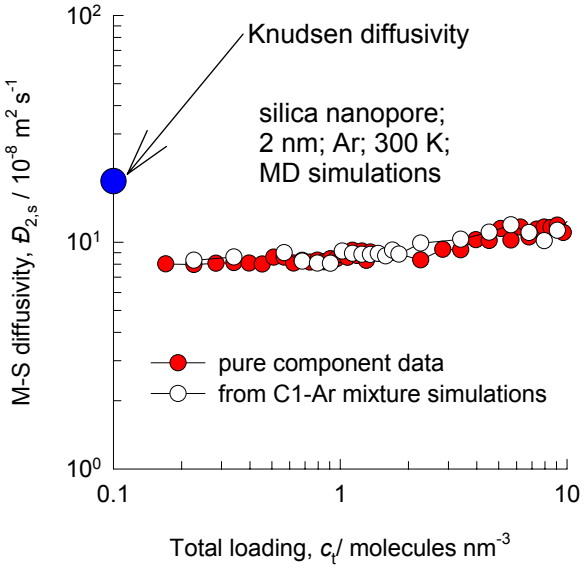

Pure C1 and pure Ar, 2 nm pore, 500 K

Figure 23

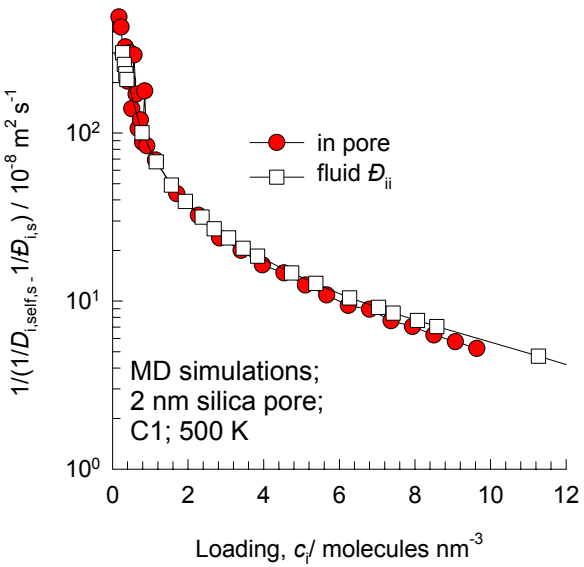

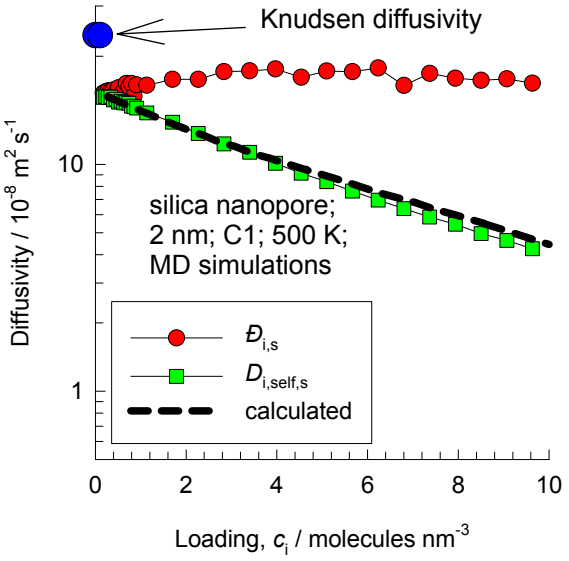

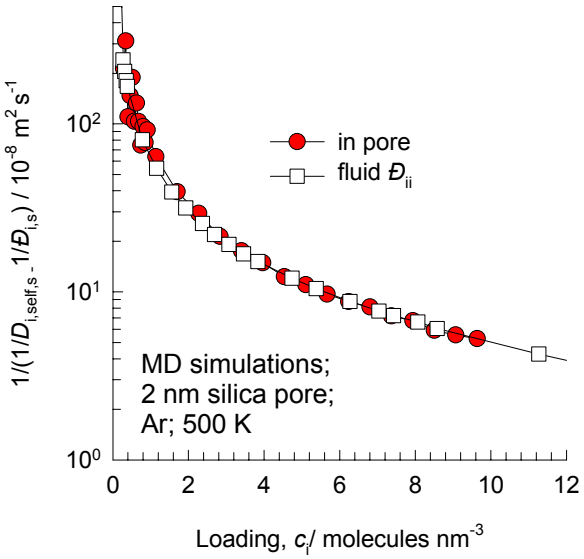

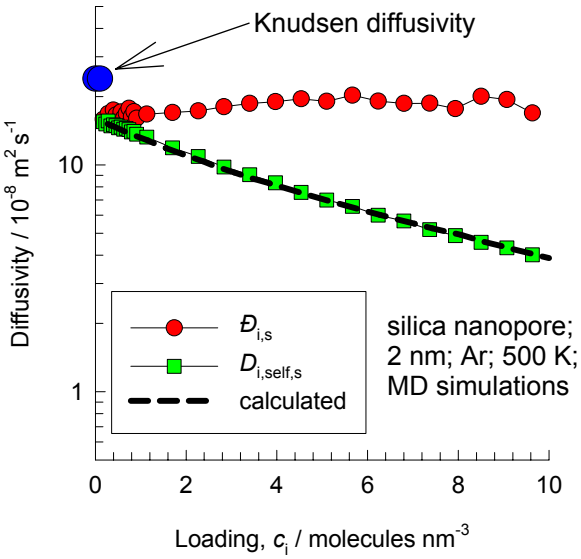

C1 –Ar mixture, 2 nm pore, 500 K

Figure 24

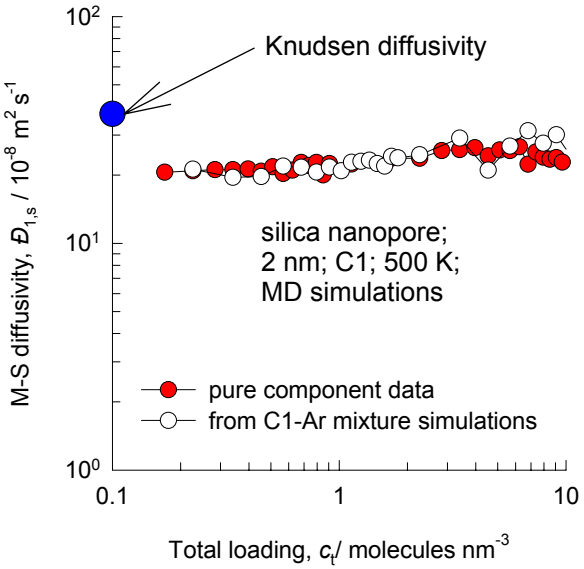

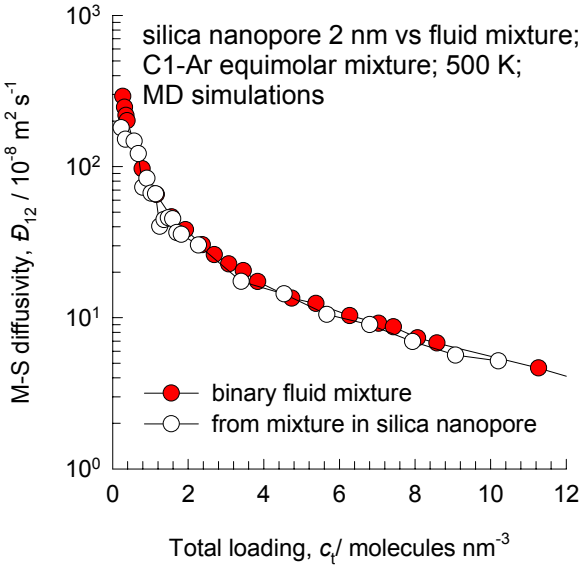

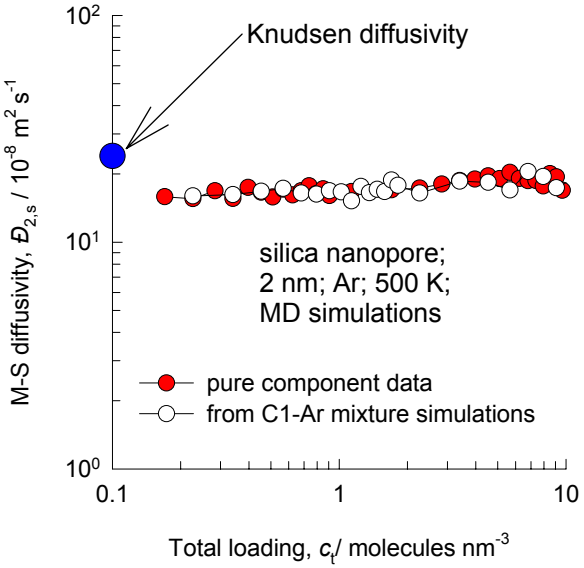

Figure 25

Pure C1, 2 nm pore, 200 K

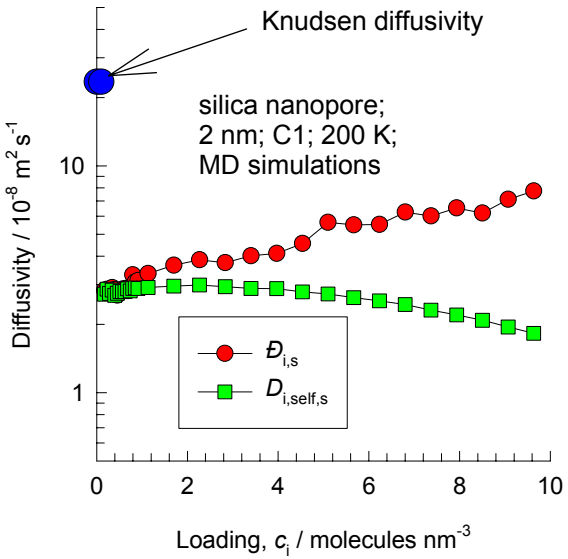

Pure Ar, 2 nm pore, 700 K

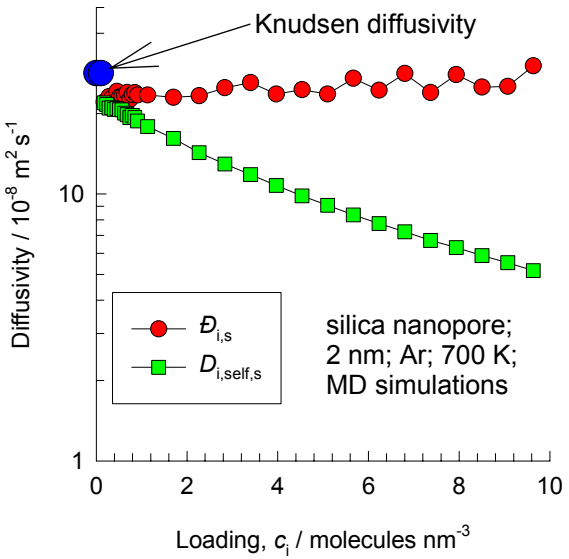

Pure Ar, 2 nm pore, 1200 K

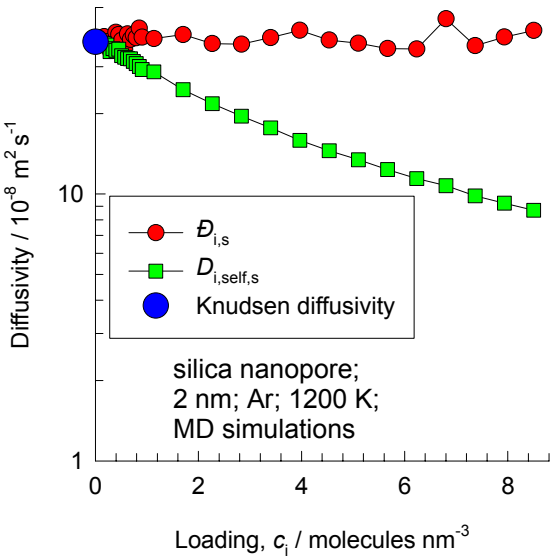

Pure Kr, 2 nm pore, 300 K

Figure 26

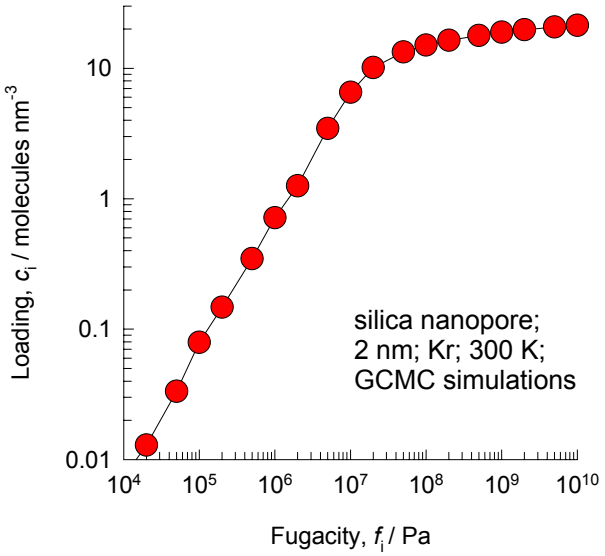

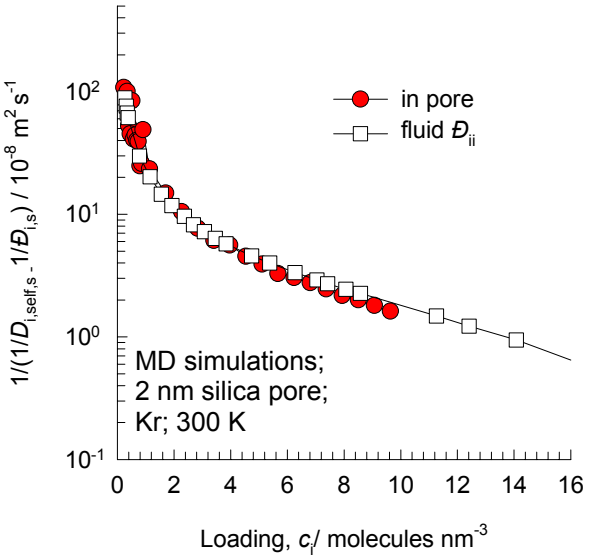

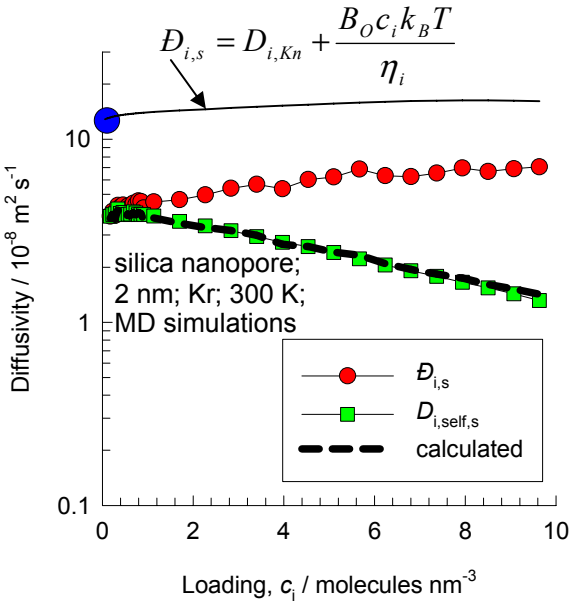

Pure C2, Pure C3, 2 nm pore, 300 K

Figure 27

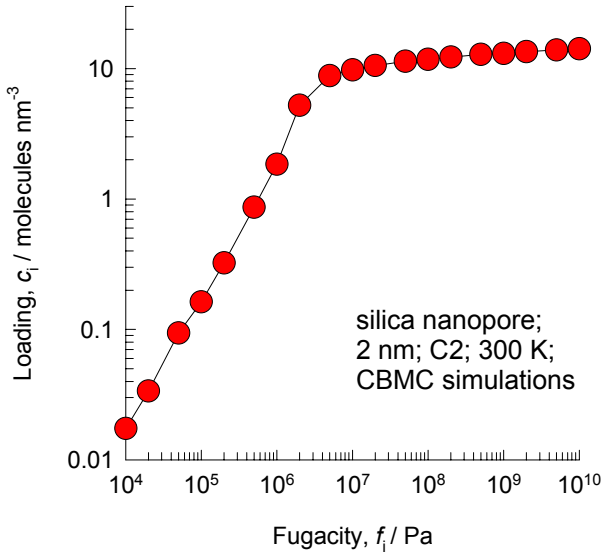

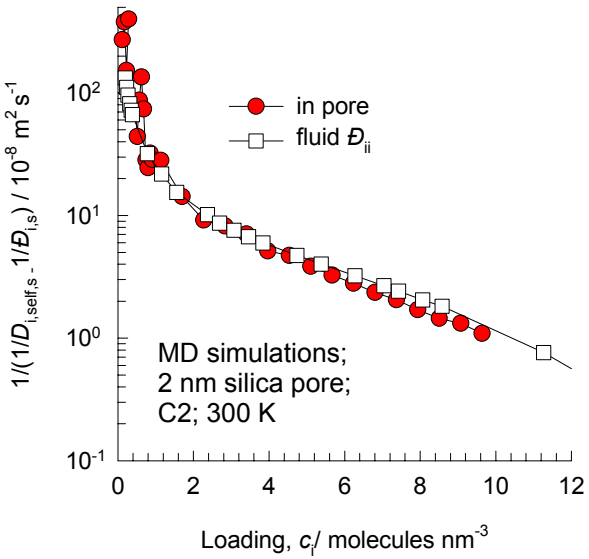

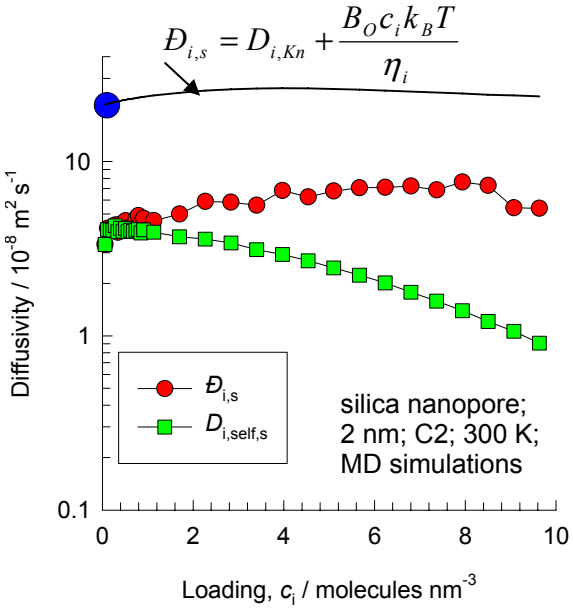

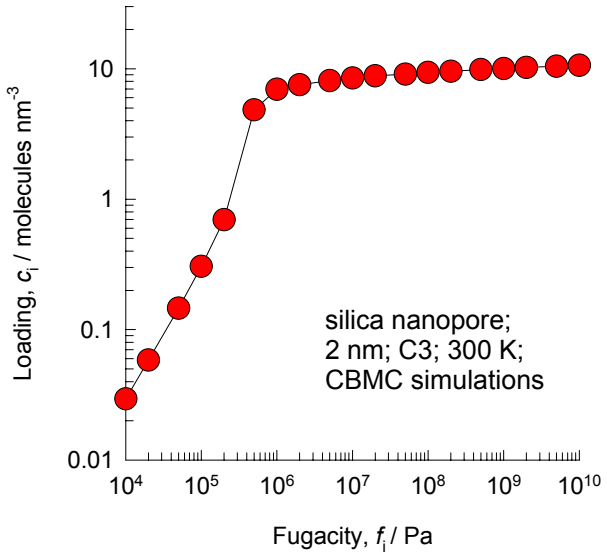

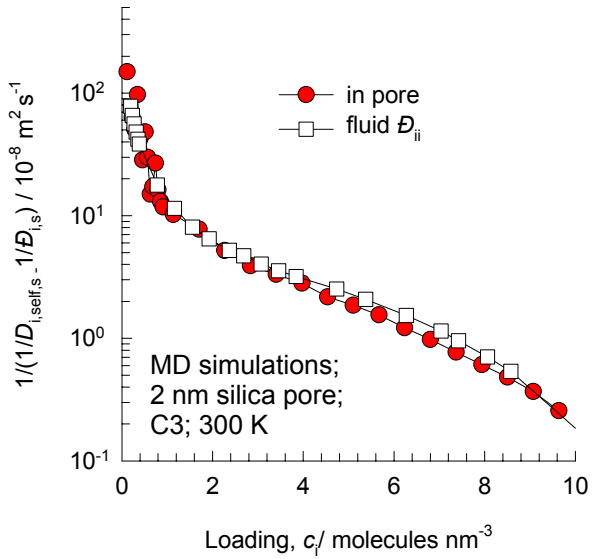

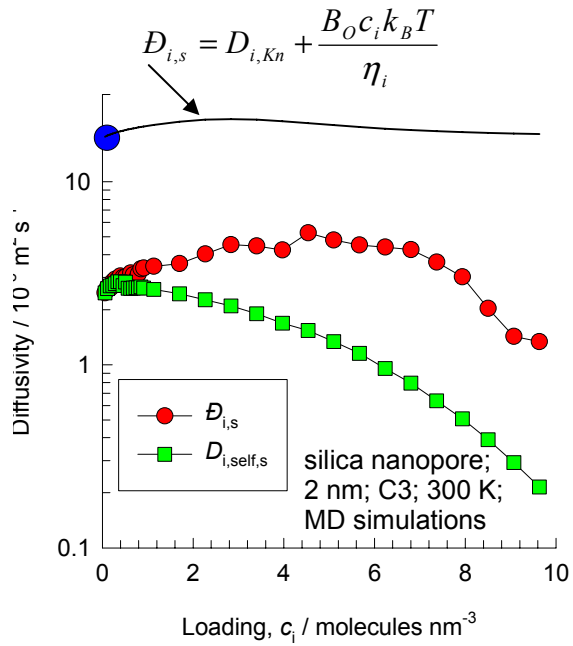

Pure nC4, Pure nC6, 2 nm pore, 300 K

Figure 28

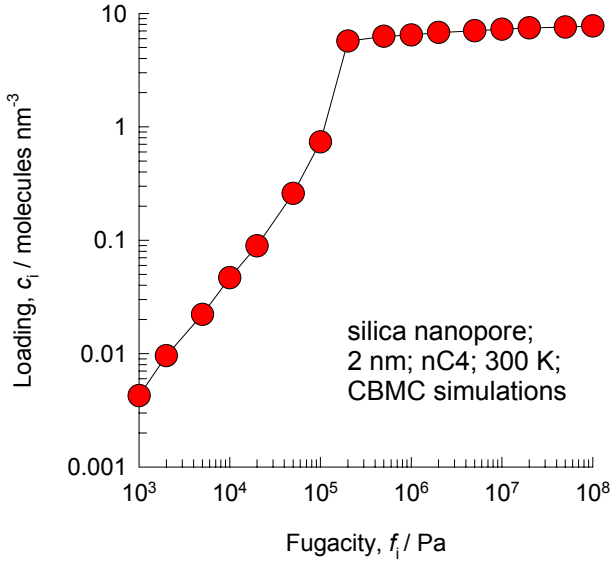

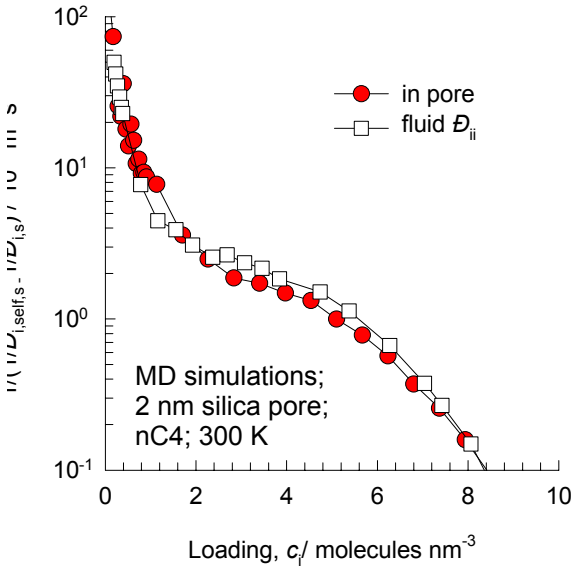

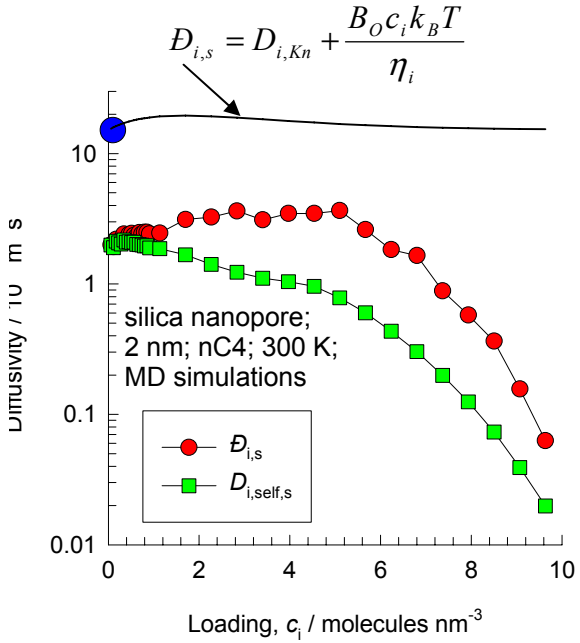

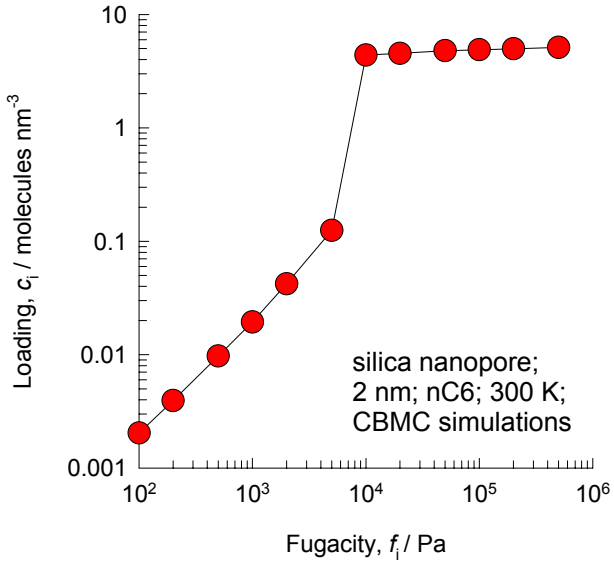

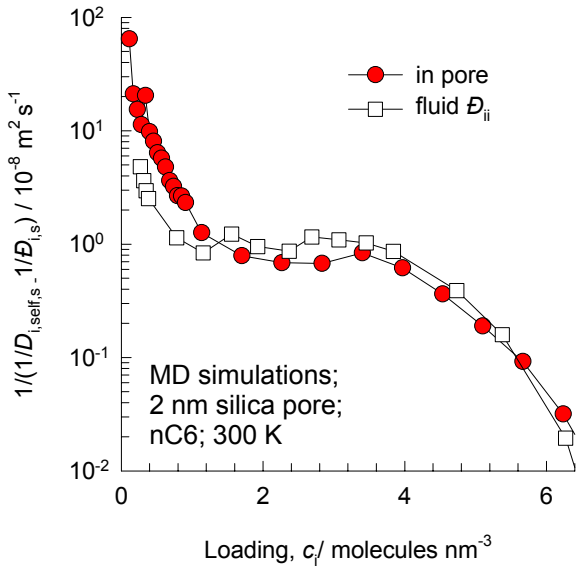

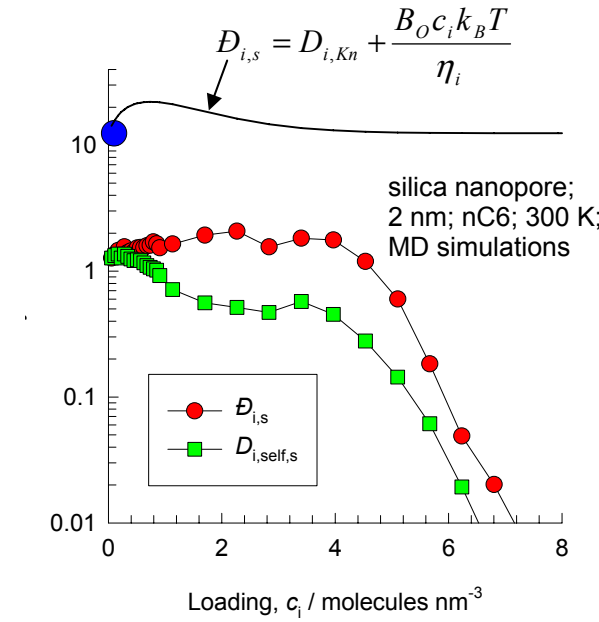

Figure 29

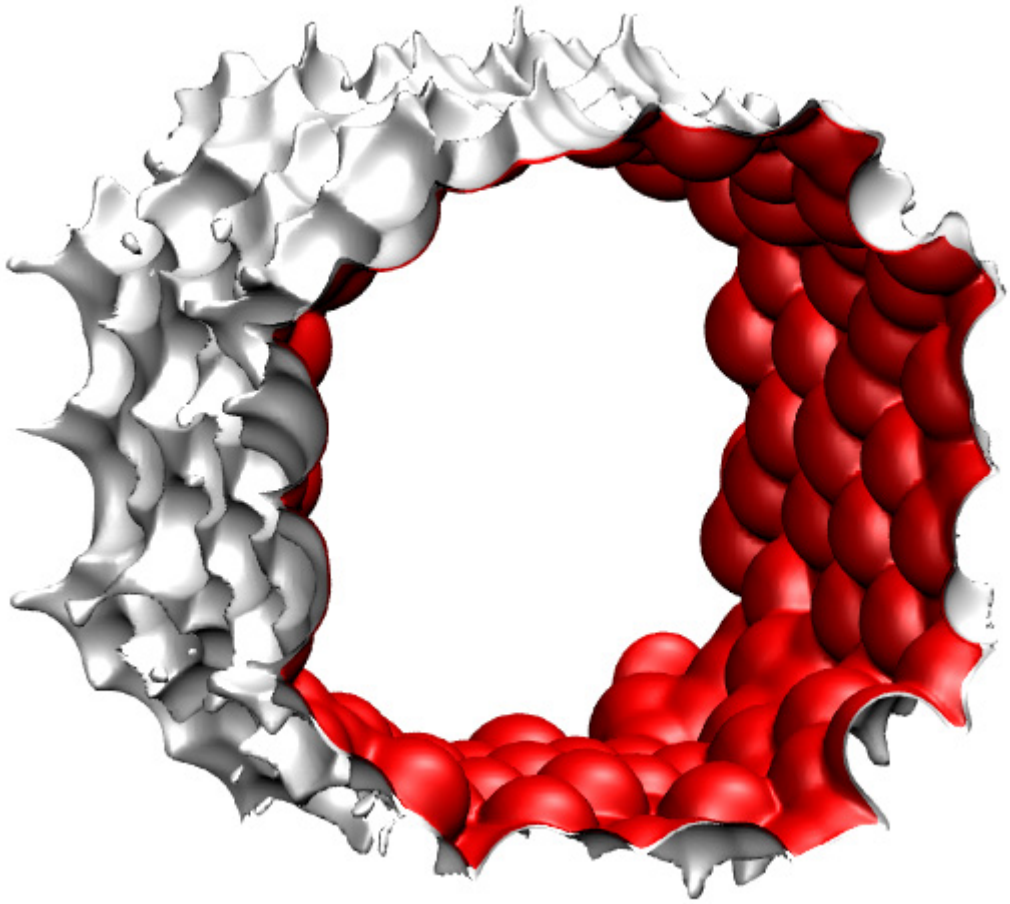

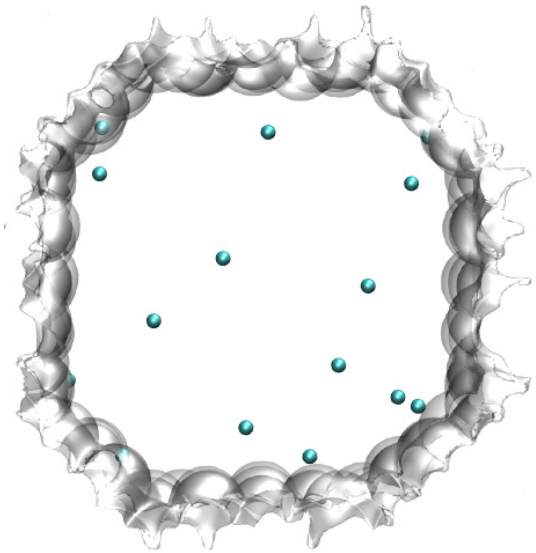

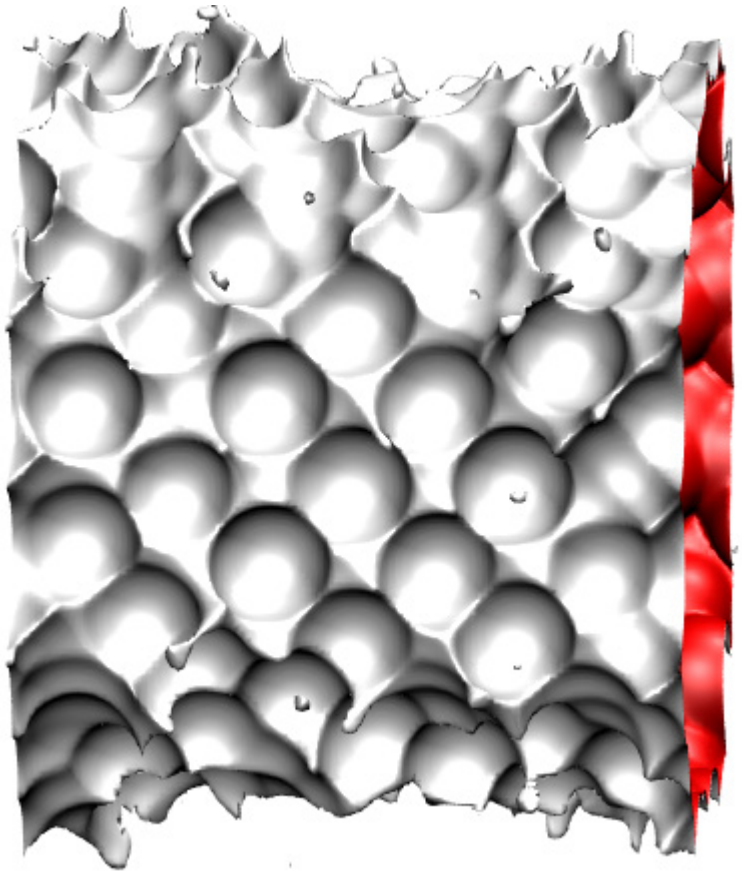

3 nm pore simulation results follow

Pure C1 and pure Ar, 3 nm pore, 300 K

Figure 30

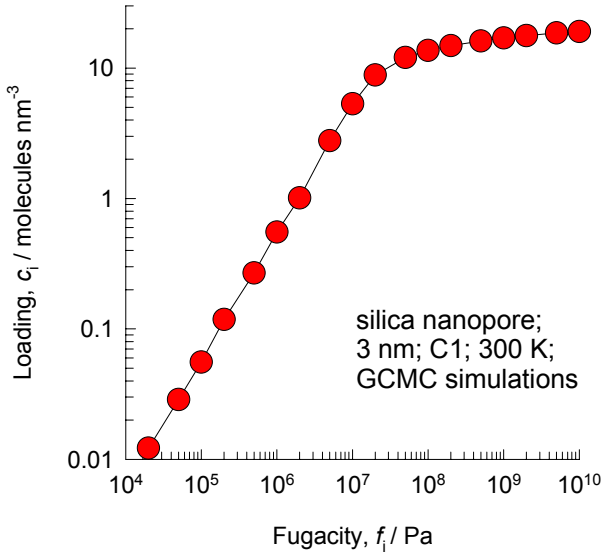

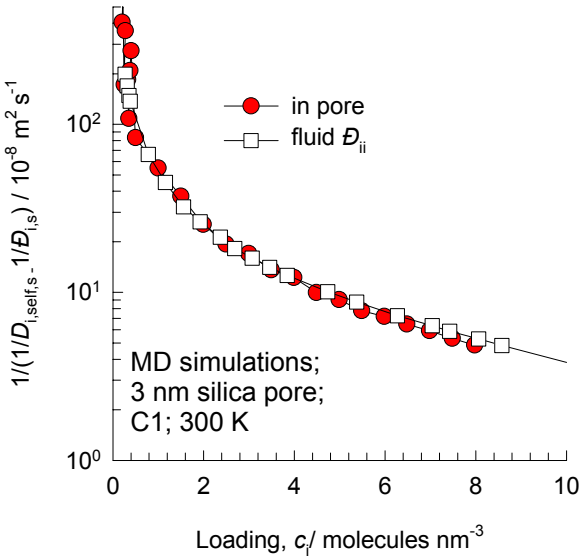

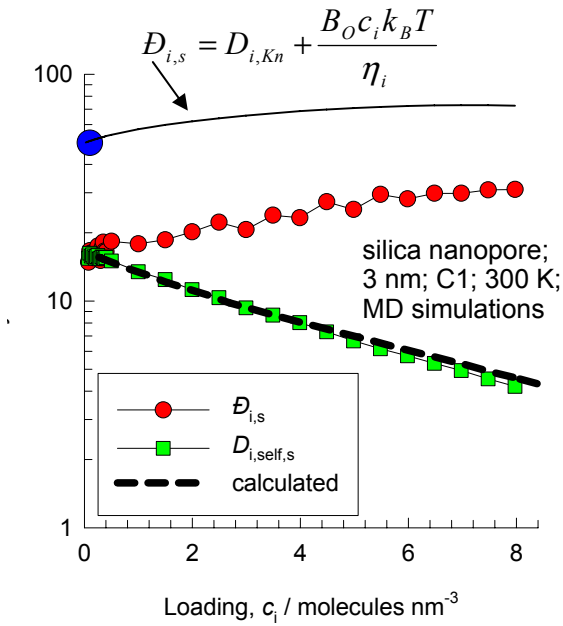

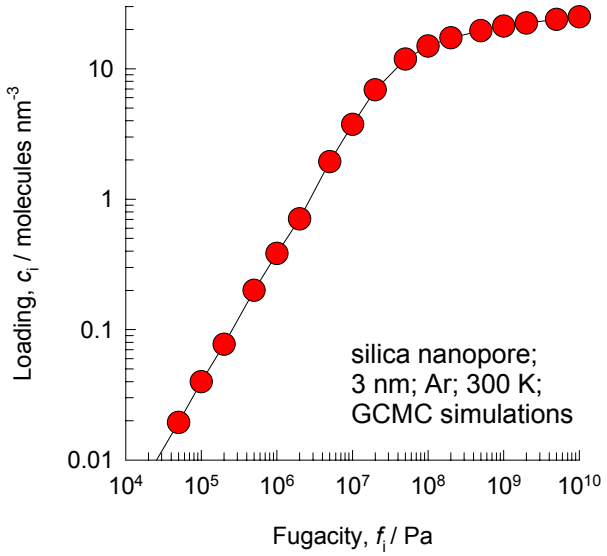

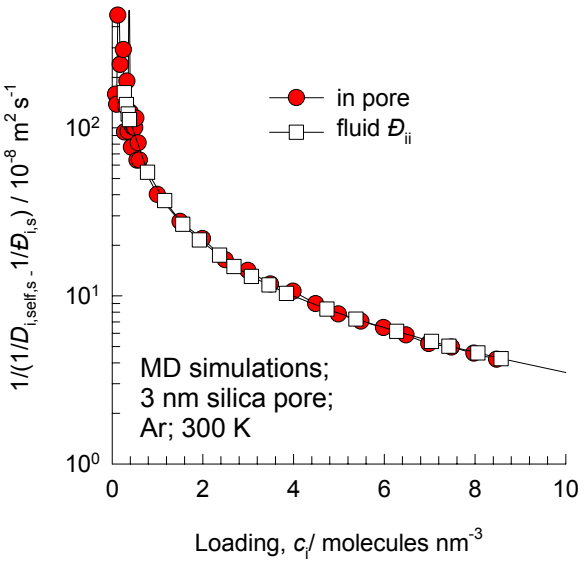

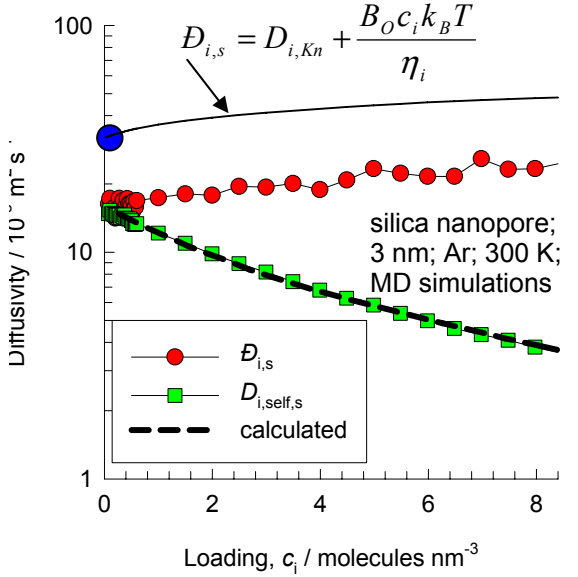

C1 –Ar mixture, 3 nm pore, 300 K

Figure 31

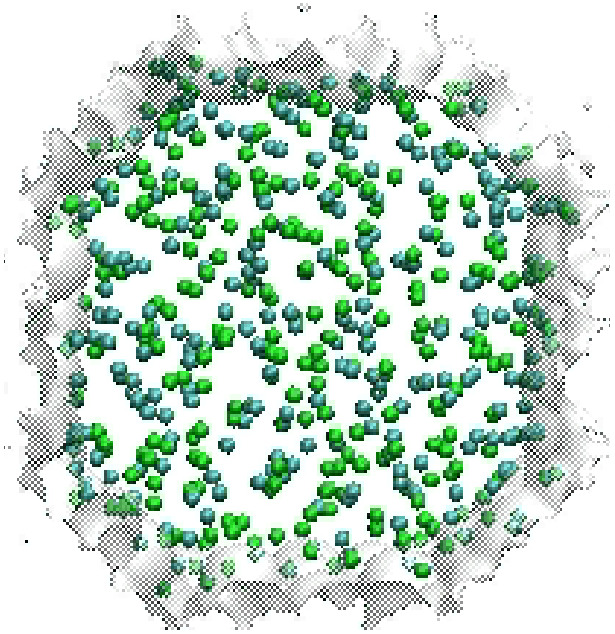

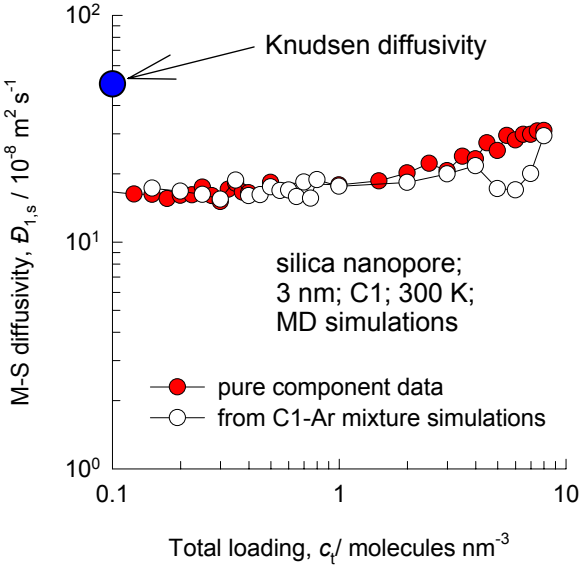

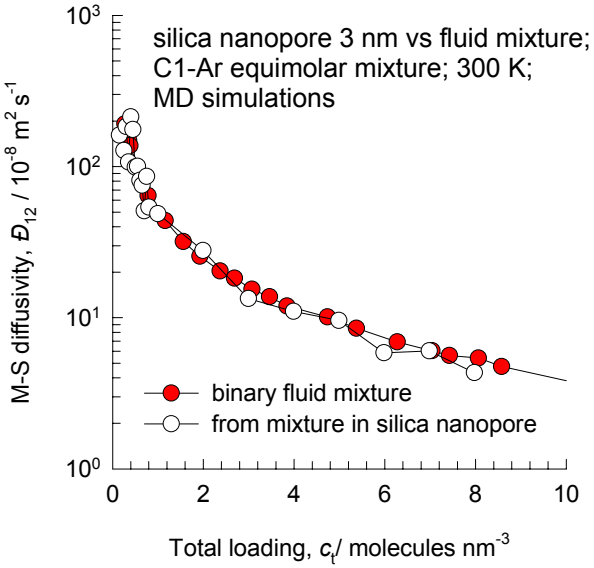

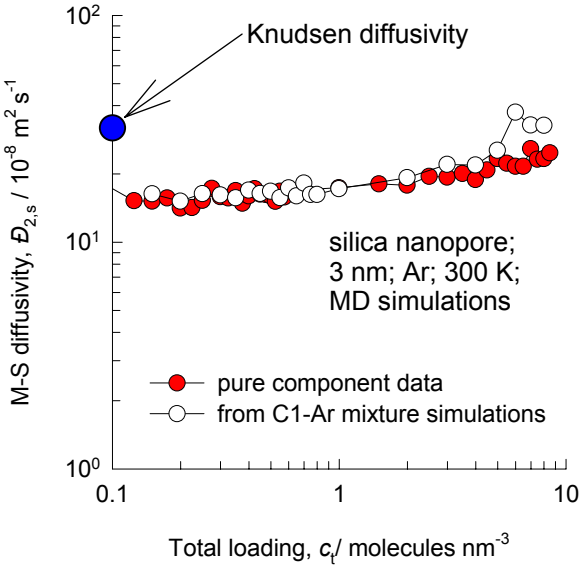

Pure C1 and pure H_2, 3 nm pore, 300 K

Figure 32

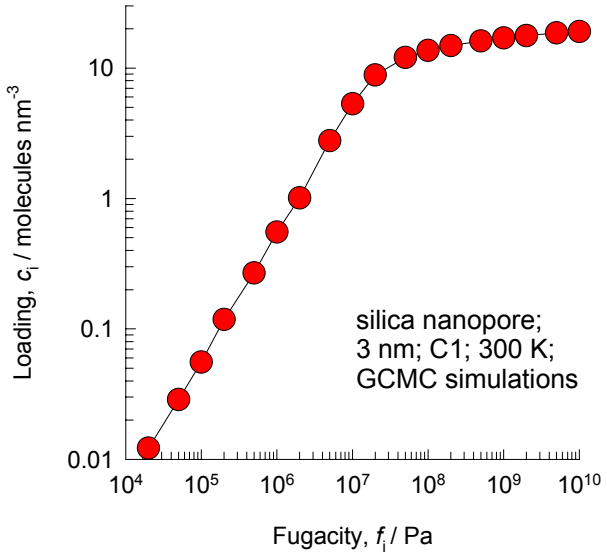

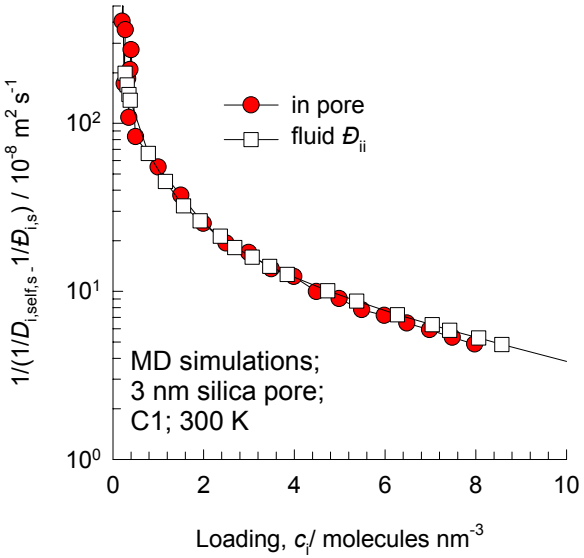

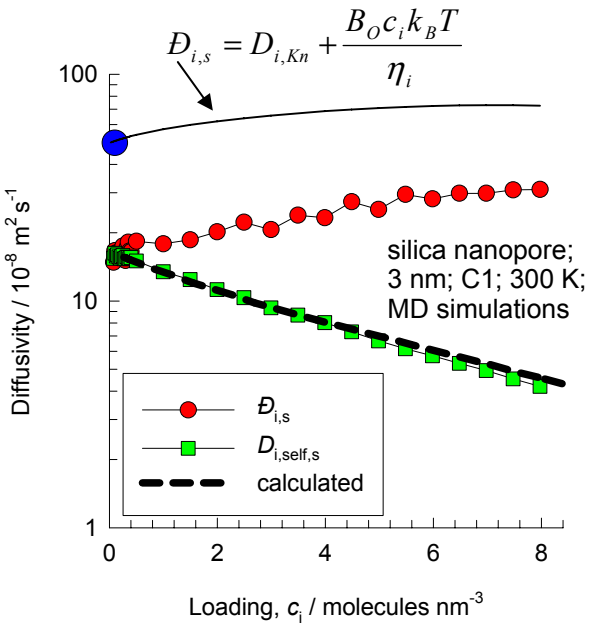

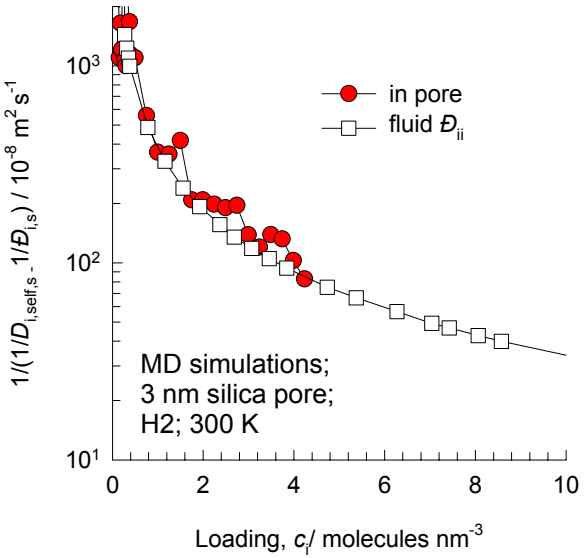

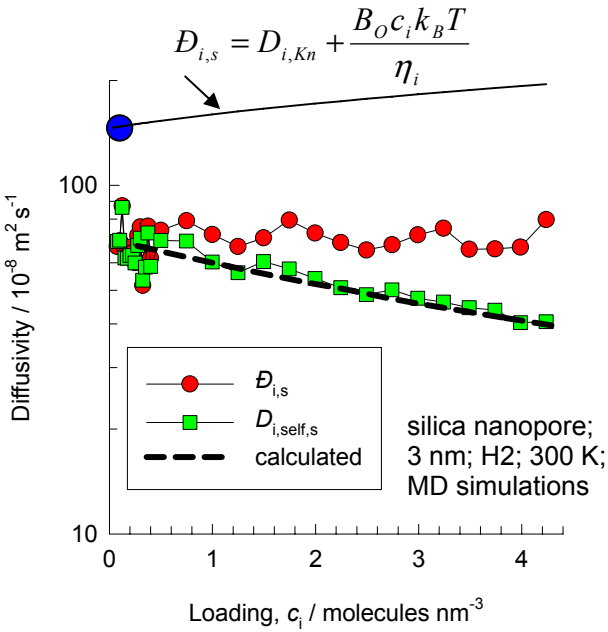

C1 –H_2 mixture, 3 nm pore, 300 K

Figure 33

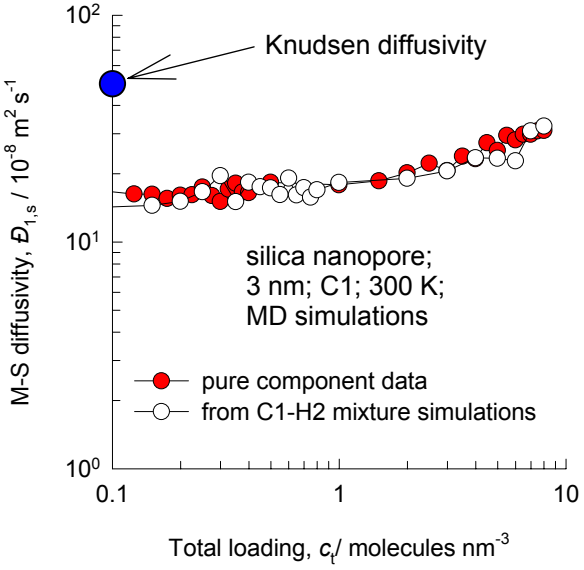

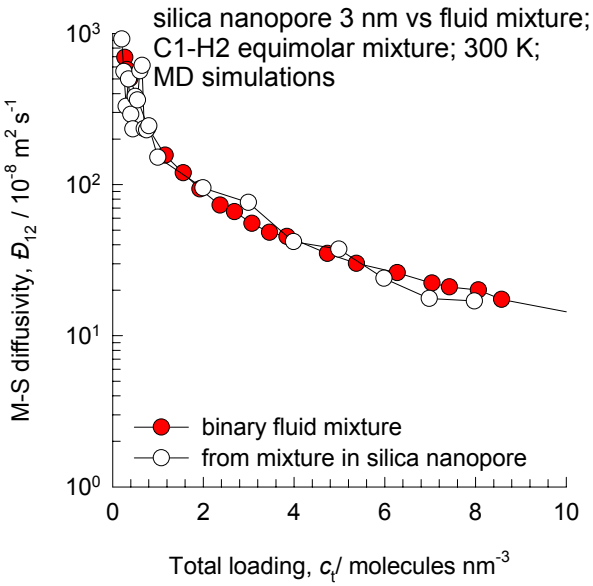

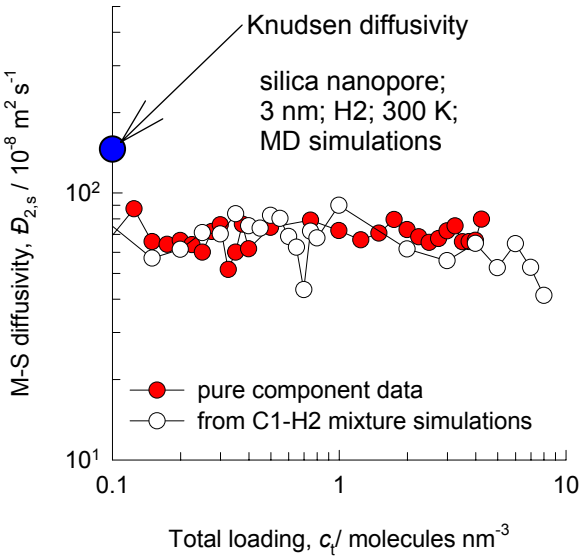

C1 –Ar mixture, 3 nm pore, 300 K

Figure 34

In these simulations the total load is kept constant at 4 molecules nm^{-3} and the composition of C1 and Ar is varied.

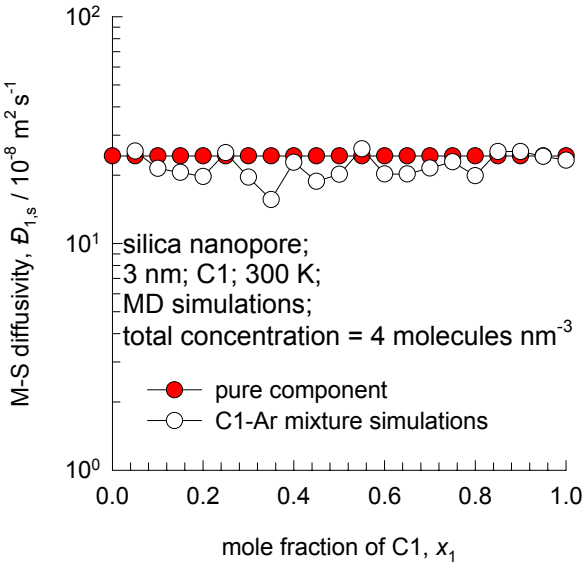

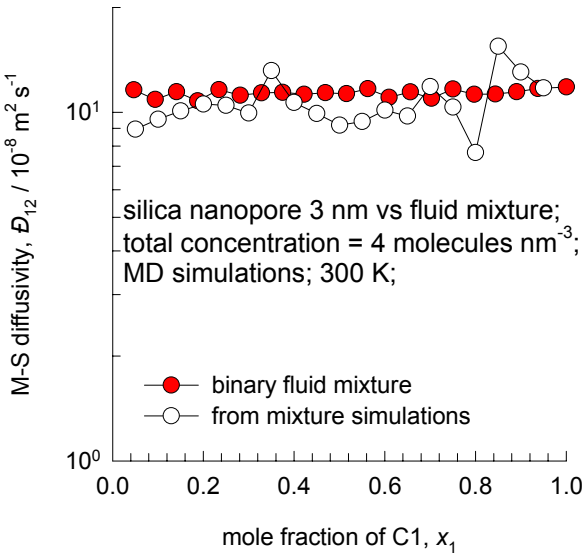

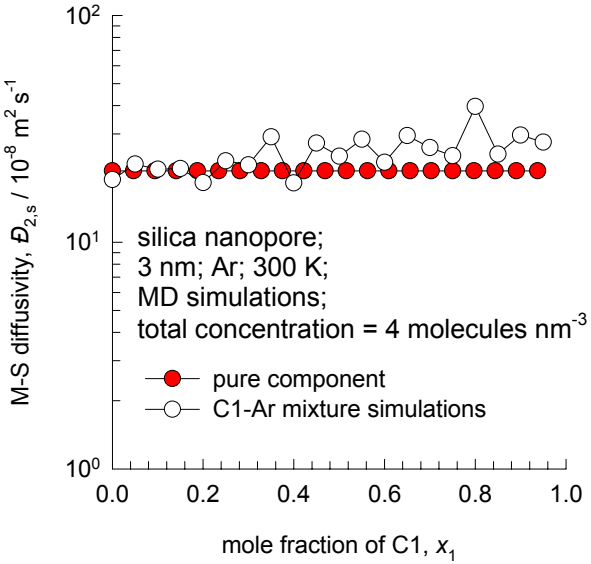

Pure C1 and pure C2, 3 nm pore, 300 K

Figure 35

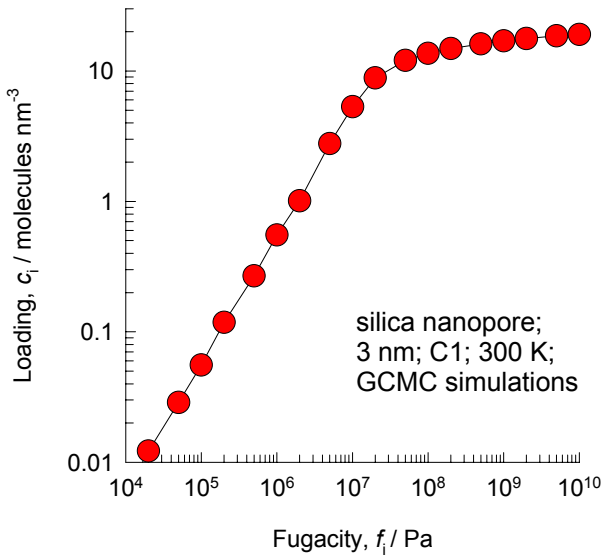

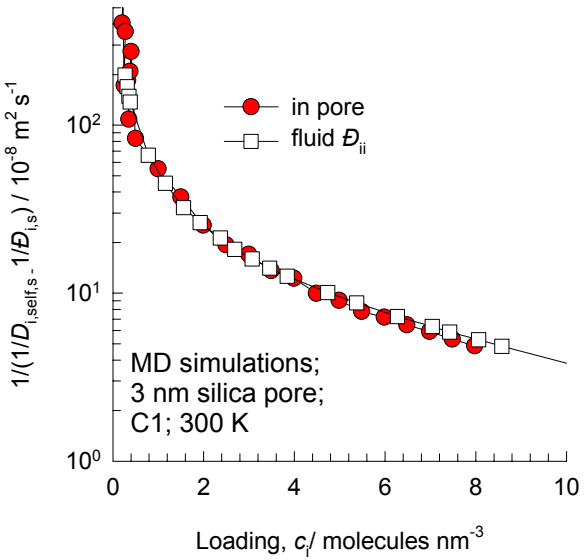

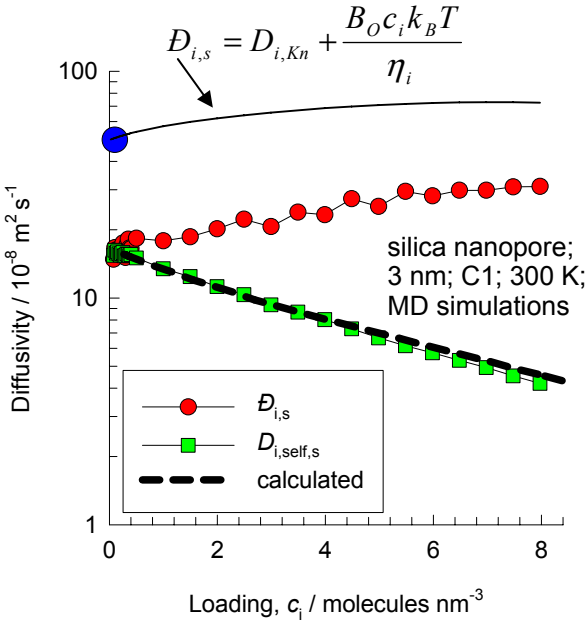

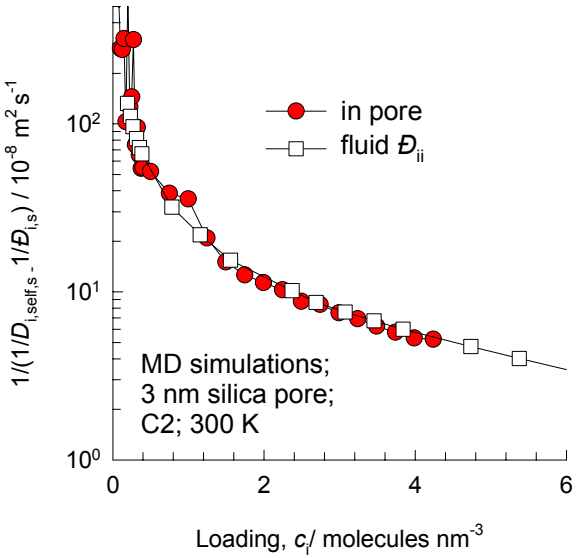

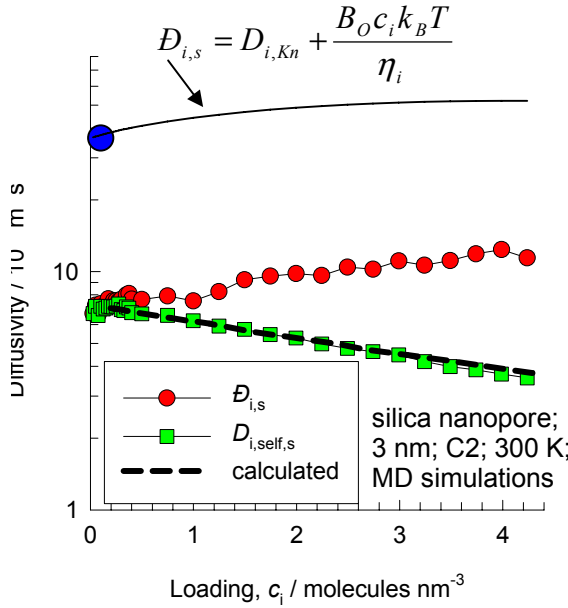

C1 – C2 mixture, 3 nm pore, 300 K

Figure 36

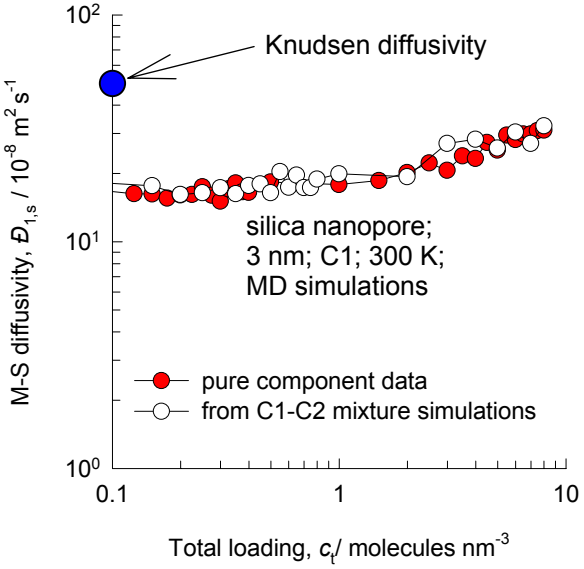

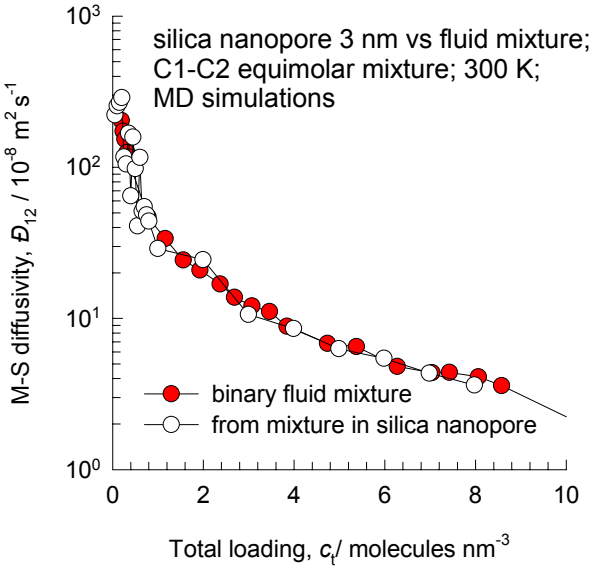

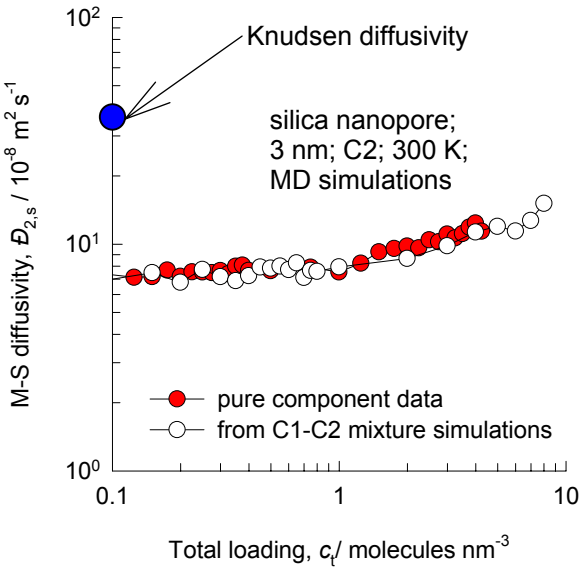

Pure C1 and pure C3, 3 nm pore, 300 K

Figure 37

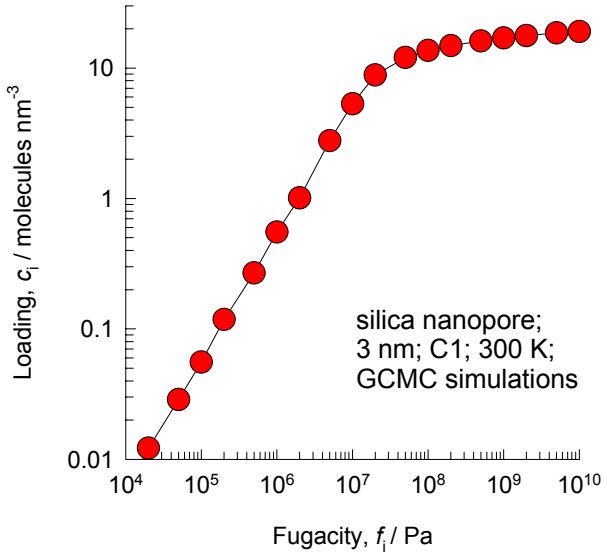

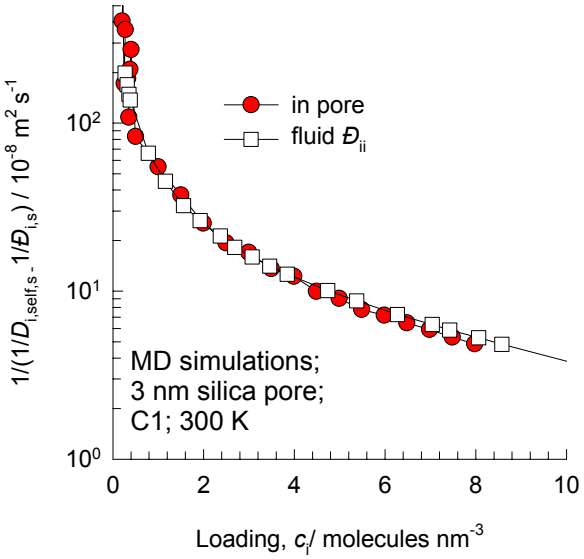

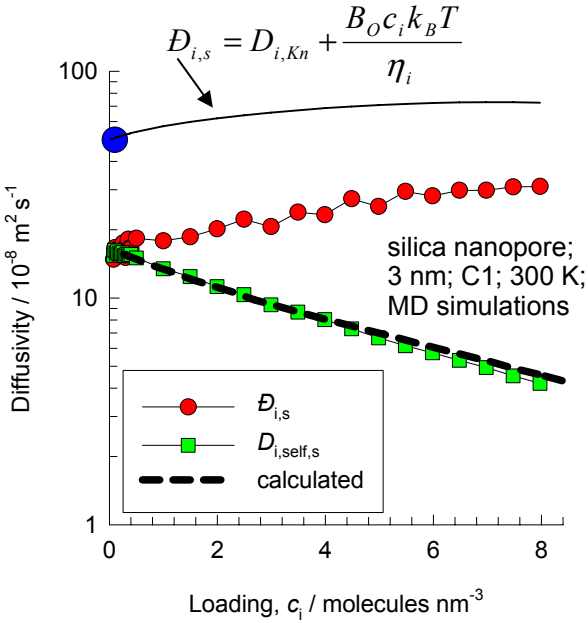

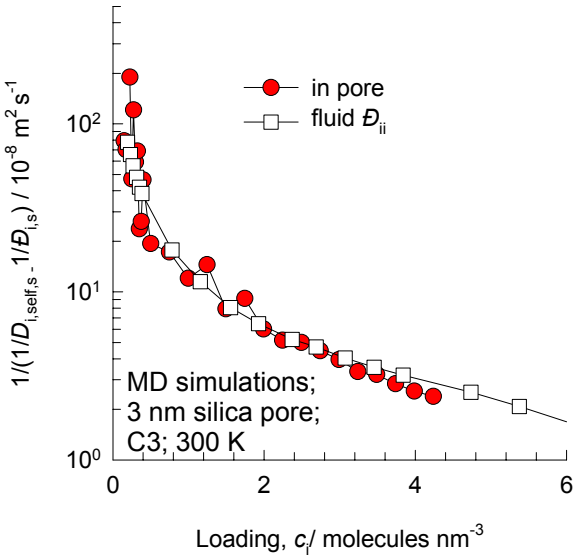

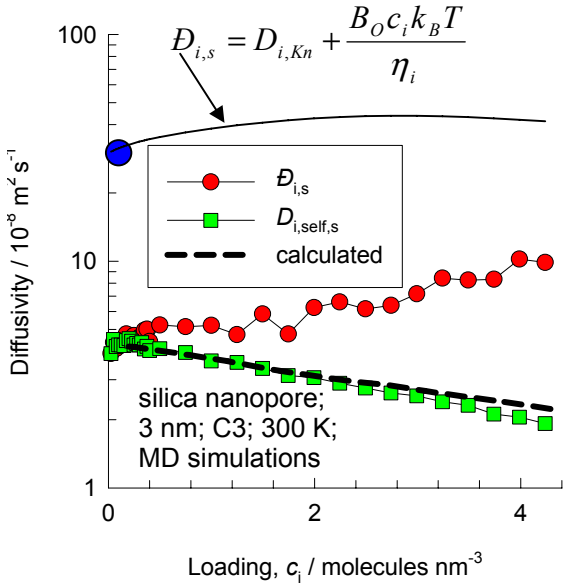

C1 – C3 mixture, 3 nm pore, 300 K

Figure 38

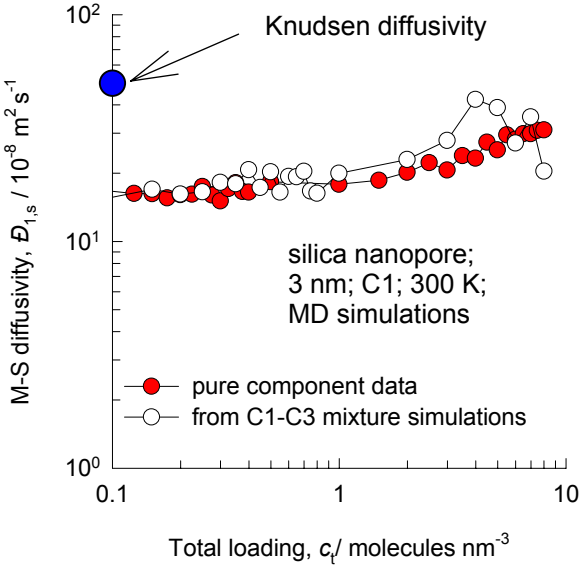

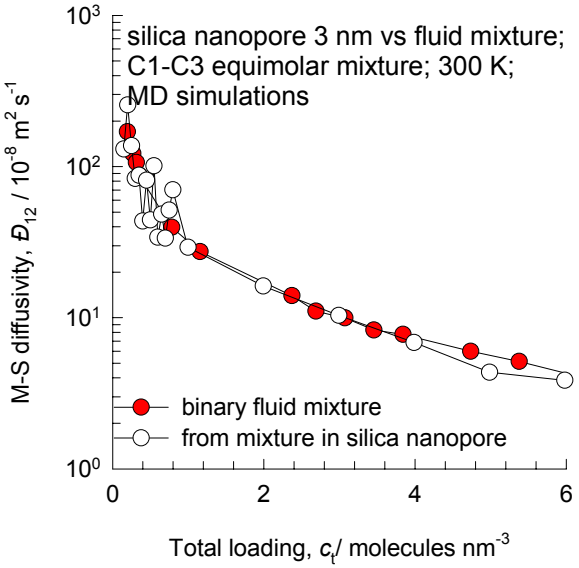

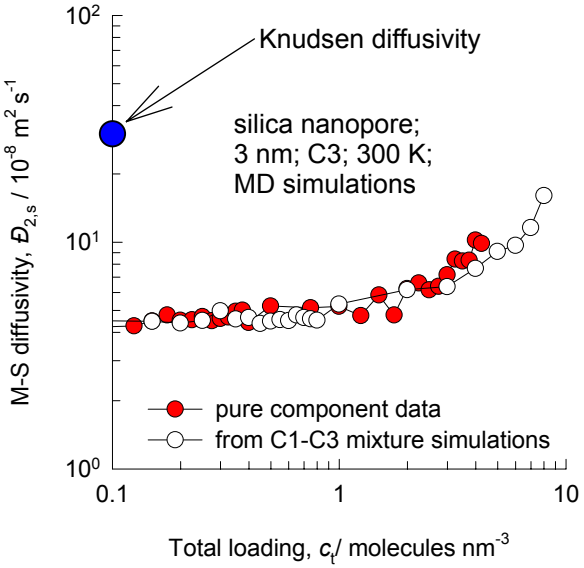

Pure C1 and pure nC4, 3 nm pore, 300 K

Figure 39

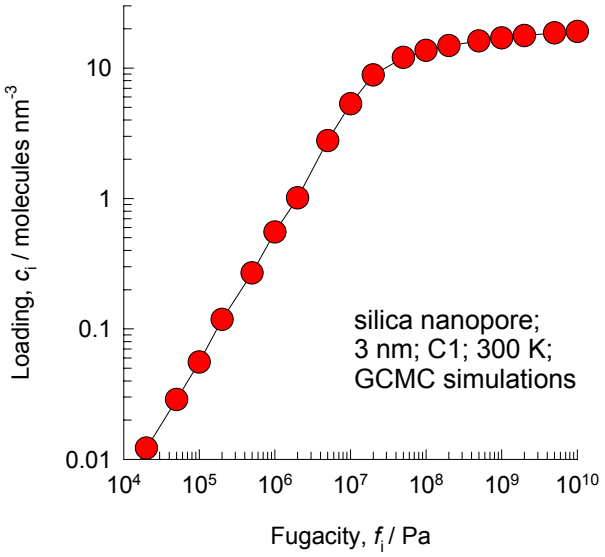

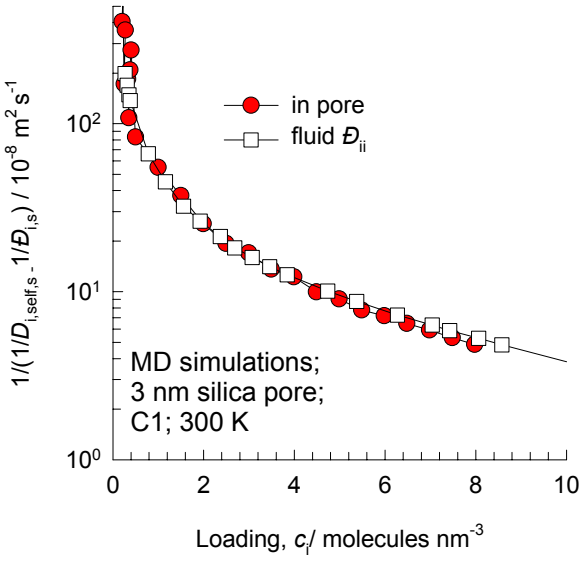

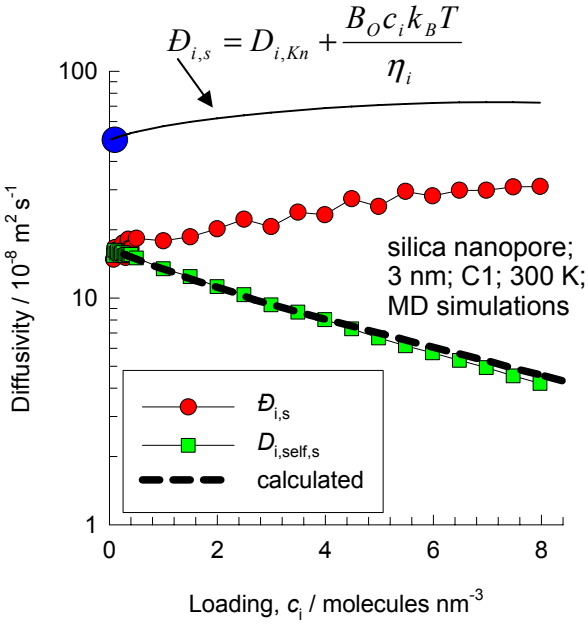

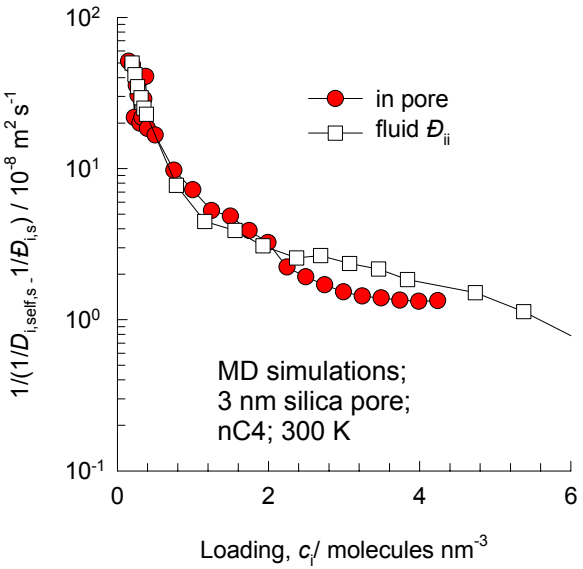

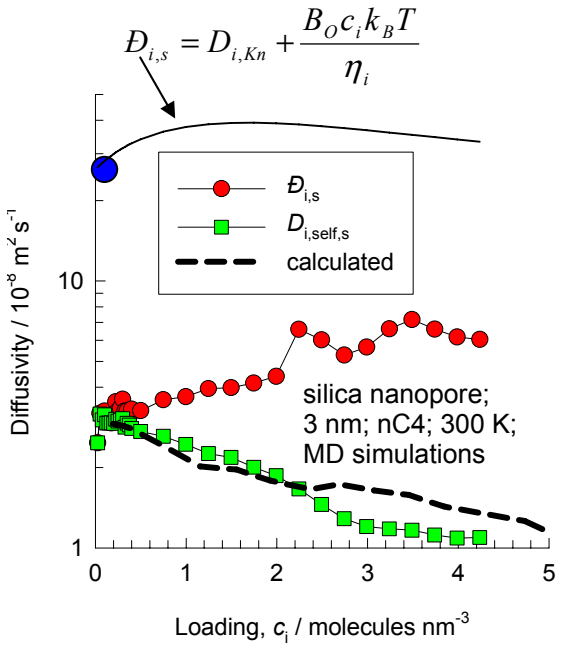

C1 – nC4 mixture, 3 nm pore, 300 K

Figure 40

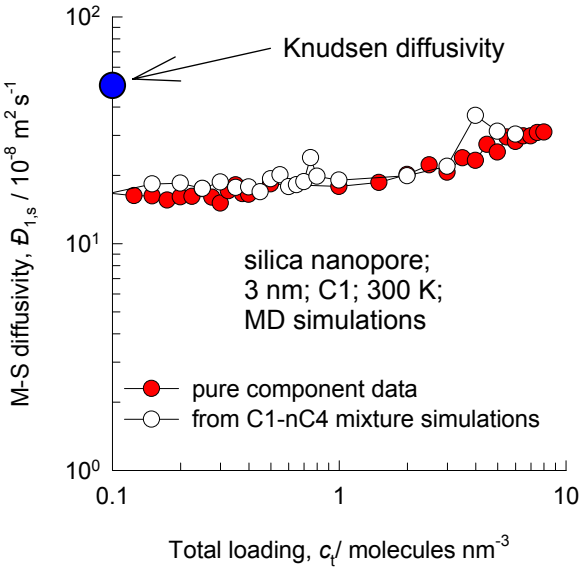

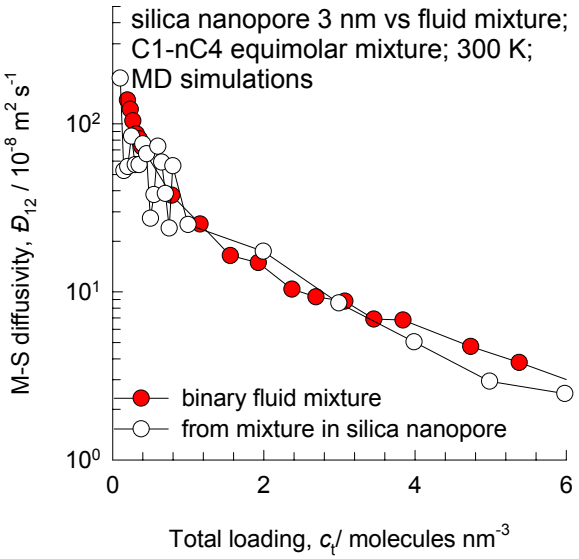

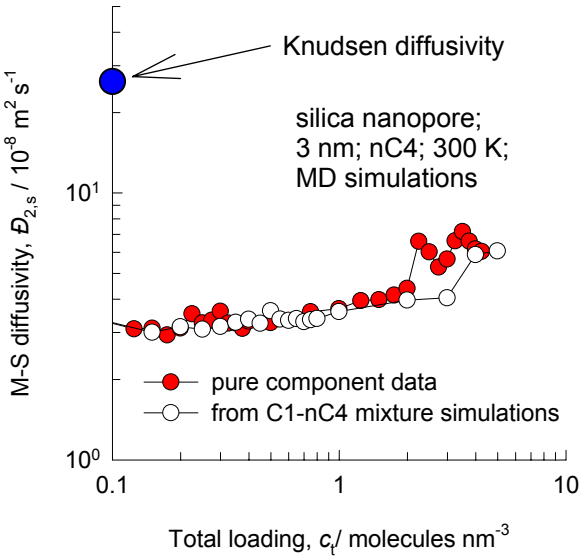

C1 – nC4 mixture, 3 nm pore, 300 K

Figure 41

In these simulations the total load is kept constant at 4 molecules nm^{-3} and the composition of C1 and nC4 is varied.

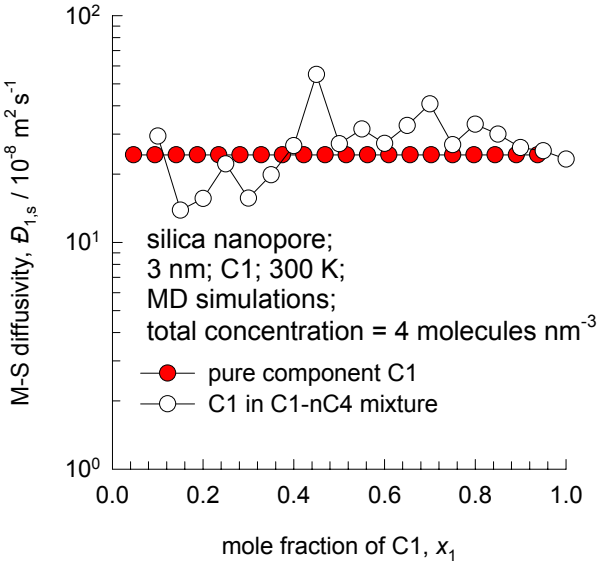

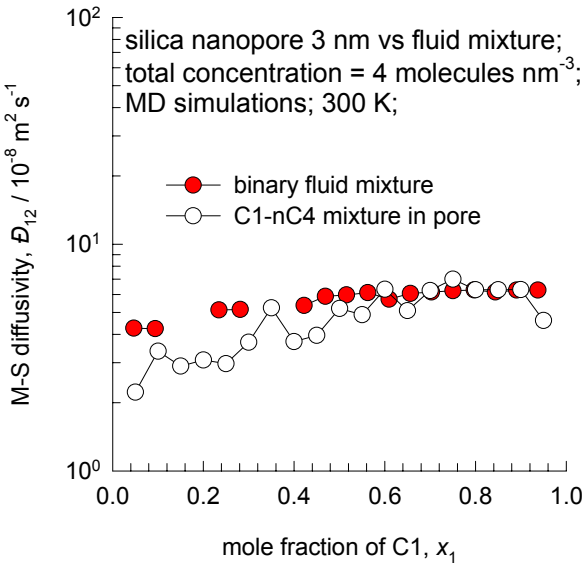

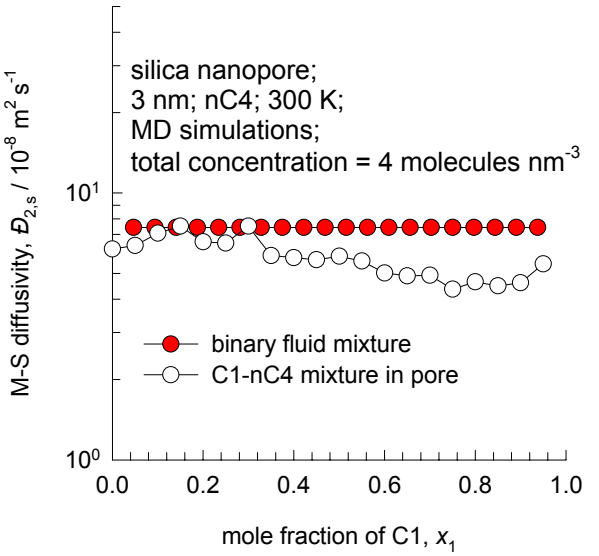

Pure C1 and pure nC6, 3 nm pore, 300 K

Figure 42

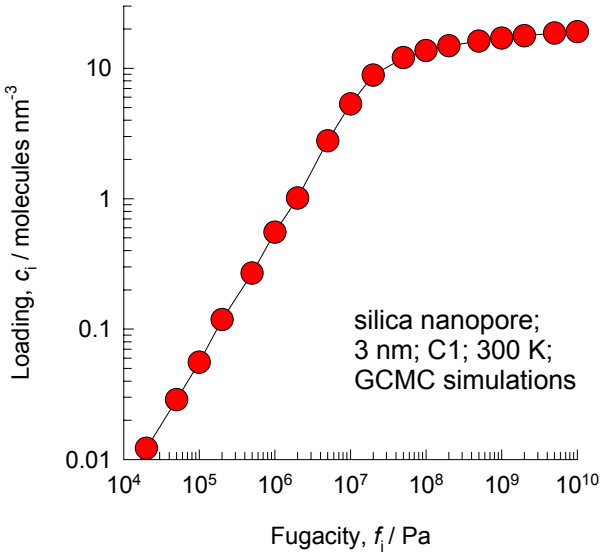

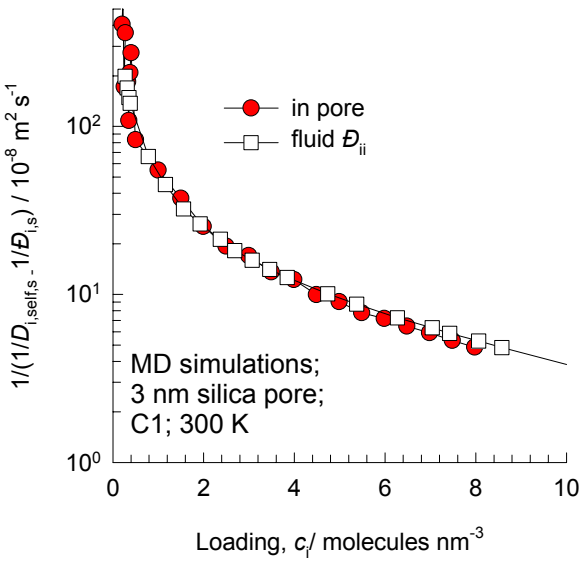

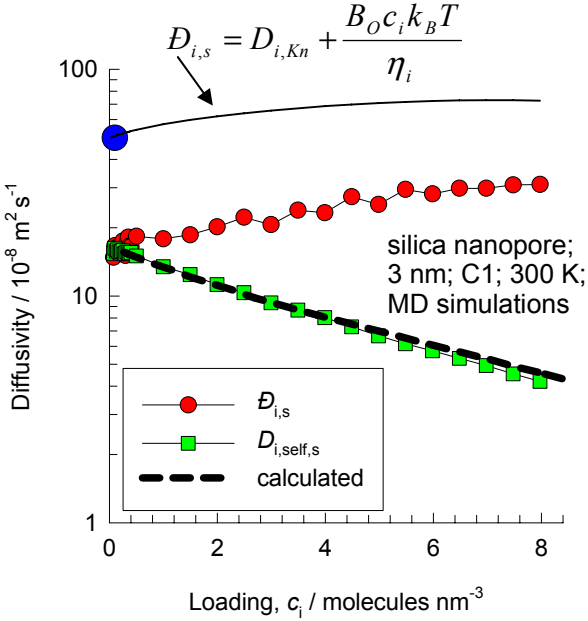

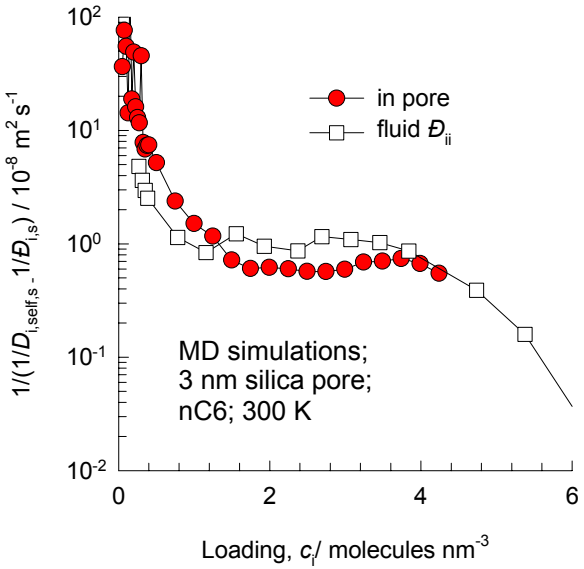

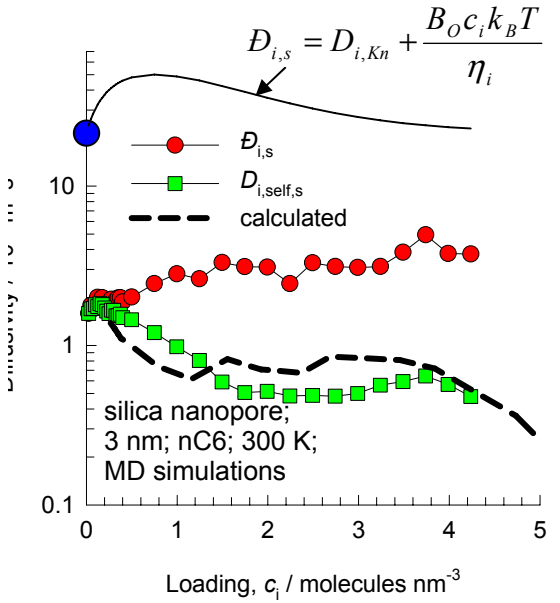

C1 – nC6 mixture, 3 nm pore, 300 K

Figure 43

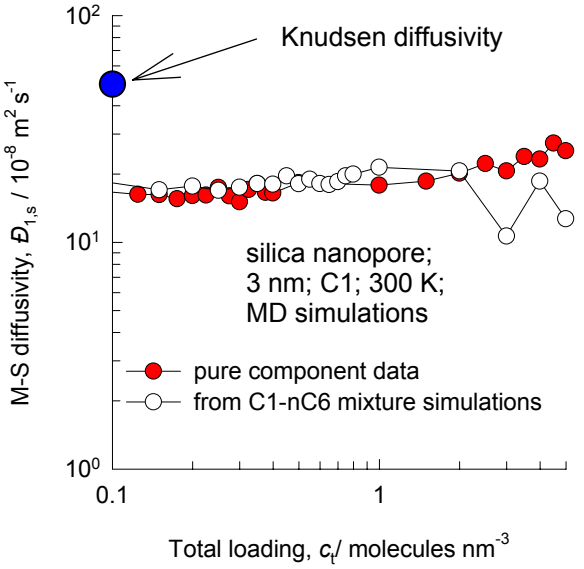

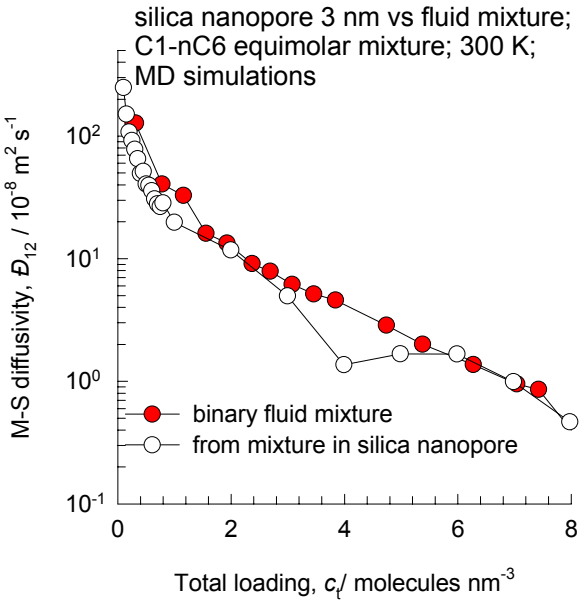

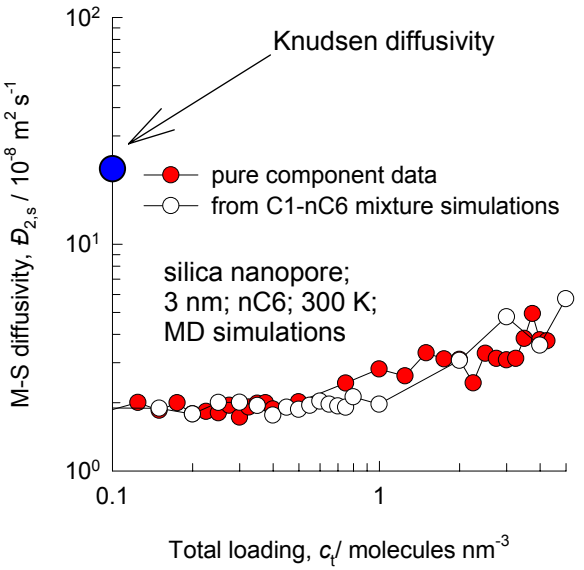

C2 – nC4 mixture, 3 nm pore, 300 K

Figure 44

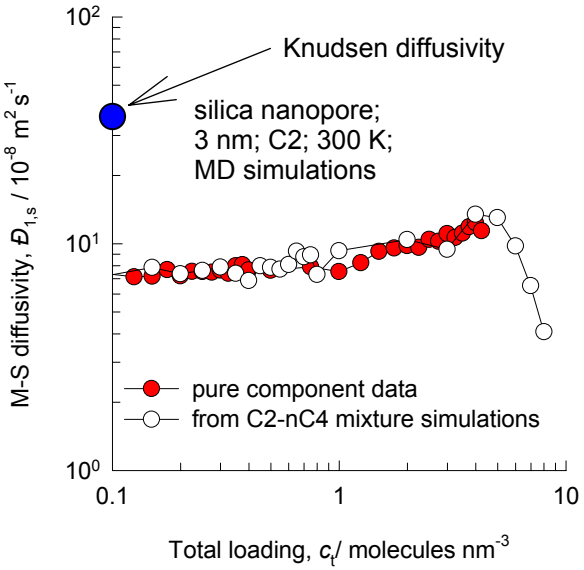

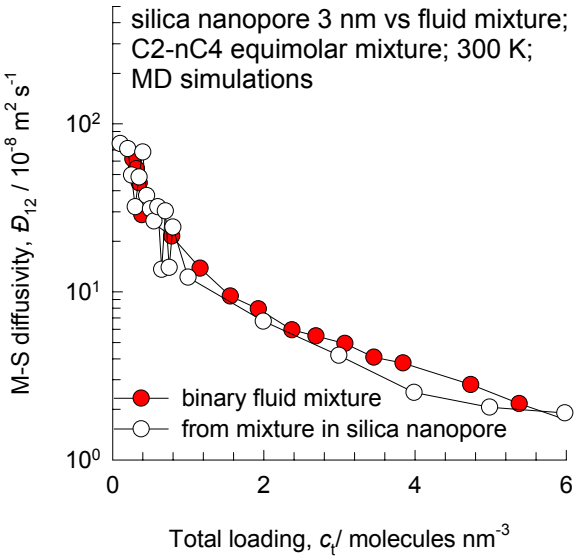

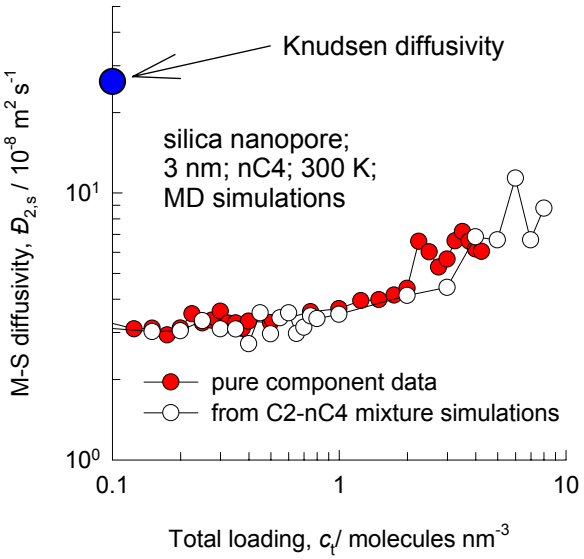

C2 – nC6 mixture, 3 nm pore, 300 K

Figure 45

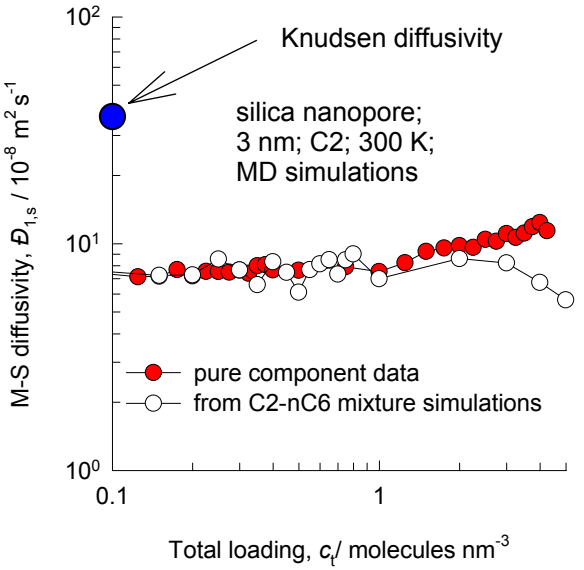

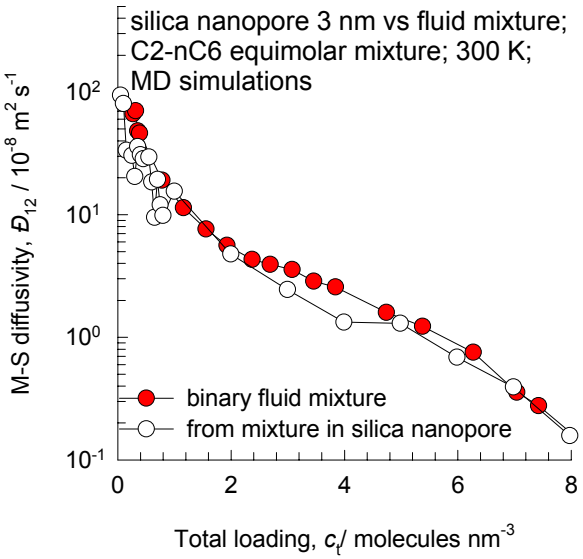

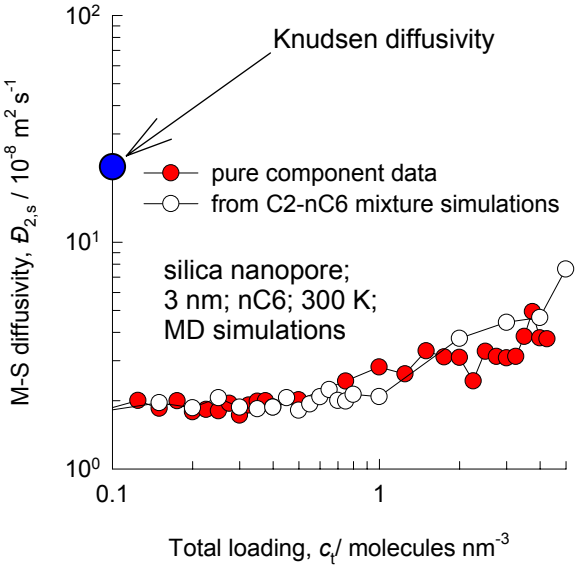

nC4 – nC6 mixture, 3 nm pore, 300 K

Figure 46

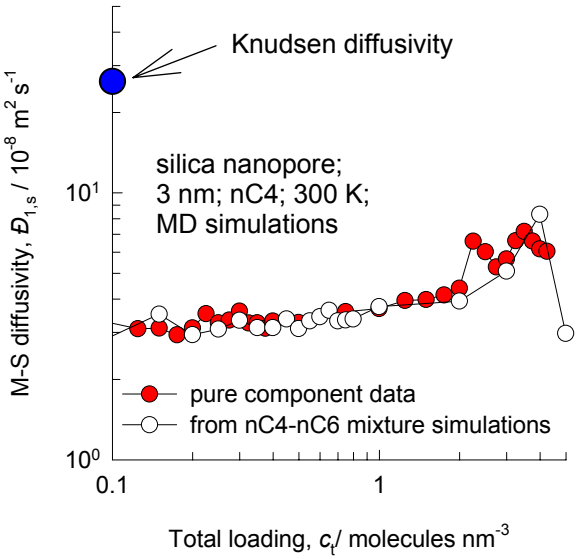

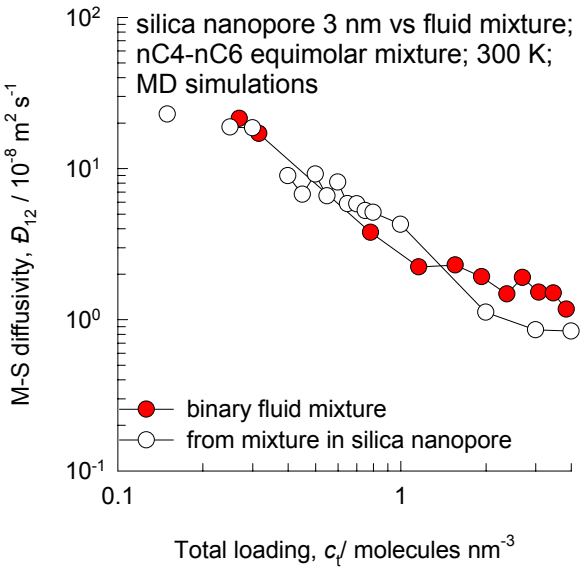

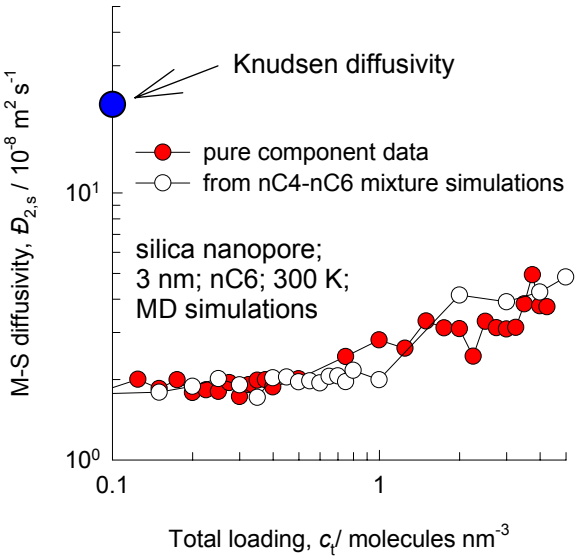

Figure 47

Pure Kr, 3 nm pore, 300 K

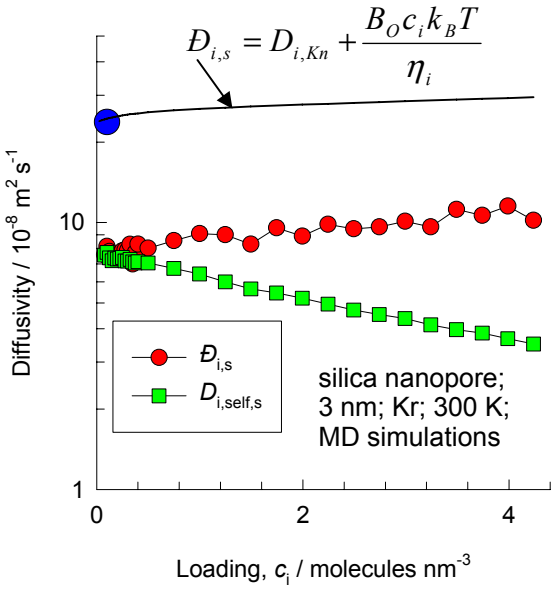

Pure nC6, 3 nm pore, 700 K

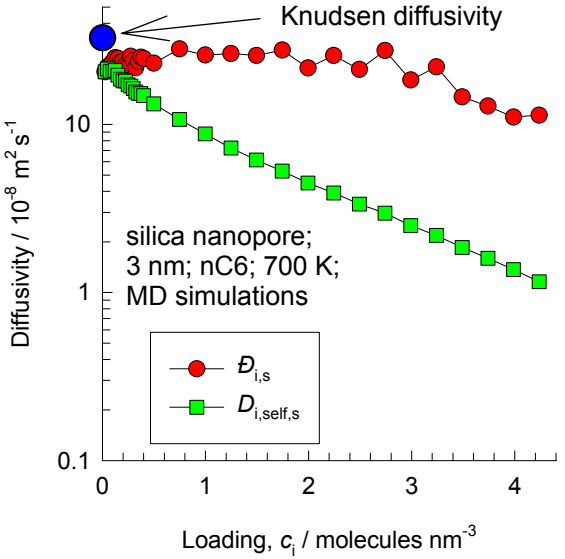

Pure nC6, 3 nm pore, 500 K

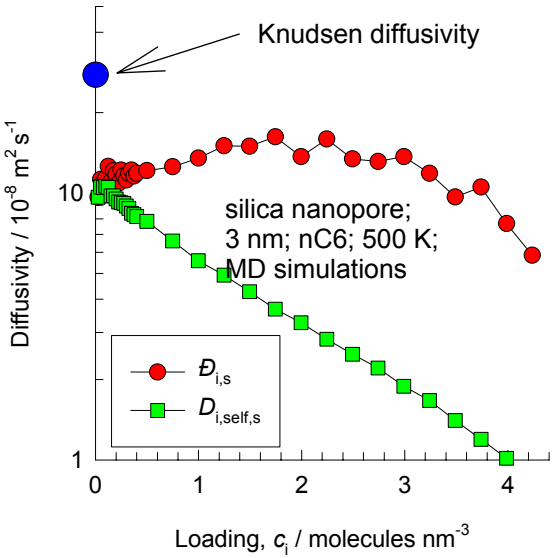

Figure 48

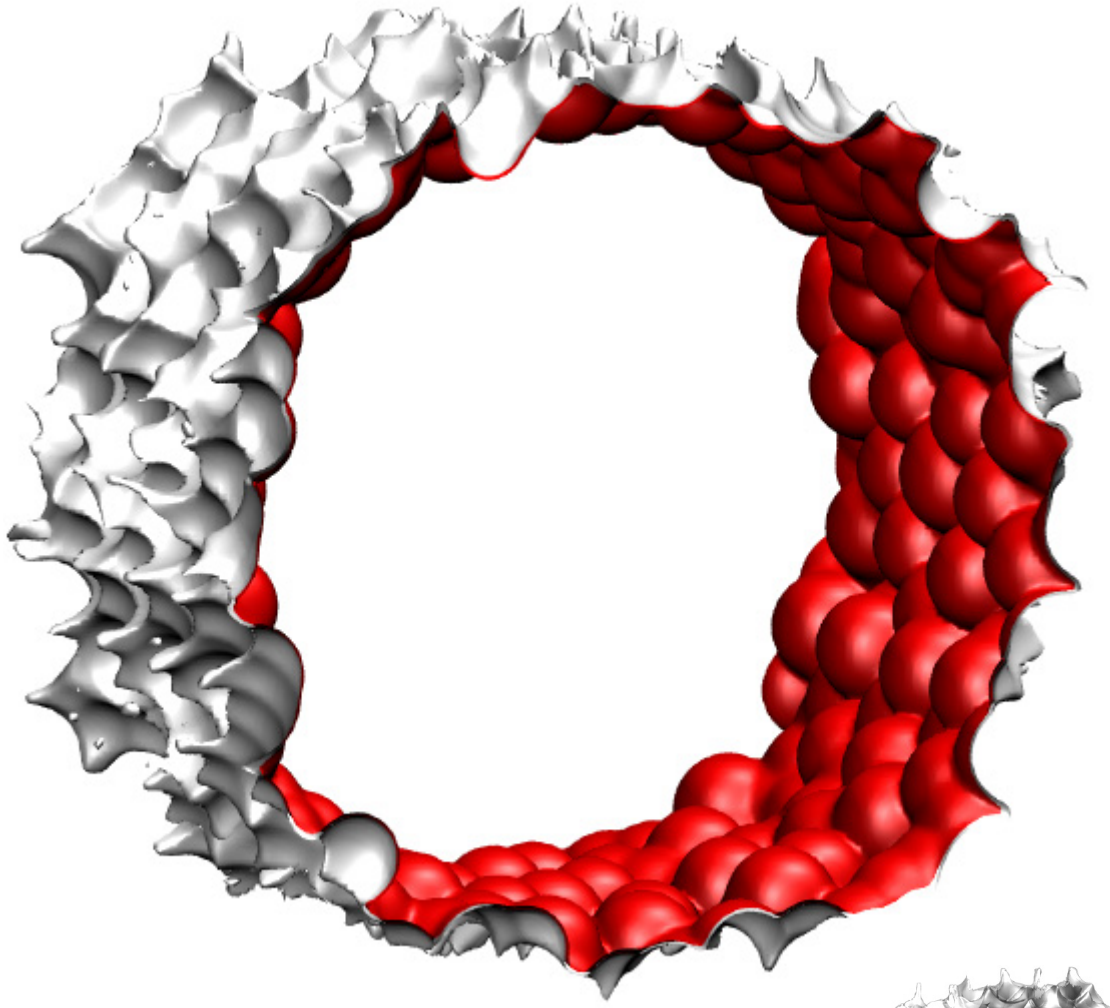

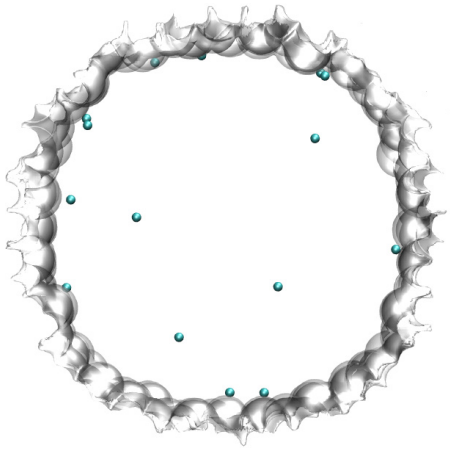

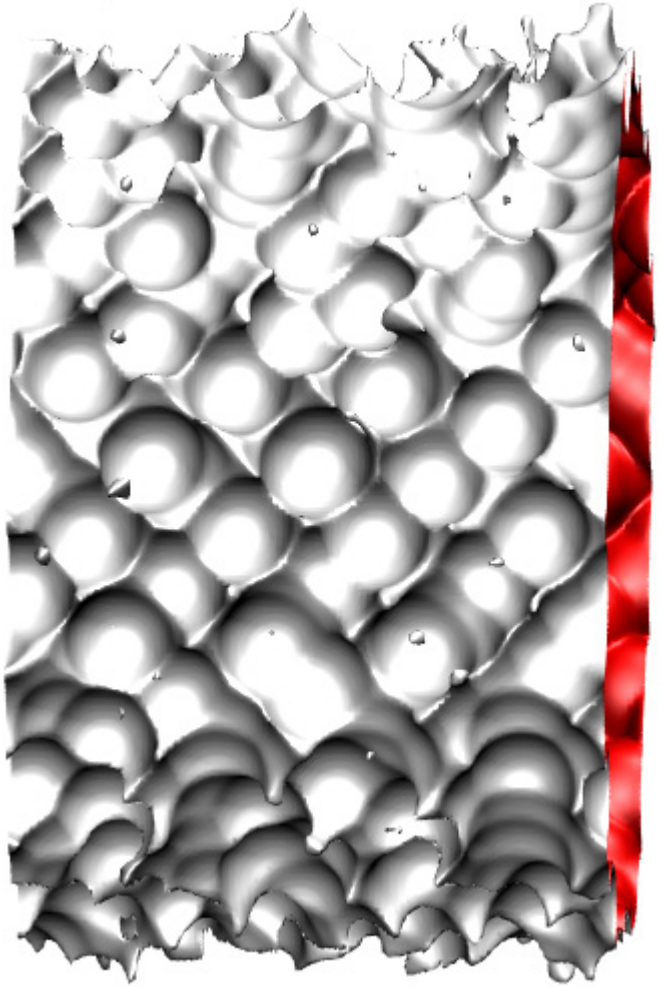

4 nm pore simulation results follow

Pure C1 and pure Ar, 4 nm pore, 300 K

Figure 49

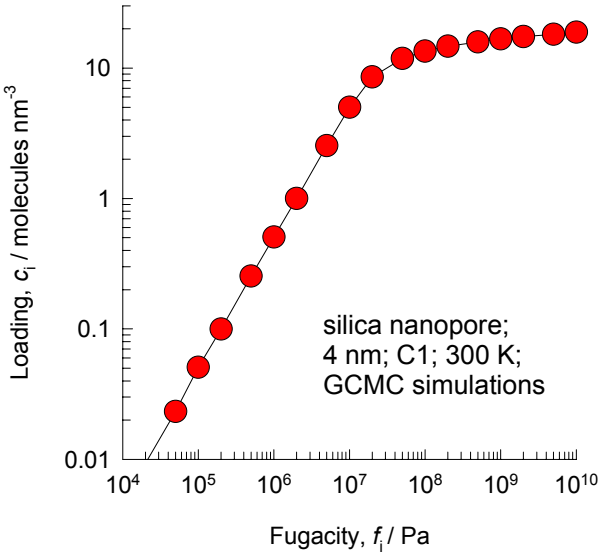

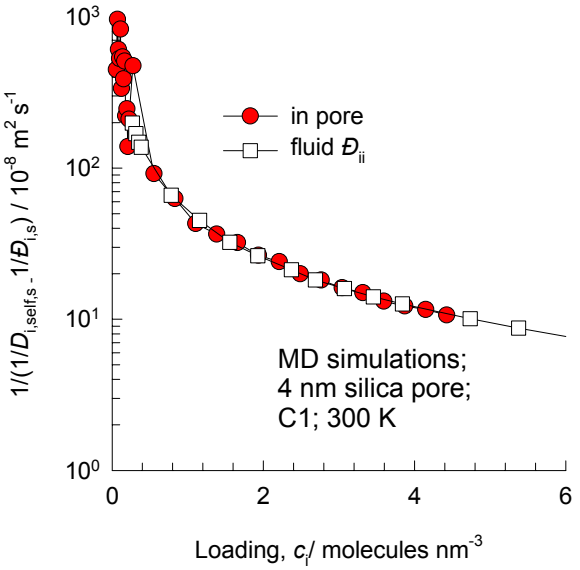

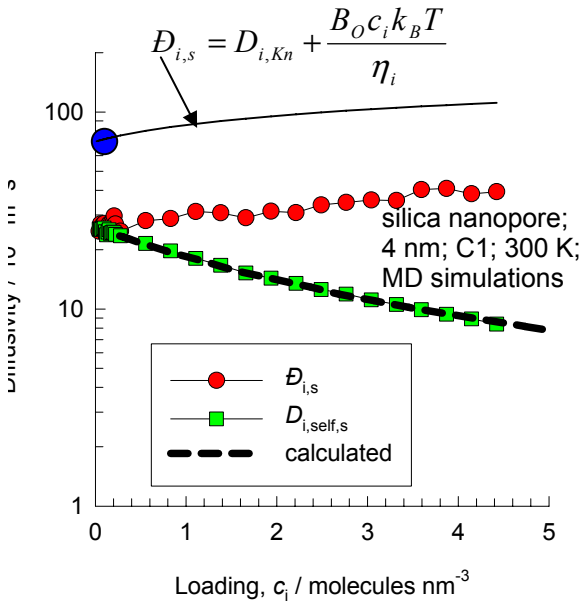

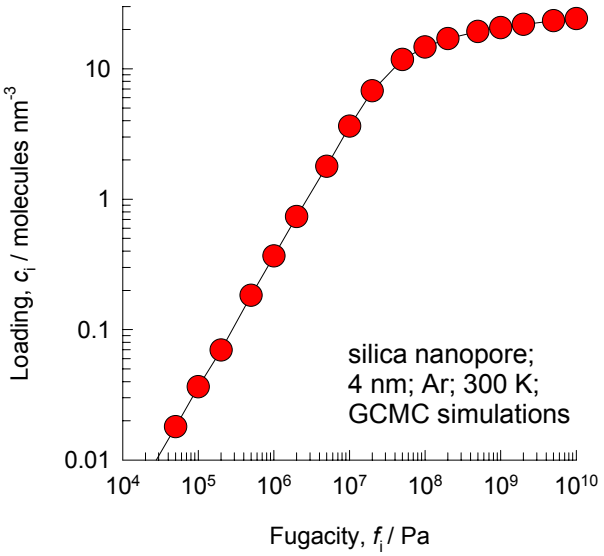

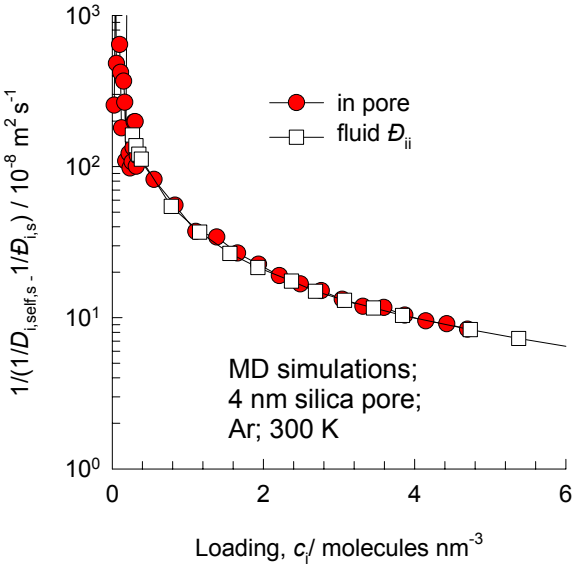

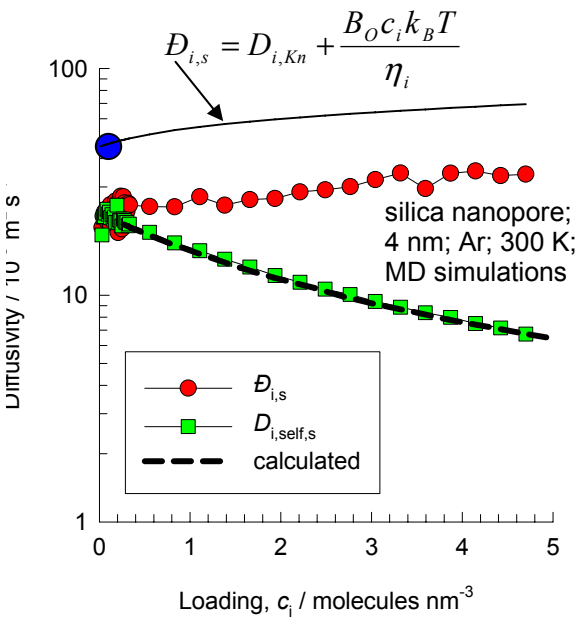

C1 –Ar mixture, 4 nm pore, 300 K

Figure 50

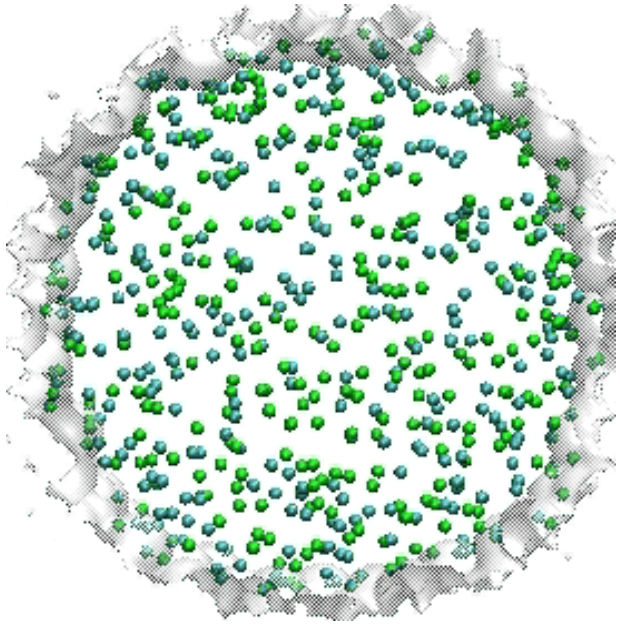

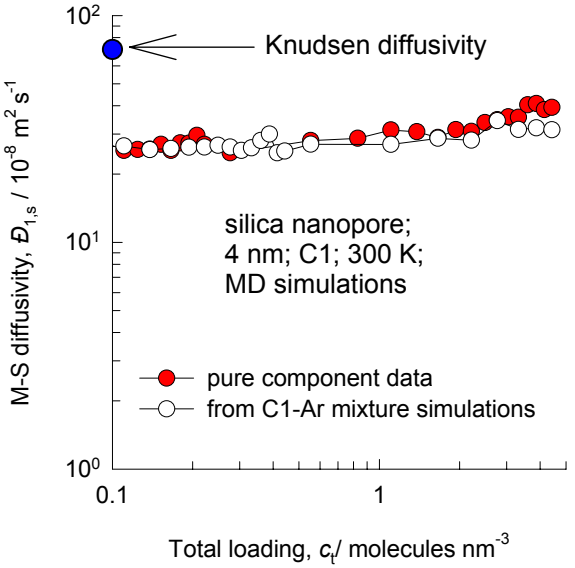

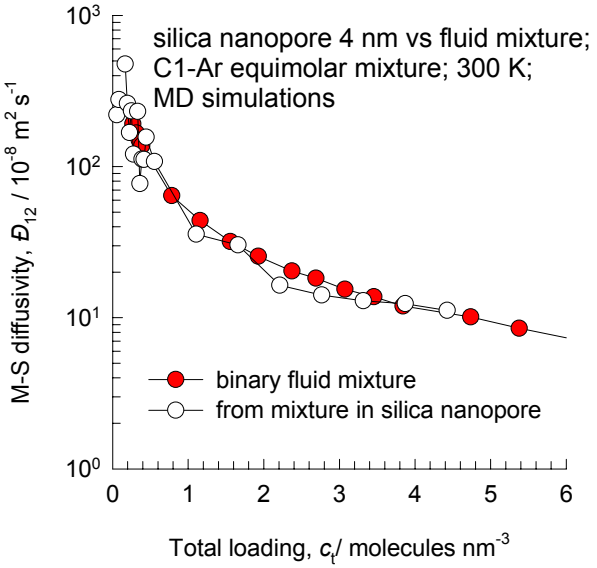

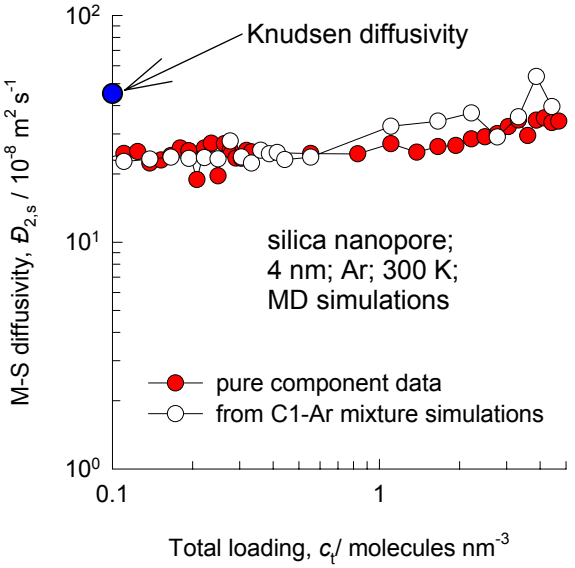

Figure 51

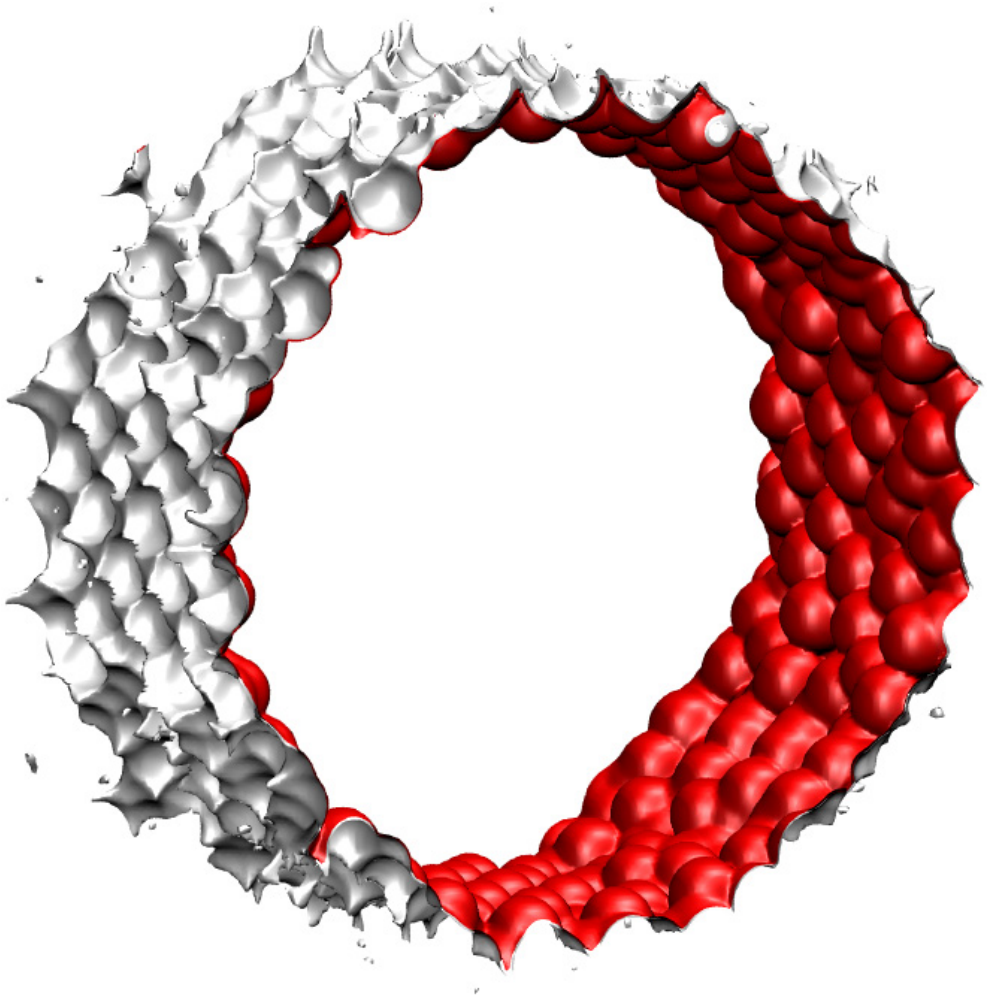

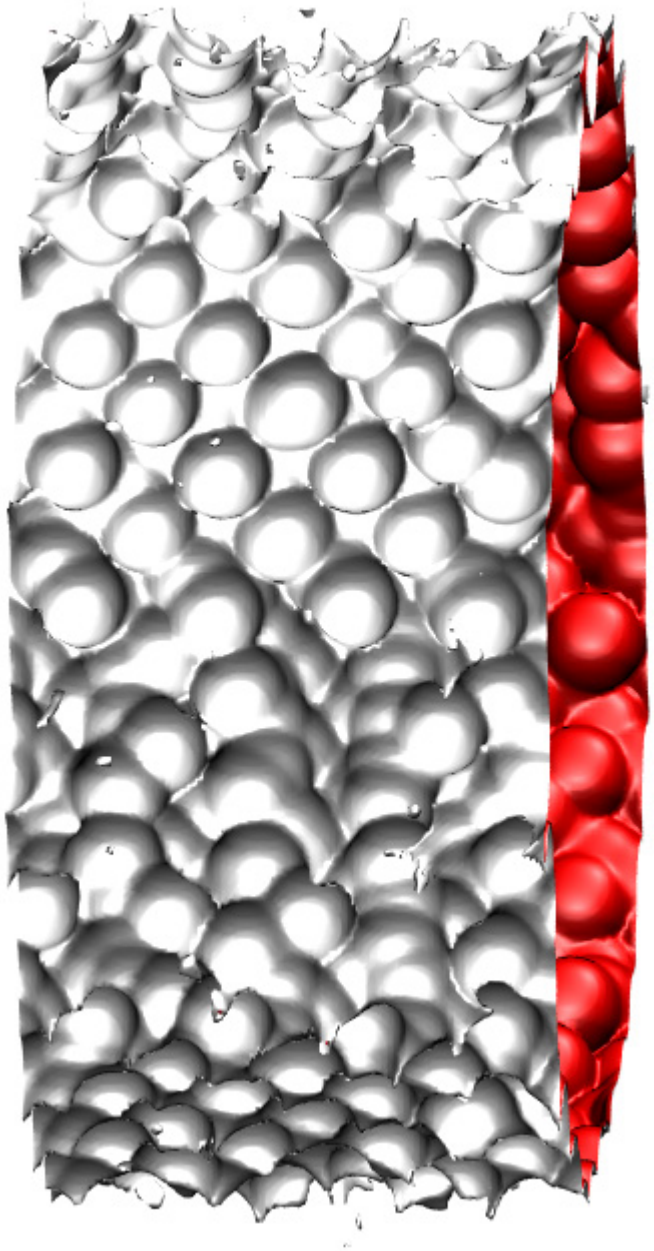

5.8 nm pore simulation results follow

Pure C1 and pure Ar, 5.8 nm pore, 300 K

Figure 52

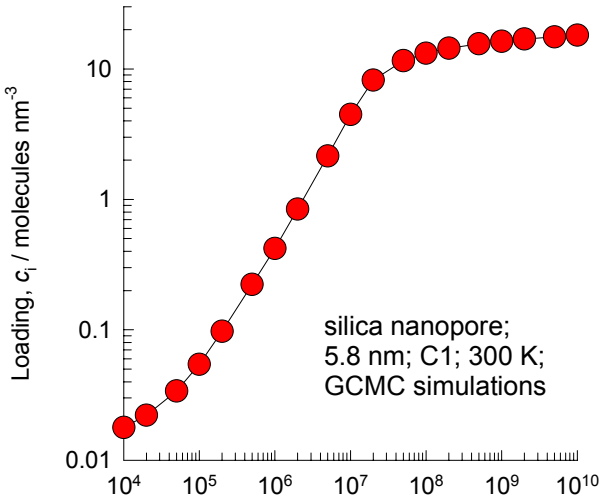

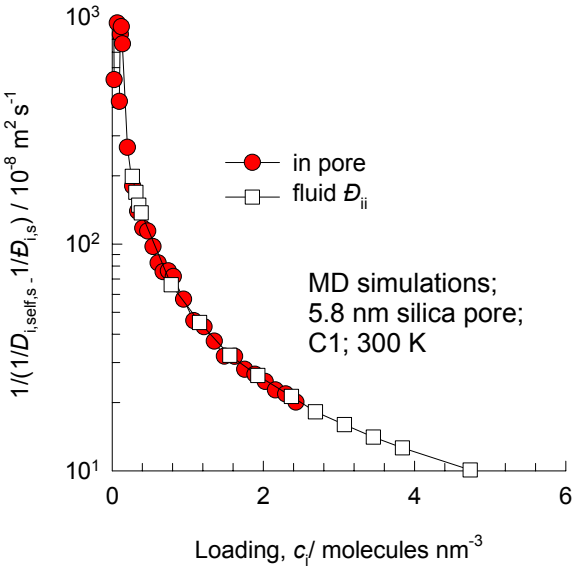

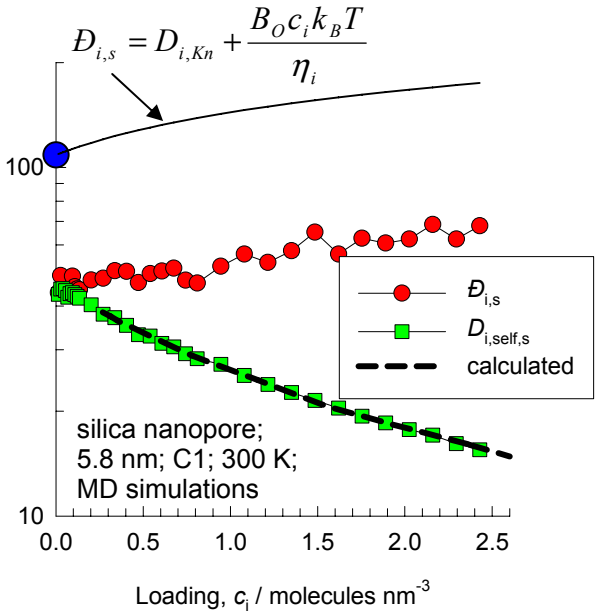

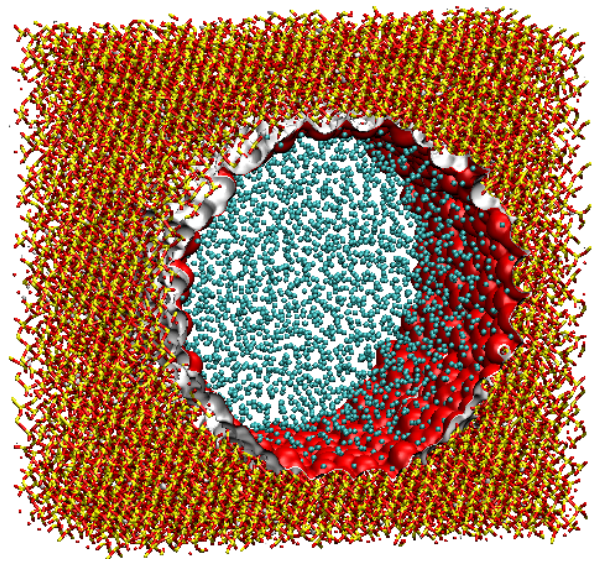

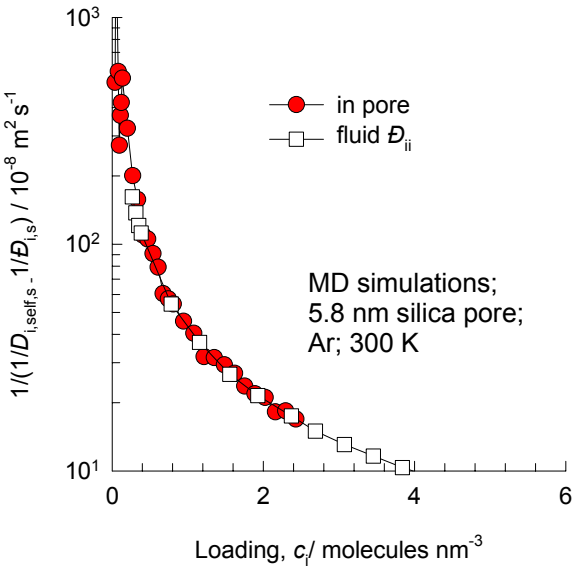

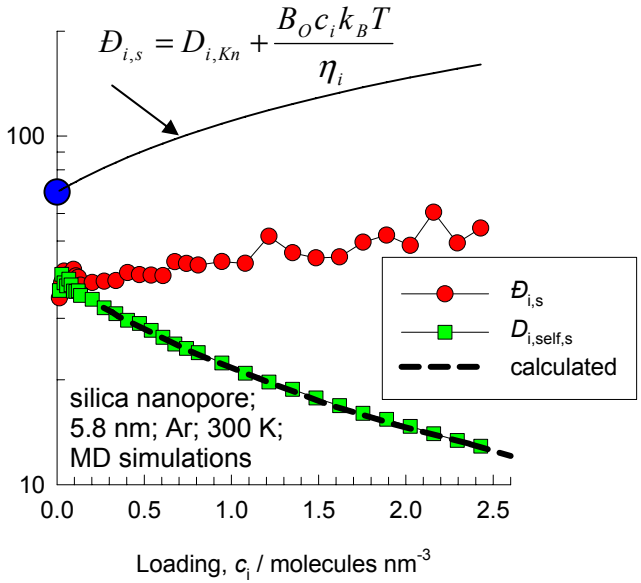

C1 –Ar mixture, 5.8 nm pore, 300 K

Figure 53

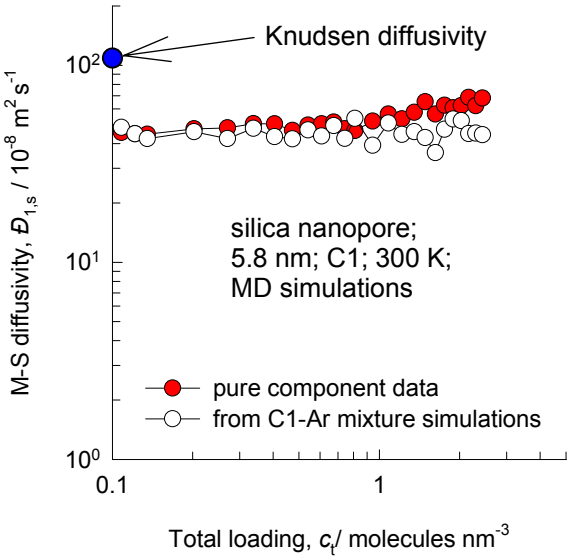

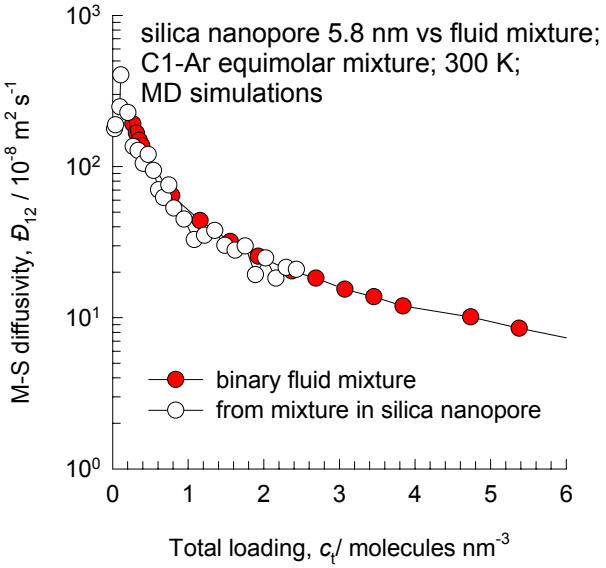

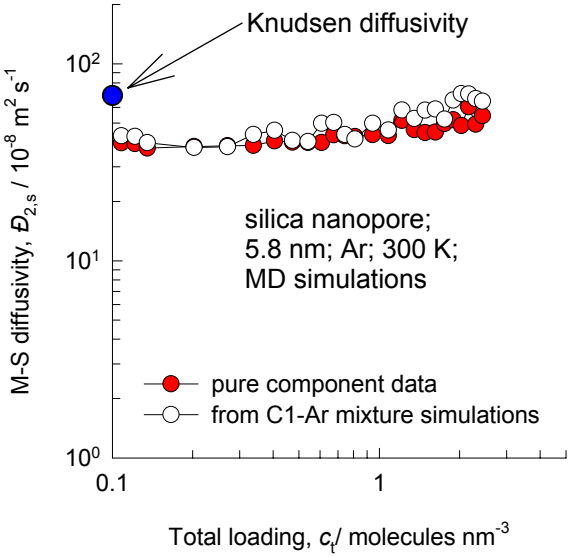

Figure 54

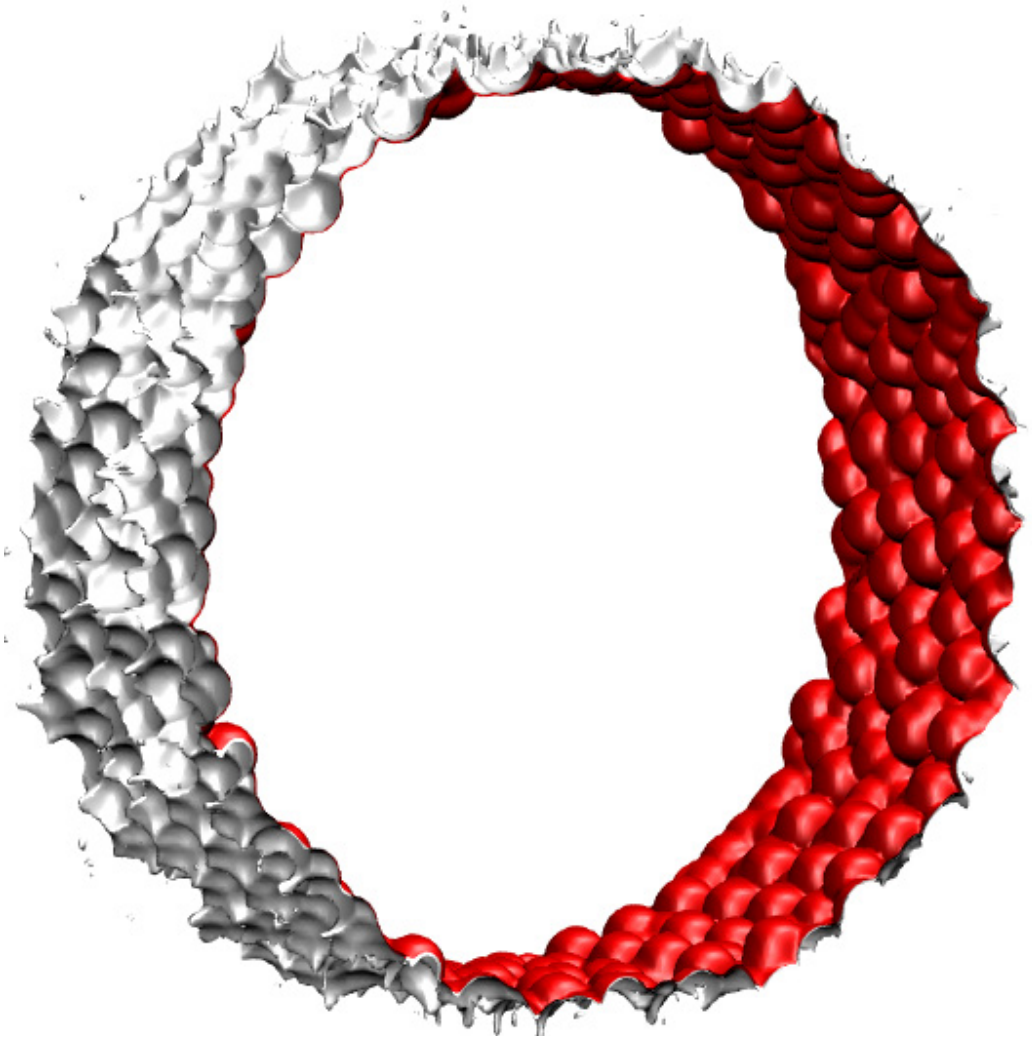

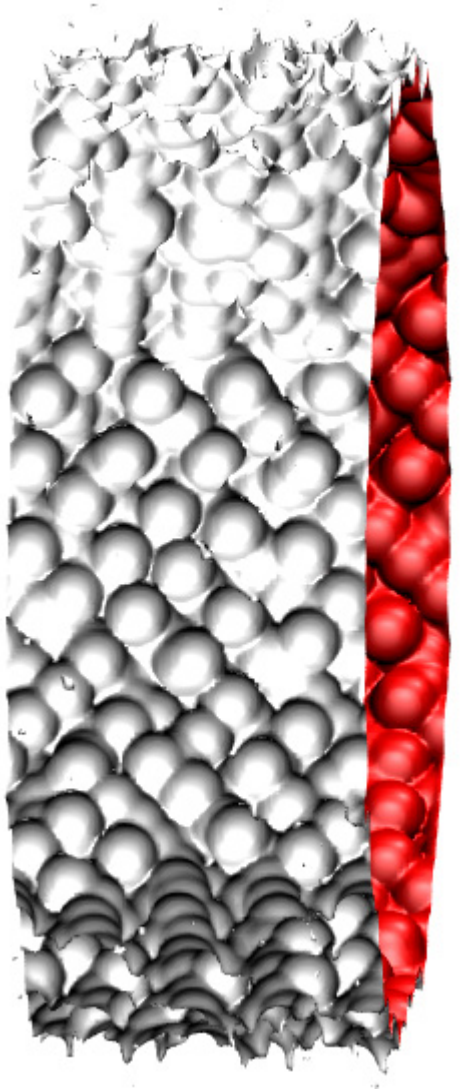

7.6 nm pore simulation results follow

Pure C1 and pure Ar, 7.6 nm pore, 300 K

Figure 55

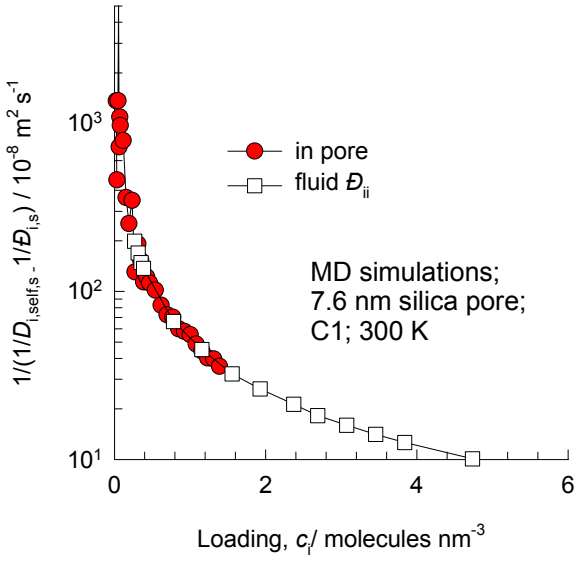

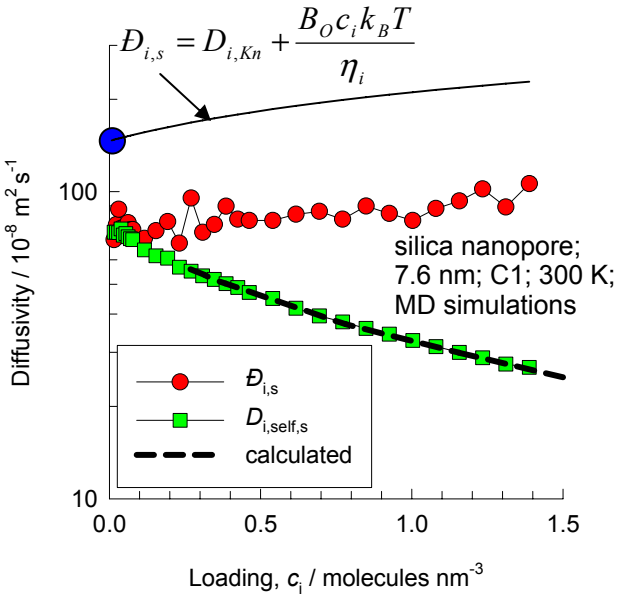

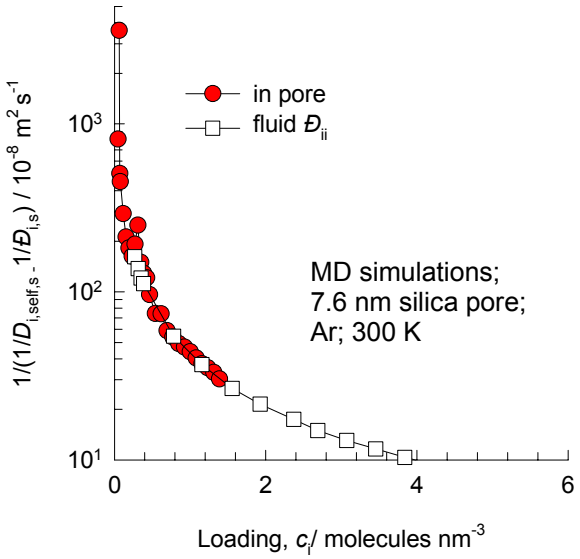

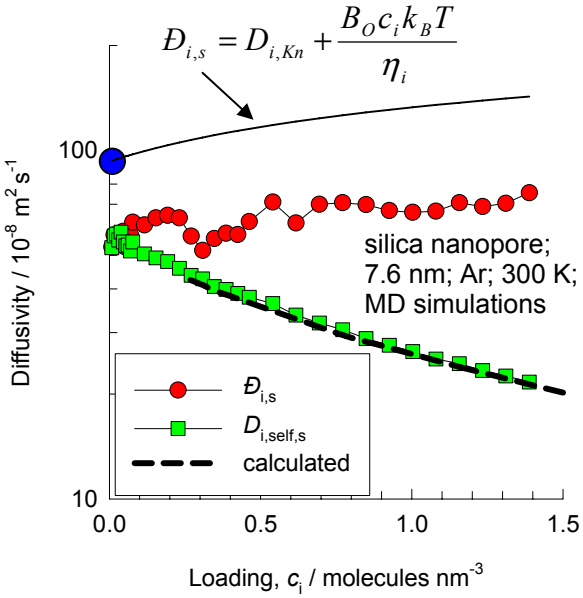

C1 –Ar mixture, 7.6 nm pore, 300 K

Figure 56

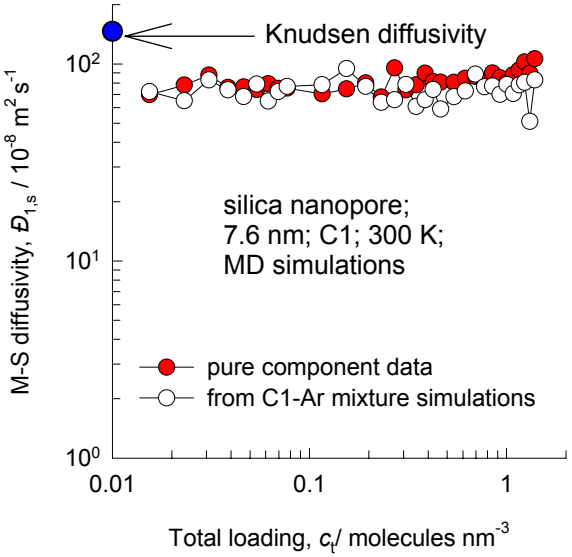

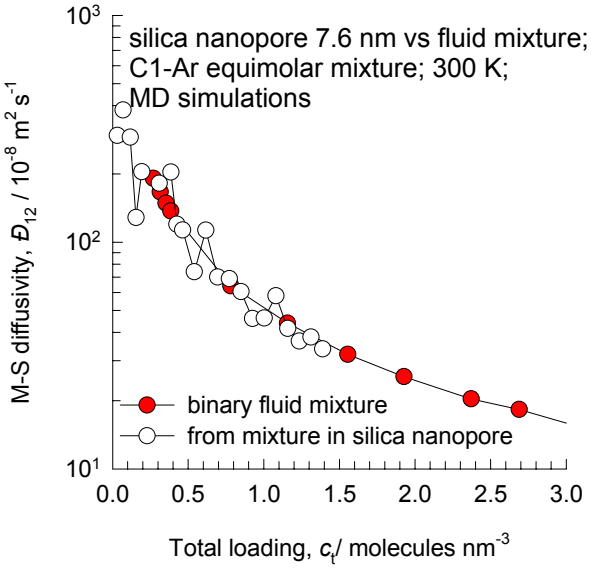

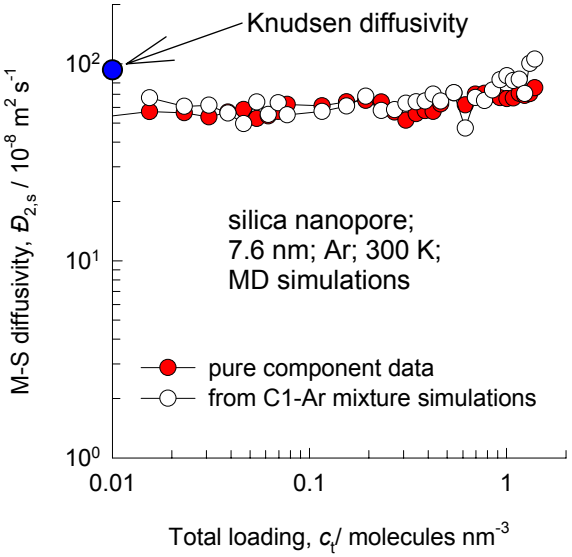

Figure 57

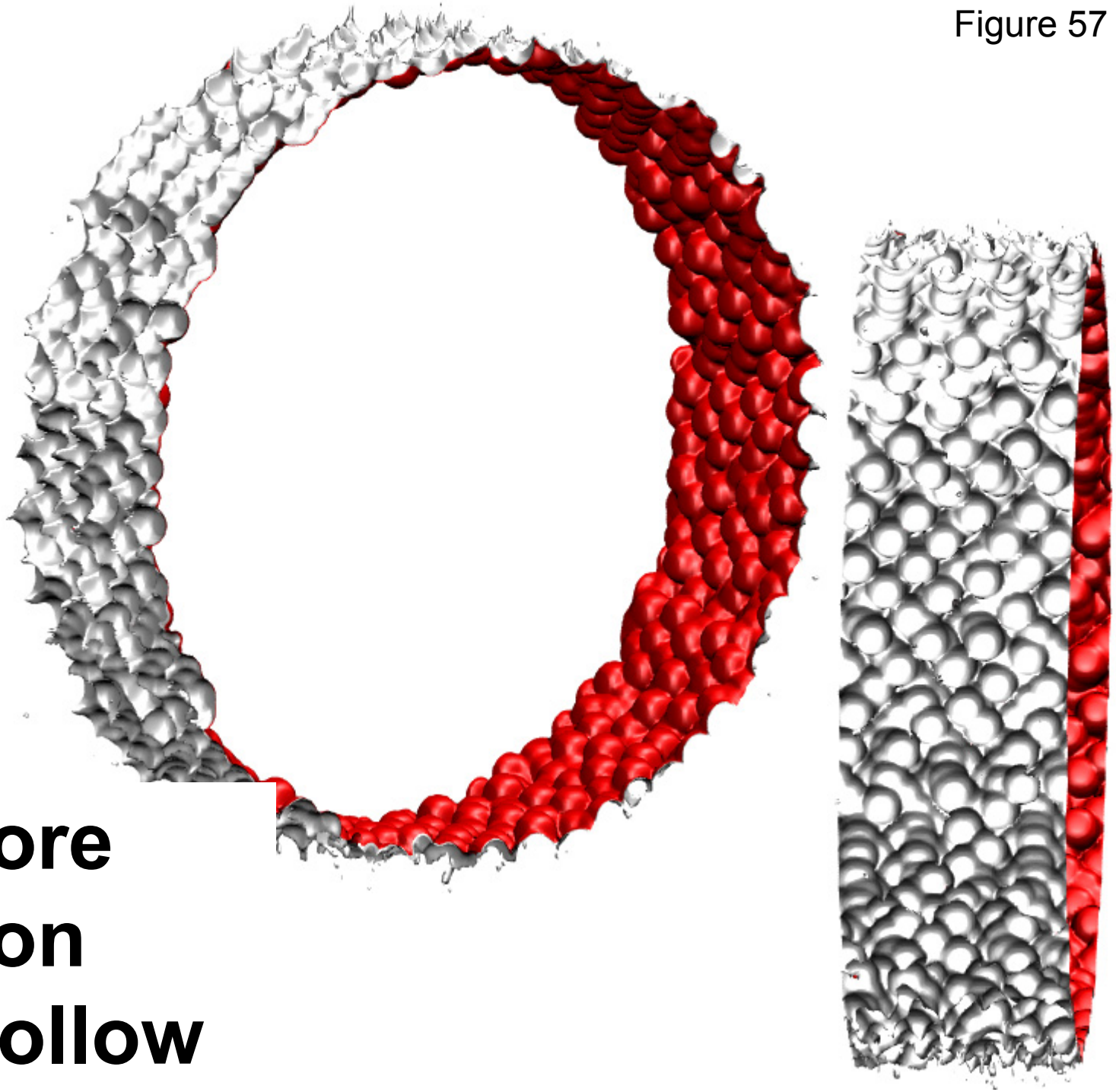

10 nm pore simulation results follow

Pure C1 and pure Ar, 10 nm pore, 300 K

Figure 58

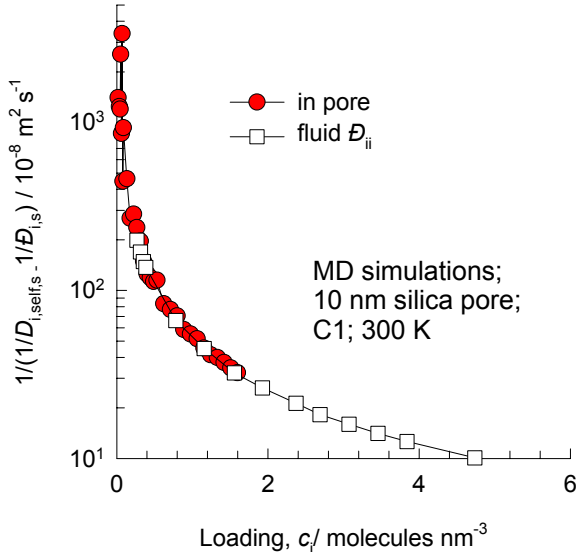

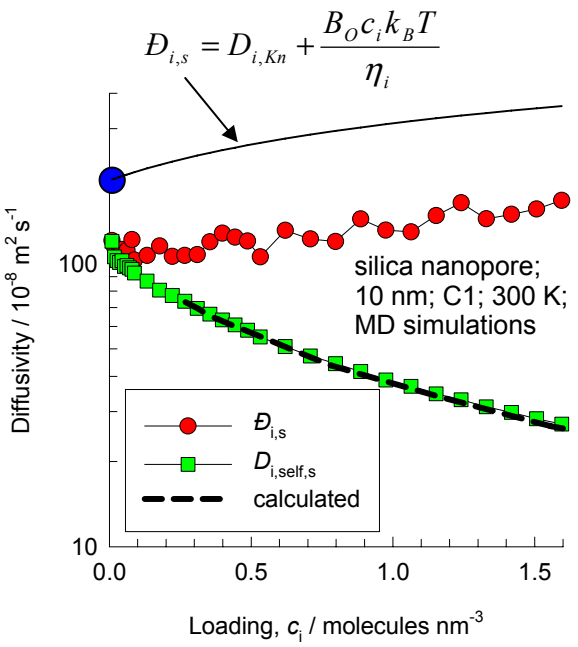

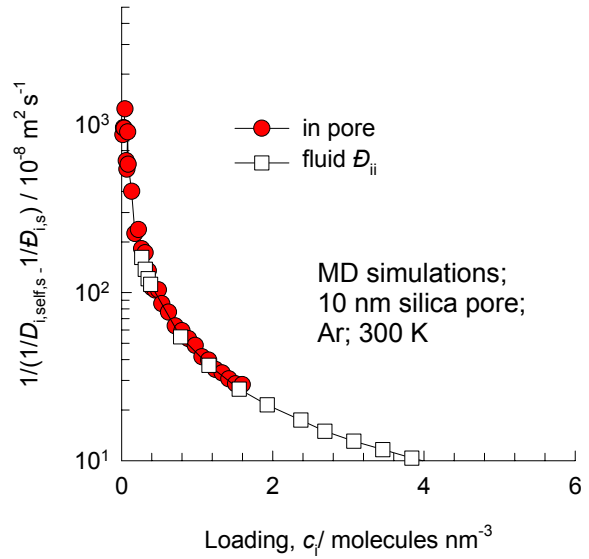

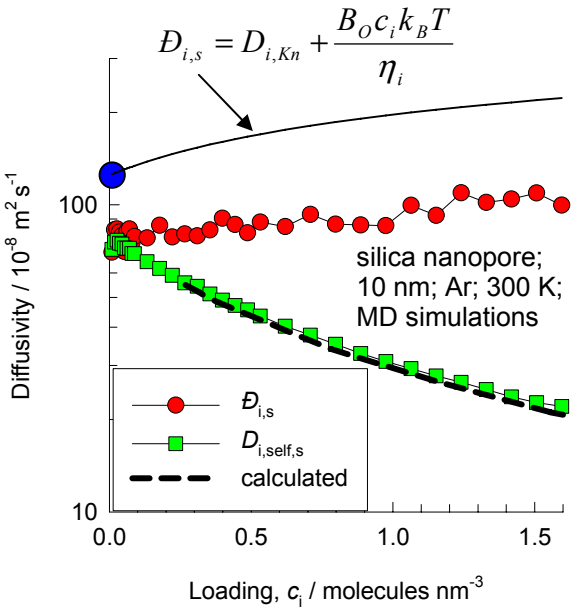

C1 –Ar mixture, 10 nm pore, 300 K

Figure 59